AD-A070 019 TEXAS INSTRUMENTS INC DALLAS F/G 7/4
STUDY OF A NUCLEAR MAGNETIC RESONANCE (NMR) GYRO USING OPTICALL--ETC(U)
MAR 79 D D MCGREGOR F49620-78-C-0056
UNCLASSIFIED AFOSR-TR-79-0728 NL

| OF |
AD
A070019

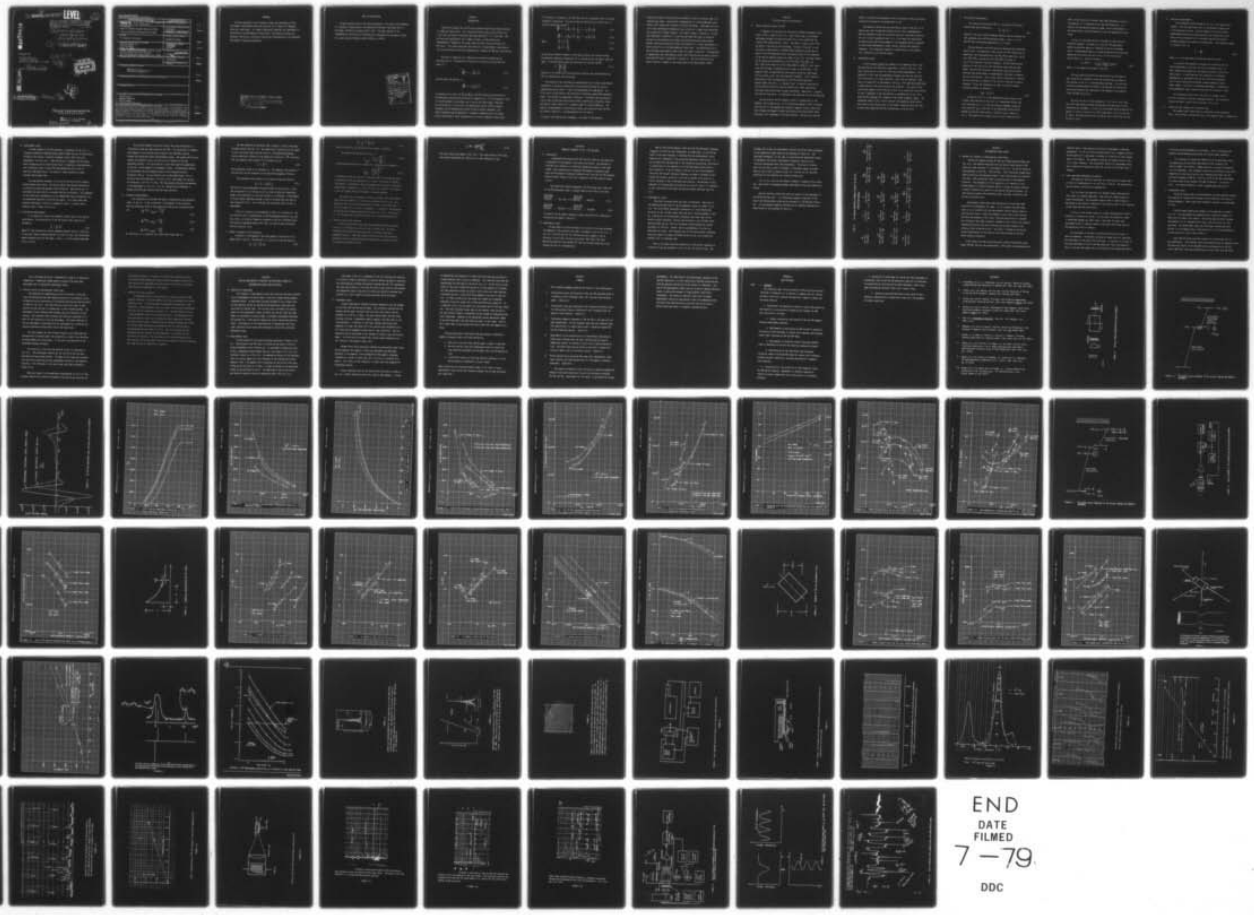

END
DATE
FILMED
7-79
DDC

(18) AFOSR-TR-79-0728 (19) **LEVEL II**

(12) 2

AD A070019

(6) STUDY OF A NUCLEAR MAGNETIC RESONANCE (NMR) GYRO USING OPTICALLY PUMPED HELIUM ISOTOPES.

(9) Final Technical Report for Period 1 April 1978 to 31 March 1979

PREPARED FOR:

Air Force Office of
Scientific Research
Bolling Air Force Base, D.C. 20332

(11) 31 Mar 79

(12) 93p.

(15) Contract No. F49620-78-C-0056

(10) Douglas D. McGregor
Principal Investigator

(16) 2305 (17) B2

TEXAS INSTRUMENTS
INCORPORATED

347 650 LB

UNCLASSIFIED

SECURITY CLASSIFICATION OF THIS PAGE (When Data Entered)

REPORT DOCUMENTATION PAGE	READ INSTRUCTIONS BEFORE COMPLETING FORM
1. REPORT NUMBER **AFOSR-TR- 79-0728** 2. GOVT ACCESSION NO.	3. RECIPIENT'S CATALOG NUMBER
4. TITLE (and Subtitle) Study of a Nuclear Magnetic Resonance (NMR) Gyro using Optically Pumped Helium Isotopes	5. TYPE OF REPORT & PERIOD COVERED Final Report 1978 April 1 - 1979 March 31
	6. PERFORMING ORG. REPORT NUMBER
7. AUTHOR(s) Dr. Douglas D. McGregor	8. CONTRACT OR GRANT NUMBER(s) F49620-78-C-0056
9. PERFORMING ORGANIZATION NAME AND ADDRESS Texas Instruments, Inc. P.O. Box 226015 Dallas, Tx 75266	10. PROGRAM ELEMENT, PROJECT, TASK AREA & WORK UNIT NUMBERS 2305/B2 61102F
11. CONTROLLING OFFICE NAME AND ADDRESS Director, Electronic & Solid State Sciences Air Force Office of Scientific Research Attn: NE Building 410 Bolling AFB, D.C. 20332 NE	12. REPORT DATE 31 MARCH 1979
	13. NUMBER OF PAGES 92
14. MONITORING AGENCY NAME & ADDRESS(if different from Controlling Office)	15. SECURITY CLASS. (of this report) Unclassified
	15a. DECLASSIFICATION/DOWNGRADING SCHEDULE

16. DISTRIBUTION STATEMENT (of this Report)

Approved for public release; distribution unlimited.

17. DISTRIBUTION STATEMENT (of the abstract entered in Block 20, if different from Report)

18. SUPPLEMENTARY NOTES

19. KEY WORDS (Continue on reverse side if necessary and identify by block number)

Optical Pumping
Magnetic Resonance
Helium Isotopes
Semiconductor Diode Lasers

20. ABSTRACT (Continue on reverse side if necessary and identify by block number)

In this experimental investigation the polarization levels and relaxation rates for optically pumped ^{4}He and ^{3}He isotopes were determined. An experiment verified that simultaneous magnetic resonance of both isotopes in a common volume may be attained. Characteristics of some experimental semiconductor diode lasers were measured with a view toward replacing helium lamps as an optical pumping radiation source with diode lasers. A semiconductor diode laser was successfully used to monitor polarized ^{4}He atoms.

DD FORM 1473

UNCLASSIFIED

FOREWORD

The work described in this technical report was performed at Texas Instruments Incorporated under the direction of Dr. Douglas D. McGregor, principal investigator. Dr. Dmetro Andrychuck conducted the experiments to characterize the semiconductor diode lasers. Bela Marton directed the apparatus fabrication, electronics design and instrumentation, and conducted the magnetic resonance experiments.

NOTE ON PUBLICATIONS

A paper covering much of the effort presented in this report was presented at a Society of Photo-Optical Instrumentation Engineers conference held in San Diego, California on August 30-31, 1978. The paper appears in the Proceedings of the Society of Photo-Optical Instrumentation Engineers, Volume 157, Laser Inertial Rotation Sensor (1978), pp. 81-88.

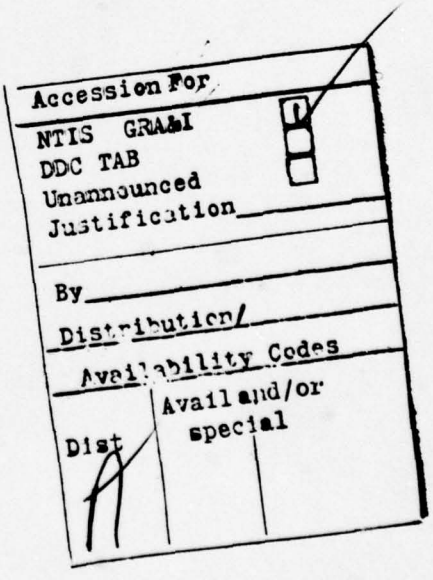

SECTION 1

INTRODUCTION

The helium isotopes ^3He and ^4He have properties which make them attractive in a NMR gyro application. Very long polarization times (up to 24 hours for a cell with no electric discharge) have been observed [1, 2, 3], with ^3He. ^4He has been used successfully for a number of years in high sensitivity magnetometers [4] because of the large signal-to-noise ratios available with ^4He cells. This report describes the results of an experimental investigation into the properties of optically pumped helium isotopes for NMR gyro applications.

The basis of operation for a NMR gyro using helium isotopes may be exhibited easily. The equation of motion of a collection of polarized ^3He atoms is [5]

$$\frac{d\vec{M}_n}{dt} = -\gamma_n \vec{M}_n \times \vec{H}; \tag{1.1}$$

for ^4He atoms the equation is

$$\frac{d\vec{M}_e}{dt} = -\gamma_e \vec{M}_e \times \vec{H}. \tag{1.2}$$

In equations (1.1) and (1.2) $\vec{M}_n$ and $\vec{M}_e$ are the ^3He nuclear polarization and ^4He metastable electron spin polarization respectively. $\vec{H}$ is the magnetic field in the environment of the atoms, and γ_n and γ_e are known atomic constants. The solutions to (1.1) and (1.2) are precessional motion of $\vec{M}_n$ at angular frequency $\gamma_n H$ and precesssional motion of M_e at angular frequency $\gamma_e H$. These frequencies may be measured in a magnetic resonance device by either optical monitoring of light transmission or by use of magnetic pickup coils.

If the device is rotated at rate $\vec{\Omega}$ there will be an apparent shift in the two precession frequencies. This may be seen by rewriting (1.1) and (1.2) in a rotating coordinate system [5]:

$$\frac{\delta \vec{M}_n}{\delta t} = -\gamma_n \vec{M}_n \times \left(\vec{H} - \frac{\vec{\Omega}}{\gamma_n}\right) = -\gamma_n \vec{M}_n \times \vec{H}_n^* \tag{1.3}$$

$$\frac{\delta \vec{M}_e}{\delta t} = -\gamma_e \vec{M}_e \times \left(\vec{H} - \frac{\Omega}{\gamma_e}\right) = -\gamma_e \vec{M}_e \times \vec{H}_e^* \tag{1.4}$$

where

$$\vec{H}_n^* = \vec{H} - \frac{\vec{\Omega}}{\gamma_n} \tag{1.5}$$

$$\vec{H}_e^* = \vec{H} - \frac{\vec{\Omega}}{\gamma_e} \tag{1.6}$$

H_n^* and H_e^* are effective magnetic fields which contain the rotation effect. The measured precession frequencies for a rotating device are hence $\gamma_n H_n^*$ and $\gamma_e H_e^*$. If we know H_n^* and H_e^* we may calculate the rotation rate $\vec{\Omega}$,

$$\vec{\Omega} = \frac{\vec{H}_e^* - \vec{H}_n^*}{\frac{1}{\gamma_n} - \frac{1}{\gamma_e}} . \tag{1.7}$$

Equation (1.7) allows us to find the device rotation rate and describes the basis of operation of the helium gyro.

The purpose of the investigation reported here was to obtain experimental information on optically pumped helium and radiation sources for optical pumping that may be used to predict the performance of an NMR gyro*. The first topic is polarization and relaxation of optically pumped ^{4}He metastable atoms. The results are presented in Section 2. The object was the accumulation of data (fractional polarization levels, polarization relaxation rates, and optical signal levels) for a computer model of a helium NMR gyro. The results of measurements of polarization levels and relaxation rates for ^{3}He are found in Section 3. The measurements will be used to

* A copy of the contract work statement is provided in the Appendix.

advance the theory of ^3He polarization behavior as well as provide input to a computer gyro model. One possible implementation of a helium NMR gyro would employ a cell containing a mixture of ^3He and ^4He gases. Experiments on such a cell were performed to demonstrate the validity of a theory which describes the interaction of these isotopes. The results appear in Section 4. In the work described in Sections 2, 3 and 4 helium lamps were used as radiation sources for the polarization process and polarization monitoring process. Another radiation source which offers the potential of a large improvement in device sensitivity is the semiconductor diode laser. The characteristics of some low power experimental diode lasers are found in Section 5. An experiment to demonstrate that semiconductor diode laser radiation may be used to monitor polarized ^4He atoms is described in Section 6. The final section of this report contains a summary of the conclusions of the experimental effort.

Section 2

^{4}He Polarization and Relaxation

A. Optical pumping process for ^{4}He

A diagram of an appartus for the optical pumping and magnetic resonance of ^{4}He is shown in Fig. 2.1. Light from a lamp is collimated and passes through a circular polarizer into a cell containing low pressure ^{4}He (approximately 1 Torr). The lamp is a glass tube of ^{4}He gas which is excited by a RF discharge. The gas in the cell is also excited by a weak electric discharge which produces a dilute sea of atoms in the 2^3S metastable level. The energy levels of ^{4}He important in the optical pumping process are shown in Fig. 2.2. The wave lengths of the radiation corresponding to the 2^3S_1-2^3P_0, 2^3S_1-2^3P_1, and 2^3S_1 -2^3P_2 transitions are in the range 10829 to 10830 Å. This radiation from the lamp is absorbed by cell atoms in the 2^3S level. The magnetic field (of magnitude H_0 and direction along the light beam) splits the 2^3S_1 level into three magnetic sublevels. Left circularly polarized D_0 light (corresponding to the 2^3S_1-2^3P_0 transition) removes atoms from the m = -1 sublevel only. Circularly polarized D_1 and D_2 radiation similarly tend to disturb the m level populations from their equilibruim state of equal population. When the m = 1 population differs from the m = -1 population, the atoms are said to be polarized.

The splitting of the 2^3S magnetic levels is proportional to the magnetic field intensity H_0. If an oscillating magnetic field is imposed upon the cell at the appropriate frequency, magnetic dipole transitions occur between the magnetic states which destroy the polarization (more precisely, the z component of the polarization). One may also view the

effect of the oscillating magnetic field as rotation of the polarization direction from parallel to perpendicular to H_0.

One method of monitoring the polarization level of the cell is to measure the light transmitted through the cell with a photodetecter. When the metastable atoms are polarized along the light beam direction, the cell is more transparent than it is if the atoms are unpolarized. By observing the oscillating magnetic field frequency which corresponds to the minimum photodetector signal one may identify the resonance frequency. This resonance frequency is proportional to the magnetic field intensity H_0 (2.8 MHz per gauss).

B. Experimental setup

A block diagram showing the elements of the apparatus used in the ^4He polarization and relaxation experiment is given in Fig. 2.3. The basic configuration is that of a self-oscillating magnetometer. The operation of this type of magnetometer depends upon the fact that the cell polarization is a vector quantity. Note that the apparatus light beam is oriented 45° to the magnetic field H_0. The light beam establishes a polarization of the atoms along the H_0 direction. The action of the oscillating magnetic field from the H_1 coil is to rotate this polarization so that a component of the polarization is perpendicular to H_0. This polarization component will precess at the Larmor frequency ($\gamma_e H_0$). The photodiode shown in Fig. 2.3 will monitor the precessing polarization and yield an oscillating signal at the Larmor frequency, which may then be amplified, phase-shifted and directed back to the H_1 coils.

C. Polarization measurements

The fractional polarization $\vec{P}_e$ of a collection of ^4He metastable atoms may be defined as:

$$\vec{P}_e = \frac{1}{\hbar} < \vec{J} >, \tag{2.1}$$

where $\vec{J}$ is the total angular momentum operator and the brackets denote averaging over the ^4He metastable atoms. Since J = 1 for the 2^3S level the maximum magnitude of P_e is unity.

One may determine the polarization by measuring the photodiode signal level. The absorption cross section for ^4He showing the D_0 absorption line (corresponding to the 2^3S_1-2^3P_0 transition), the D_1 line (2^3S_1-2^3P_1), and the D_2 line (2^3S_1-2^3P_2) is given in Fig. 2.4 as function of optical frequency. The ^4He lamp emission spectrum in the limit of no self absorption would have the same shape. One can also calculate a monitoring cross section which describes the effectiveness of monochromatic radiation in determining cell polarization. Such a cross section (the dichroic monitoring cross section) is plotted in Fig. 2.5 as a function of optical frequency. Using the information in Figs. 2.4 and 2.5 one may calculate S_D which is defined by

$$I_{SIG} = P_e \, S_D \, I_L \tag{2.2}$$

In equation (2.2) I_L is the photodiode current caused by the incident lamp radiation to the cell (i.e. photodiode current with cell discharge out). P_e is the polarization component along the light beam and I_{SIG} is the part of the photodiode current which depends on the cell polarization. Typically I_{SIG} is about 1% of I_L. The quantity S_D is shown in Fig. 2.6 as a function of $\tilde{A}$,

which is the fraction of incident lamp light absorbed by the cell. The quantity τ_L is a measure of the lamp self absorption. It affects the lamp emission spectral shape. With a spectrometer τ_L was established to be approximately 2.5 for the experimental conditions.

In Fig. 2.7 the polarization is plotted for three cells of differing pressure. The abscissa is the cell 2^3S metastable density n_4 which we employ as a measure of the cell discharge level. The metastable density is found by measuring the fractional absorption $\tilde{A}$ and using the plot of Fig. 2.8 to find the cell optical depth τ_c. The n_4 is given by

$$n_4\ (cm^{-3}) = \frac{\tau_c}{L\ (cm) \times 0.865 \times 10^{-12}} \qquad (2.3)$$

where L is the length of the beam in the cell.

The I_{SIG} used to calculate the polarization was the peak-to-peak value of the sinusoidal signal and the polarization shown as the ordinate of Fig 2.7 is correspondingly defined. This polarization may be demonstrated by analysis to be one-half of the polarization established by the light beam in the absence of any magnetic fields (neither H_0 nor H_1).

The cells of Fig. 2.7 have dimensions 1 1/2" OD X 1 3/4" long. The total lamp radiation passed through the cells was about 1.54 mW (absorption not included). In Fig. 2.9 are plotted the polarizations for several 2" cells (2 1/16" OD X 2 1/16" long) and 6" cells (2 1/16" OD X 6" long). The lamp radiation was 1.54 mW for the 2" cells and 1.24 mW for the 6" cells.

D. Relaxation measurements

In the apparatus block diagram of Fig. 2.3 a box labelled $\Delta\phi$ appears. This box adds either zero or 5.9 degrees of phase shift to the electronic circuit. From the theory of self oscillating magnetometer operation one may show that if we change the circuit phase shift by an amount $\Delta\phi$ (in radians) then the oscillation frequency changes by an amount $\Delta\omega$ (radians/sec). The frequency change is related to $\Delta\phi$ by

$$\frac{1}{\tau} = \frac{\Delta\omega}{\Delta\Phi} \quad , \tag{2.4}$$

where $1/\tau$ is the metastable polarization relaxation rate.

In practice the procedure to measure the relaxation rate involves measurement of the self oscillation frequency (near 1.5 MHz), changing the phase shift and measuring the oscillation frequency again. In recording data the frequency of a reference magnetometer is subtracted from the self oscillator frequency. This is easily done with the Hewlett-Packard computing counter (Model 5360A). The use of a reference magnetometer is necessitated by geomagnetic noise, random fluctuations of the earth's field.

The relaxation rate of the 1 3/4" cells is plotted in Fig. 2.10 as a function of the cell metastable density. The relaxation results for the 2" and 6" cells are given in Fig. 2.11.

E. Effect of light intensity on relaxation rate

The pumping light itself tends to contribute to the relaxation rate. The variation in relaxation rate as the pumping light is reduced with

optical filters is presented in Fig. 2.12. By extrapolation to zero light intensity we see that the light contribution is about 2×10^3 sec^{-1} for the conditions stated.

F. Signal-to-noise ratio and gyro drift

The signal-to-noise ratio $(S/N)_e$ is a useful measure of signal strength. A plot of $(S/N)_e$ (the RMS photo-diode signal divided by the RMS noise in a 1 Hz bandpass) for the ^4He cells is given in Fig. 2.13 as a function of the metastable density n_4. The noise is assumed to be shot noise only and is calculated from the DC photo diode current. For typical situations the photo diode shot noise dominates the amplifier noise.

Given the signal-to-noise ratio and the relaxation rate one may determine with the following expression the contribution to random drift from the ^4He cell:

$$\sigma_e(\tilde{\phi}) = \frac{\gamma_n (t/\Delta f)^{\frac{1}{2}}}{2 \gamma_e \tau \left(\frac{S}{N}\right)_e} , \qquad (2.5)$$

In this relation $\sigma_e(\tilde{\phi})$ is the drift angle, γ_n is the ^3He 1^1S_0 gyromagnetic ratio, γ_e is the ^4He 2^3S_1 gyromagnetic ratio, t is the gyro operation time (usually 1 hour), and Δf is the bandwidth of the noise in $(S/N)_e$ ($\Delta f = 1Hz$). The quantity $\sigma_e(\tilde{\phi})$ in degrees (after 1 hour of operation) for the various ^4He cells versus n_4 is shown in Fig. 2.14.

SECTION 3

^{3}He POLARIZATION AND RELAXATION

A. Optical pumping process for ^{3}He

Apparatus for the optical pumping and magnetic resonance of ^{3}He is similar to that of Fig. 2.1, except now the cell contains ^{3}He gas at low pressure (0.2 to 10 Torr). The lamp may contain either ^{3}He or ^{4}He gas and is excited by a RF discharge. A weak RF discharge is also maintained in the ^{3}He cell to maintain a population of metastable atoms. The energy levels of ^{3}He which are important in the optical pumping process are shown in Fig. 3.1. Circularly polarized lamp radiation polarizes the two ^{3}He 2^3S levels in the same fashion as ^{4}He metastables are polarized. By metastability exchange collisions angular momentum in the 2^3S levels is transferred to the 1^1S_0 ground level. This process may be written as

$$\underbrace{^3\text{He}\ (2^3S)}_{\text{polarized}} + \underbrace{^3\text{He}\ (1^1S)}_{\text{unpolarized}} \longrightarrow \underbrace{^3\text{He}\ (1^1S)}_{\text{polarized}} + {}^3\text{He}\ (2^3S). \qquad (3.1)$$

After the polarization of the nuclei (i.e. the 1^1S_0 level atoms) has been established, one may perform magnetic resonance on the nuclei. If an oscillating magnetic field is applied at angular frequency $\gamma_n H_0$, then the z component of the nuclear polarization is destroyed. Because of the coupling of the 1^1S and 2^3S levels through exchange collisions, the polarization of the metastables is also destroyed. This change in polarization may be observed optically by transmission monitoring of the pumping radiation. If one directs a monitoring beam through the cell in a direction perpendicular to the magnetic field a sinusoidal signal at the nuclear precession frequency will be observed.

B. Experimental setup

A block diagram of the ^3He apparatus is presented in Fig. 3.2. A frequency synthesizer (Hewlett-Packard Model 3330B) delivers an oscillating voltage at the nuclear precession frequency (about 1725 Hz for this experiment) to the H_1 coil. When the switch is engaged, the ^3He nuclei begin precessing, and an oscillating signal is observed at the photodiode. This sinusoidal signal is amplified and demodulated with a lock-in amplifier (PAR Model JB-5). The output is then directed to a chart recorder (Brush Model 250).

The experimental procedure is to turn off the H_1 drive for several minutes before data taking. During this period the nuclear polarization is building up along the magnetic field direction. When the H_1 coil is activated, the polarization is rotated from the H_0 direction. The component of the polarization perpendicular to H_0 immediately begins precessing, and the photodiode registers an oscillating signal. This signal amplitude gradually decreases in time to an asymptotic value. A typical chart recorder trace is shown in Fig. 3.3.

C. Polarization measurements

It is possible to relate the asymptotic signal level to the nuclear polarization. The polarization of the ^3He ground level atoms may be defined as

$$\vec{P}_n = \frac{2}{\hbar} \langle \vec{I} \rangle \tag{3.2}$$

where $\vec{I}$ is the nuclear spin angular momentum operator (which is identical to the total angular momentum operator for the 1^1S level) and the brackets denote averaging over the ^3He atoms. Since I = 1/2 the maximum magnitude of P_n is unity.

The relation between the nuclear signal level and polarization is calculated in much the same fashion as for ^4He. The calculation is somewhat more complex in that account must be made of the imperfect coupling between the precessing ground and metastable atoms. The nuclear polarization results are plotted in Figs. 3.4 and 3.5 as a function of the cell metastable density. This polarization is that which would be established in the cell in the absence of any magnetic fields. The metastable density was calculated from the measured values of the transverse nuclear relaxation time T_2. This calculation will be described below. All of the cells have the dimensions 1 1/2". OD x 2 1/2" long except for one cell of dimensions 1 1/2" OD x 5" long. ^4He lamp pumping radiation was employed in the experiments of Fig. 3.4. Fig. 3.5 indicates the difference in pumping with ^3He lamp radiation and ^4He lamp radiation.

D. Relaxation measurements

The relaxation of polarized ^3He atoms is described by two relaxation times, T_1 and T_2. If the z direction is the magnetic field direction, then the relaxation terms of the equations of motion for the polarization are

$$\frac{d}{dt}\langle I_z\rangle \Big|_{relax} = -\frac{\langle I_z\rangle}{T_1} \tag{3.3}$$

$$\frac{d}{dt}\langle I_x\rangle \Big|_{relax} = -\frac{\langle I_x\rangle}{T_2} \tag{3.4}$$

$$\frac{d}{dt}\langle I_y\rangle \Big|_{relax} = -\frac{\langle I_y\rangle}{T_2} . \tag{3.5}$$

For ^3He nuclei T_1 is typically 10 to 100 times longer than T_2.

We next describe the procedure used to obtain T_1 and T_2 from chart recorder traces like Fig. 3.3. The quantities T^* and the ratio a/b shown in Fig. 3.6 may be taken from the trace in a straightforward manner. From an analytical solution to the equations of motion of $\langle\vec{I}\rangle$, one finds that the apparent time constant T^* is related to T_1 by

$$T_1 = \frac{a}{b} T^*. \tag{3.6}$$

This expression allows us to calculate T_1. The apparent time constant T^* and the ratio a/b are functions of the oscillating magnetic field H_1.

The transverse time constant T_2 is found by using the relation

$$\frac{1}{T^*} = \frac{1}{T} + \gamma_n^2 H_1^2 T_2. \tag{3.7}$$

The field H_1 may be determined from the current to the H_1 coils. Since the calculation of T_2 involves H_1 and T_1, both of which are imperfectly known, the uncertainty in T_2 by this method is of interest. A measurement of T_2 by another technique yielded a value of T_2 about 18% less than by use of equation (3.7). This indicates the uncertainty level of the T_2 measurement.

Plots of T_1 versus T_2 are presented in Figs. 3.7, 3.8 and 3.9. The T_2 relaxation time is proportional to the ^{3}He metastable density, n_3 (see Fig. 3.10), so T_2 may be viewed as a measure of the cell discharge level. The values of metastable density for Figs. 3.4 and 3.5 were calculated from T_2 using Fig. 3.10.

E. Effect of magnetic field gradients

A gradient in the magnetic field environment of the ^{3}He cell will reduce both T_1 and T_2. The decrease in T_1 and T_2 is given by theory as

$$\frac{1}{T_1} = \frac{1}{T_1'} + \left(\frac{1}{T_1}\right)_{\Delta H} \tag{3.8}$$

$$\frac{1}{T_2} = \frac{1}{T_2'} + \left(\frac{1}{T_2}\right)_{\Delta H}, \tag{3.9}$$

where T_1' and T_2' are the relaxation times without a gradient.

The theoretical expression for $T_{1\,H}$ is

$$\frac{1}{T_{1\Delta H}} = \frac{u^2 \tau_o \left(\frac{\partial H_z}{\partial z}\right)^2}{2H_o}. \tag{3.10}$$

A preliminary expression for T_2 based on a simplified cell geometry is

$$\frac{1}{T_{2\Delta H}} = \frac{L^4 \gamma_n^2 \left(\frac{\partial H_z}{\partial z}\right)^2}{72\, u^2 \tau_o}. \tag{3.11}$$

In equations (3.10) and (3.11) u is the RMS speed of the atoms and may be calculated from the gas temperature ($u = 0.908 \times 10^5$ cm/sec for 300°K). The quantity τ_0 represents a mean time between collision and is inversely proportional to pressure ($\tau_0 = 2.2 \times 10^{-7}$ sec for 1 Torr[6]). The length L is the cell length along the direction of maximum gradient.

The results of an experiment in which a gradient field from magnetic field coils was applied to a ^{3}He cell are exhibited in Fig. 3.11. Also plotted in Fig. 3.11 are the predictions of theory. The sensitivity of T_2 to the choice of L in (3.11) is apparent. L = 4.24 cm is the projection of the cell axial length along the z axis (see Fig. 3.12). The choice of L = 4.77 cm was made on the basis of best fit to the experimental data.

F. Signal-to-noise ratio and drift

Plots of the RMS ^{3}He signal from the photodiode divided by the RMS noise in a 1 Hz bandpass are given in Fig. 3.13 and 3.14. The noise (assumed purely photodiode shot noise) was calculated from the DC photodiode current. Given the signal-to-noise ratio and the transverse relaxation rate, one may determine the contribution to random drift from an optically monitored ^{3}He cell:

$$\sigma_n(\phi) = \frac{(t/\Delta f)^{1/2}}{2T_2 \left(\frac{S}{N}\right)_n} \qquad (3.12)$$

The drift results are shown in Fig. 3.15. The large values of drift mean that optical monitoring of a ^3He cell is a poor technique to use.

SECTION 4

MAGNETIC RESONANCE IN ^3He - ^4He MIXTURES

A. Introduction

A gyroscope with separate ^3He and ^4He cells would be very sensitive to gradients of the magnetic field within the shield. One approach to alleviate this problem is to place both precessing species in the same volume. With consideration of adequate ^3He magnetic resonance signal level and ^4He magnetic resonance linewidth, one finds that the ^3He pressure should be small (0.001 to 0.01 Torr) compared to the ^4He pressure (about 1 Torr).

The coupling of angular momentum of the ^3He ground level atoms and of the ^4He metastable atoms is accomplished by collisions of the form

$$\underbrace{^4He(2^3S)}_{\text{polarized}} + {}^3He\,(1^1S) \longrightarrow \underbrace{^3He(2^3S)}_{\text{polarized}} + {}^4He(1^1S) \qquad (4.1)$$

$$\underbrace{^3He(2^3S)}_{\text{polarized}} + {}^4He(1^1S) \longrightarrow \underbrace{^3He(1^1S)}_{\text{polarized}} + {}^4He(2^3S) \qquad (4.2)$$

The details of the angular momentum transfer obtained from a theoretical calculation are shown in Table 4.1.

B. Experimental setup

An experiment to verify processes (4.1) and (4.2) has been performed. The elements of the apparatus are shown in schematic form in Fig. 4.1. A cell of 1 Torr ^4He and 0.01 Torr ^3He was optically pumped in the H_0 direction (z axis) with circularly polarized light from a ^4He lamp. Monitoring radiation from another ^4He lamp was directed along the y axis through the cell to a photodetector.

When an oscillating magnetic field near the ^{4}He metastable resonance frequency (1.49 MHz for this experiment) is established, an oscillating-signal at the same frequency is observed from the photodetector, which monitors the y component of the precessing metastable polarization. It can be shown that the amplitude of the transverse (precessing) polarization is proportional to the component of the ^{4}He metastable polarization in the z direction. If we now impose on the cell an oscillating magnetic field near the nuclear resonance frequency, we expect a decrease in the nuclear polarization along the z axis and by process (4.1) and (4.2) a similar decrease in the z metastable polarization. The decrease in the z component of the metastable polarization in turn will result in a decrease in the y polarization and hence the observed signal amplitude (see Fig. 4.1).

C. Experimental results

The effect discussed above did occur as predicted. Some plots of the demodulated amplitude of the photodetector signal are shown in Fig. 4.2. The curve marked "metastable resonance" is a trace showing the variation of the 1.49 MHz signal amplitude with a scanning magnetic field H_0. With H_0 set on the metastable resonance, the three lower curves marked "nuclear resonance" indicate the variation in the 1.49 MHz signal amplitude when the H_{1n} field was frequency scanned through the nuclear resonance (at 1725 Hz). Several curves corresponding to various H_{1n} magnitudes are shown. The frequency scan for the three nuclear resonance curves was begun at slightly different points on the x axis, hence the apparent shift in resonance peak.

Plots of the peak fractional modulation of the nuclear resonance as a function of H_{1n} are presented in Fig. 4.3 for two values of H_{1e}. The

diamonds and circles are experimental results; the solid curves correspond to the theoretical model based on the processes of Table 4.1. One adjustable parameter, T_1', was used in calculating the theoretical curves. T_1' represents the nuclear longitudinal relaxation time due to all relaxation mechanisms other than metastables. The value of T_1' which best fits the data is only 2.3 seconds, a time which seems very short when we look at the T_1 curves of Figs. 3.7, 3.8 and 3.9 for pure ^3He. Resolution of this question will require further work.

Fig. 4.4 is a plot of the nuclear linewidth in magnetic units versus H_{1n}. Again there is agreement between experimental points and theoretical curves.

One may state two conclusions from the results of the experiment on the ^3He-^4He mixture cell: (1) simultaneous magnetic resonance of ^3He nuclei and ^4He metastable atoms may be achieved in a ^3He-^4He gas mixture; and (2) the observed magnetic resonance may be adequatey modeled with a theory based on the processes of Table 4.1.

TABLE 4.1 THE ANGULAR MOMENTUM EXCHANGES BETWEEN ^3He AND ^4He.

INTERACTION FORMULA

$$\overbrace{1\hbar}^{} \quad \overbrace{0}^{} \quad \overbrace{0}^{} \quad \overbrace{\frac{5}{6}\hbar}^{} \quad \overbrace{\frac{1}{6}\hbar}^{}$$

$$^4He\ (2^3S) + {}^3He\ (1^1S) \longrightarrow {}^4He\ (1^1S) + {}^3He\ (2^3S,\ F = \tfrac{3}{2}) + {}^3He\ (2^3S,\ F = \tfrac{1}{2})$$

$$\overbrace{1\hbar}^{} \quad \overbrace{0}^{} \quad \overbrace{\frac{1}{3}\hbar}^{} \quad \overbrace{\frac{2}{3}\hbar}^{}$$

$$^3He\ (2^3S,\ F = \tfrac{3}{2}) + {}^4He\ (1^1S) \longrightarrow {}^3He\ (1^1S) + {}^4He\ (2^3S)$$

$$\overbrace{1\hbar}^{} \quad \overbrace{0}^{} \quad \overbrace{-\frac{1}{3}\hbar}^{} \quad \overbrace{\frac{2}{3}\hbar}^{}$$

$$^3He\ (2^3S,\ F = \tfrac{3}{2}) + {}^4He\ (1^1S) \longrightarrow {}^3He\ (1^1S) + {}^4He\ (2^3S)$$

$$\overbrace{1\hbar}^{} \quad \overbrace{0}^{} \quad \overbrace{\frac{10}{9}\hbar}^{} \quad \overbrace{-\frac{1}{9}\hbar}^{} \quad \overbrace{0}^{}$$

$$^3He\ (1^1S) + {}^4He\ (2^3S) \longrightarrow {}^3He\ (2^3S,\ F = \tfrac{3}{2}) + {}^3He\ (2^3S,\ F = \tfrac{1}{2}) + {}^4He\ (1^1S)$$

SECTION 5

SEMICONDUCTOR DIODE LASERS

A. Reasons for interest in semiconductor diode lasers

The optical pumping process for ^4He has already been described (see Fig. 2.2). One problem associated with the optical polarization of ^4He atoms with lamp radiation is illustrated in Fig. 5.1. D_0 and D_1 radiation (corresponding to the $2^3S_1 - 2^3P_0$ and $2^3S_1 - 2^3P_1$ transitions respectively) tends to polarize the metastable atoms in one direction while D_2 radiation (the $2^3S_1 - 2^3P_2$ transition) tends to polarize atoms in the opposite direction. The consequence of this opposition is a reduction in the effectiveness of a helium discharge lamp as a source of pumping radiation. A similar situation also applies in the optical monitoring process. D_2 lamp radiation reduces the photodiode signal from what it would be with D_0 and D_1 radiation only.

Semiconductor diode lasers have characteristics which make them attractive as replacements for lamps. In its simplest form the diode laser is a p-n junction with the semiconductor crystal heavily doped so that the Fermi level is above the bandgap on the n side of the junction and below the bandgap on the p side. With the application of a forward bias voltage to the diode, electrons injected on the n side of the junction recombine with holes from the p side and give up their energy to the radiation field inside the cavity. The cavity is formed by cutting the crystal perpendicular to the junction plan and polishing the surface (which should be parallel).

Diode lasers have been constructed which radiate considerable power (about 150 mW)[7] and are very monochromatic. Both power and monochromaticity

features imply a large potential sensitivity improvement in NMR gyro performance. In Fig. 5.2 the calculated sensitivity in magnetic units of the ^{4}He portion of a gyroscope is plotted as a function of laser radiant power in milliwatts. The parameter relating the several curves in Fig. 5.2 is laser linewidth. The considerable sensitivity improvement which may be realized by replacing a lamp with a 10 mW, 0.07 Å diode laser is apparent.

B. Laser wavelength dependence on material

The materials which are available for construction of diode lasers are the III-V combinations of In, Ga, Al-As, P and Sb. The combinations may be binaries, tertiaries or quaternaries.

Fig. 5.3 gives the spectrum of an AlGaAsSb double heterojunction laser grown on a GaAsSb substrate[8]. Note that the intensity peaks at several wavelengths. The wavelength region 0.995 to 1.000 microns is determined by the physical dimensions of the diode as well as the injection current amplitude and pulse nature.

In Fig. 5.4 the radiant output of a double heterojunction laser[9] is plotted as a function of current. In this laser the InGaAs p-n region is sandwiched between two InGaP layers. Note that the laser peak wavelength occurs at 1.064 μm, which is only about 200 Å away from the ^{4}He absorption lines at 1.083 μm.

The wavelength of the band of radiation emitted by the laser is material dependent. Furthermore the material composition will determine the wavelengths of the peaks within the band. If the peak is to occur at the exact wavelength of one of the ^{4}He absorption lines, one should be able to fine-tune the composition of the material even though other means

of tuning the peak wavelength are available. This is so because non-material tuning mechanisms may affect the radiant power adversely.

It is possible to choose the composition of the quaternary alloy $In_{1-x}Ga_xP_{1-z}As_z$ so that diode lasers made of such a material will lase at 1.0830 μm(1.145 eV). Common practice is to grow this material on an InP substrate. This produces an additional constraint on the alloy composition in that the alloy unit cell dimension must match the InP unit cell dimension (5.869 Å). From Fig. 5.5[10] we see that the bandgap of 1.145 eV and lattice constant of 5.869 Å requires x = 0.12 and z = 0.27. The required material is then $In_{0.88}Ga_{0.12}As_{0.27}P_{0.73}$/In P.

C. Experimental setup

The diode lasers used in the experimental work were supplied through the courtesy of Profesor Nick Holonyak of the University of Illinois at Urbana-Champaign. These lasers were designed to operate in a pulsed mode at 77°K.

A block diagram showing the elements of the apparatus is shown in Fig. 5.6. The spectrometer was manufactured by Jarrell-Ash (Model 82-020) with a 0.5 meter focal length. The grating used has 1180 lines/mm. The detector is a S-1 photomultiplier tube. Both 40 and 10 μm slits were used. The pulsed power supply was fabricated in-house and could deliver 0 to 1.0 amperes with a pulse duration of 1 to 20 microseconds at a pulse repitition rate of 100 to 1000 Hz.

Light from the diode laser was focused into the entrance slit of the spectrometer. The dispersed light was detected by the S-1 photomultiplier. The electrical output of the photomultiplier was detected by a PAR 220 lock-in amplifier, which was synchronized with the signal from the diode

laser power supply. The current peak, pulse duration and repetition rates were measured on a Tektronix 454 oscilloscope. A Keithly chart recorder was used to record the output signal from the lock-in amplifier.

The arrangement shown in Fig. 5.7 was used to vary the temperature of the diode. The diode was mounted on a TO-18 header, which itself was mounted on an insulator type terminal block. The header was held in place by a copper strip which served to transfer heat away from the header. This copper strip was screwed to the Dewar. A heater coil was wrapped around the copper cold transfer strip. This arrangement permitted variation of the temperature of the TO-18 header and hence of the diode. An Iron-Constantan thermocouple, clamped between the header and the cold transfer strip, was used to measure the temperature.

D. Laser spectral characteristics

The spectra of the emission from diode laser D-2 is given in Fig. 5.8. The current of 0.24 amperes is near the threshold for laser operation. One notes six peaks due to the different axial modes. The splitting of the peaks may be due to transverse modes. One further notes that there is a peak at 10830.36 Å, almost in coincidence with the ^{4}He absorption line at 10830.341 Å. Only a small amount of tuning is required to match the laser emission wavelength with the absorption line.

The laser linewidth is an important quantity because of optical pumping considerations (see Fig. 5.2). A comparison of one of the modes of the D-2 diode laser and the ^{4}He lamp emission spectrum is presented in Fig. 5.9. It is apparent that the two lines have a comparable width, which is probably the limit of the spectrometer resolution.

We next consider the effect of injection current on the laser spectrum. A recorder trace is shown in Fig. 5.10 which corresponds to a current of 0.8 amperes peak. At the repetition rate of 200 pulses per second and a pulse duration of 3 microseconds, the primary effect of the current increase was to increase the output radiant energy by increasing the linewidth and secondarily the height. The peak position does not change to any extent. These two effects are shown in Fig. 5.11 for one of the modes. The current pulse duration and amplitude change the peak position such a small amount that it is not a good method for tuning the laser wavelength.

Increase in temperature decreases the bandgap of the semiconductor and the band of emitted radiation shifts to longer wavelength. This effect may be observed in Figs. 5.12, 5.13 and 5.14, which correspond to three values of heater current. With no heater current the emission is in the spectral band 10763.60 to 10797.75 Å. A heater current of 0.5 amperes increases the temperature of the diode, and the emission shifts to the region 10780.7 to 10808.4 Å. With 1.0 amperes of heater current, the diode emission has moved to the region 10789.2 to 10840.4 Å, which includes the helium absorption wavelength of 10830 Å.

A second effect of temperature is the alteration of a given peak within the band. With no heater current there is a peak at 10791 Å. At 0.5 amperes of heater current, the temperature rise in the diode caused this peak to shift to 10793 Å and the amplitude to decrease. At 1.0 ampere this peak has shifted to 10796 Å and the peak has further decreased in value.

Fig. 5.15 shows the shift in angstroms of a peak as a function of temperature. Temperature change permits tuning of the laser peak wavelength over a considerable wavelength region.

E. External cavity to semiconductor diode laser

One technique for augmenting one oscillation mode of the diode laser and suppressing the other modes involves use of an external cavity. An external cavity consisting of a diffraction grating and coupling optics is shown in Fig. 5.16. The light from one side of the laser is made parallel by the lens and is directed upon a 1180 lines/mm grating. The wavelength of the reflected light depends upon the orientation of the grating. The reflected light re-enters the diode and stimulates it to emit all the radiation at this one wavelength. The diode radiation at the one wavelength is monitored with the spectrometer by collecting the radiation emitted from the other side of the diode laser.

The tests showed that the turnable external cavity permitted the concentration of radiant power into essentially a single line, which may be chosen among the various modes. It did not allow selection of any wavelength between two modes.

The results of a test with the external cavity are presented in Fig. 5.17. The three peaks labelled #1, #2, and #3 on the left were obtained with the grating blocked. The peaks on the right were recorded with the cavity operating and the spectrometer scanning in the opposite direction. The difference in the two #2 peak amplitudes represents a factor of 33.

There was concern in the experiment corresponding to Fig. 5.17 that possibly some of the radiation reflected by the grating was entering the

spectrometer directly. In order to eliminate this possibility a dove prism was inserted between the Dewar and the spectrometer entrance slit. The results of an experiment with dove prism in place (Fig. 5.18) show that the gain in amplitude is a real effect.

F. Absorption of laser radiation

If the diode laser is to be useful as a radiation source for NMR pumping of helium, it must be tunable to the exact wavelength of a helium absorption line. In the experiment to demonstrate absorption of laser radiation, a helium absorption cell was placed in the optical path between the laser and the spectrometer entrance slit. The spectrometer was set at the wavelength of one of the absorption lines. The wavelength of the laser emission was tuned, by increasing the diode temperature, through the diode emission peaks. When the peak was passed the heater was turned off and the diode temperature was decreased until the emission again passed through the peak (See Fig. 5.19). This step was done (a) with the absorption cell excited (so that absorption is possible) and (b) with the cell unexcited. The two peaks on the right correspond to the cell excited, and the two peaks on the left correspond to the cell unexcited. The large fraction of absorption is apparent.

SECTION 6

OPTICAL MONITORING OF POLARIZED ^{4}He METASTABLE ATOMS WITH SEMICONDUCTOR DIODE LASER RADIATION

A. Objective of experiment

The interest in semiconductor diode laser derives from their possible use as replacements for helium lamps in optically pumped helium magnetic resonance device. An experiment has been designed to use a diode laser as the radiation source for monitoring ^{4}He metastable atoms which are polarized by a helium lamp. The low duty cycle (and hence low average power) of the experimental lasers available and the fact that the laser power is distributed in several modes of different wavelength eliminated the possibility of both optical pumping and optical monitoring with the laser. The objective of the experiment was to demonstrate that diode laser radiation can be successfully employed to monitor ^{4}He polarized metastable atoms.

B. Experimental setup

A block diagram of the laser monitoring experiment is shown in Fig. 6.1. The purpose of the ^{4}He lamp is to polarize the atoms of the cell along the magnetic field direction H_0. If we gradually change the value of H_0, a photodiode placed beneath the cell (not shown in Fig. 6.1) will indicate a signal as in Fig. 6.2. The maximum dip occurs at the resonance point $H_0 = \omega_0/\gamma_e$, where ω_0 is the frequency of the imposed oscillating magnetic field. The magnetic coils producing the oscillating field were driven by an oscillator at 1.2 MHz. In order to produce an AC photodiode signal H_0 was modulated at 90 Hz. The amplitude of the H_0 oscillation was chosen to maximize the 90 Hz photodiode signal (see Fig. 6.2).

Note that in Fig. 6.1 a component of the cell polarization along H_0 is visible to either a horizontal or vertical monitoring beam of radiation. The laser beam was directed horizontally through the cell for convenience. The laser was pulsed at a 21.51 KHz rate with a duty cycle of 1.05 percent. The photodiode signal (consisting of pulses and the 90 Hz envelope) was directed to a lock-in amplifier which extracted the 90 Hz signal.

C. Experiment result

Several experimental problems presented themselves when the attempt to find the laser monitoring was begun. One difficulty involved the low average radiant power available from the diode laser (about 0.03 mW compared to 1.5 mW for a lamp). The peak radiant power from the laser was about 2.90 mW, a respectable amount; however, the duty cycle is low (1.05 percent). In addition to the laser average power being small compared to a lamp, only about 6% of the radiation was absorbed by the cell (this may be compared to about 50% for lamp radiation). The low absorption can be attributed to the presence of several laser oscillation modes. This low value of average laser radiant power absorbed by the cell implied a low expected signal level.

Another factor which adversely affected the anticipated signal level was the magnetic environment in which the experiment was performed. Gradients in the magnetic field broadened the ^4He magnetic resonance linewidth by a factor of about four over its value in a gradient free region. This factor of four reduction in signal level was accepted for convenience reasons.

A chart recording trace of the laser monitoring signal is shown in Fig. 6.3. Several features of the trace require some comment. In order

to demonstrate the presence of a signal the laser beam was periodically blocked manually with a piece of cardboard. The times the laser beam was unobstructed are indicated at the top of Fig. 6.3. The RC filter on the output of the lock-in amplifier was set to a time constant of 3 seconds. The laser monitoring signal was easily visible while the laser beam was interrupted and the 1.2 MHz oscillating magnetic field was on (see Fig. 6.3). In order to check that the signal was indeed due to magnetic resonance of the cell atoms, the 1.2 MHz oscillator was turned off. As is apparent in Fig. 6.3 the signal did vanish when the RF field was turned off. The large transient spikes seen on the recorder trace are due to the step function change in photodiode current caused by interrupting the laser light beam. Compared to the photodiode current modulation caused by the polarized atoms the step function signal is very large. Part of this signal made its way through the lock-in amplifier and showed up as a spike.

One may draw several conclusions from the success in obtaining a magnetic resonance signal with laser monitoring:

1. Even with a very low laser radiant power a signal is obtained.
2. One can tune the laser with temperature control to match the laser emission wavelength (of one made) with a helium absorption line.
3. A sufficient fraction of the laser emission spectrum is in the helium absorption bandwidth to allow a signal.

These conclusions are encouraging when viewed in the light of future semiconductor lasers which the literature suggests may be made continuous and single mode.

SECTION 7

SUMMARY

The following statements sumarize the results of the investigation.

1. Polarization levels and relaxation rates for ^4He have been found as a function of cell discharge level, cell size and lamp radiation power. (Section 2)

2. Polarization rates and longitudinal and transverse relaxation rates for ^3He have been found as functions of cell discharge level and magnetic field gradient. (Section 3)

3. Simultaneous magnetic resonance of ^3He and ^4He in the same cell has been accomplished. The ^3He resonance amplitude and linewidth agree with predictions of a theory which treats a system of coupled ^3He and ^4He precessing species. (Section 4)

4. Measurements of the characteristics of experimental semiconductor diode lasers indicate that the laser radiation may be tuned by temperature control to coincide (in part) with a helium absorption line. The diode lasers may be forced to oscillate in essentially one axial made by use of an external cavity. (Section 5)

5. Optical monitoring of polarized ^4He atoms with semiconductor diode laser radiation has been accomplished in a ^4He magnetic resonance experiment. (Section 6)

The results of Sections 2 and 3 allow one to develop mathematical models of the polarization and (in part) the relaxation processes for ^4He and ^3He. Such models will be useful in estimating helium gyro

performance. The importance of the simultaneous resonance of ^3He and ^4He (Section 4) in a cell containing a ^3He-^4He mixture derives from the possible application of this effect in a NMR gyro. The use of the semiconductor diode laser as an optical pumping radiation source is attractive because of large potential sensitivity improvement. The results of Sections 4 and 5 for low power experimental lasers are encouraging in that they demonstrate that the lasers have characteristics such that they can be used to monitor polarized atoms in a magnetic resonance device.

APPENDIX A

WORK STATEMENT

0001 1. RESEARCH

The Contractor shall furnish scientific effort during the period indicated in Paragraph 1.a. of Section H, together with all related services, facilities, supplies and materials, needed to conduct the following research:

a. Experimental and theoretical studies to assess the feasibility and potential of using optically pumped helium isotopes for NMR gyro application, including:

1. Design, construction and testing of He^3 and He^4 magnetic resonance measurement apparatus.

2. Measurements of polarization of He^4 and He^3 to establish polarization levels attained, at various cell pressures and discharge levels, when irradiated by He^3 and He^4 lamps.

3. Measurements of relaxation time of polarized $He^4(2^3S)$ atoms to determine collisional and radiation interaction effects.

4. Determination of the longitudinal and transverse relaxation times of polarized He^3 atoms for various cell discharge, pressure and wall conditions, including the effect of a magnetic field gradient.

b. Investigation of the suitability of semi-conductor lasers for NMR optical pumping: dependence of radiation spectrum on injection current, temperature and on application of an external resonator.

c. Exploration of techniques for tuning the laser wavelength on appropriate lines of He^4 and He^3 absorption spectrum; of techniques for monitoring the polarized helium atoms employing a laser cross beam with pumping radiation either from a lamp or laser.

1. Research concerning NMR effects which relate to gyro operation, determination of operational trade offs, and parameters of optimal conditions.

REFERENCES

1. Fitzsimmons, W.A., L.L. Tankersley, and G.K. Walters, "Nature of Surface-Induced Nuclear-Spin Relaxation of Gaseous He^3", Phys. Rev. 179, 156 (1969).

2. Timsit, R.S., J.M. Daniels, and A.O. May, "Nuclear Relaxation of ^3He Gas on Various Solid Surfaces", Canadian Jour. Phys 49, 560 (1971).

3. Slocum, R.E. and B.I. Marton, "A Nuclear Free Precession Magnetometer using Optically Polarized He^3 Gas", IEEE Trans. Magnetics MAG-10, 528 (1974).

4. Slocum, R.E. and B.I. Marton, "Measurement of Weak Magnetic Fields Using Zero-Field Parametric Resonance in Optically Pumped He^4", IEEE Trans. Magnetics MAG-9, 221 (1973).

5. Pake, G.E. Paramagnetic Resonance. New York: W.A. Benjamin, Inc., 1962. p. 23.

6. Schearer, L.D. and G.K. Walters, "Nuclear Spin-Lattice Relaxation in the Presence of Magnetic-Field Gradients", Phys. Rev. 139, A1398 (1965).

7. Sugino, T., M. Wada, H. Shimizu, K. Itoh and I. Teramoto, "Terraced-Substrate GaAs-(GaAl) As Injection Lasers", Appl. Phys. Lett. 34, 270 (1979).

8. Nahory, R.E., M.A. Pollock, E.D. Beebe, J.C. De Winter, and R.W. Dixon, "Continuous Operation of 1.0 μm $GaAs_{1-x}Sb_xAl_yGa_{1-y}As_{1-x}Sb_x$ Double-Heterostructure Injection Lasers at Room Temperature", Appl. Phys. Lett. 28, 1 (1976).

9. Nuese, C.J., G.H. Olsen, M. Ettenberg, J.J. Garmon and T.J. Zamerowski, "CW Room-Temperature InGaAsInGaP 1.06 μ Lasers", Appl. Phys. Lett. 29, 12 (1976).

10. Wright, P.D., E.A. Rezek, and N. Holonyak, Jr., "Lattice Matching and Dislocation in LPE $In_{1-x}Ga_xP_{1-z}As_z$ - InP Heterojunctions", Jour. Crystal Growth 41, 254 (1977).

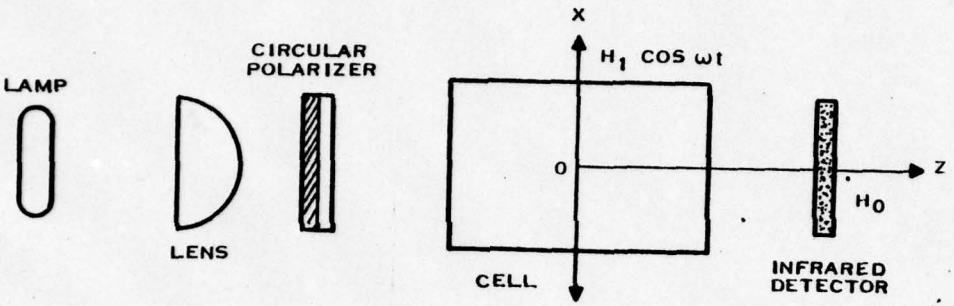

FIGURE 2.1 OPTICAL PUMPING MAGNETOMETER SENSOR SCHEMATIC.

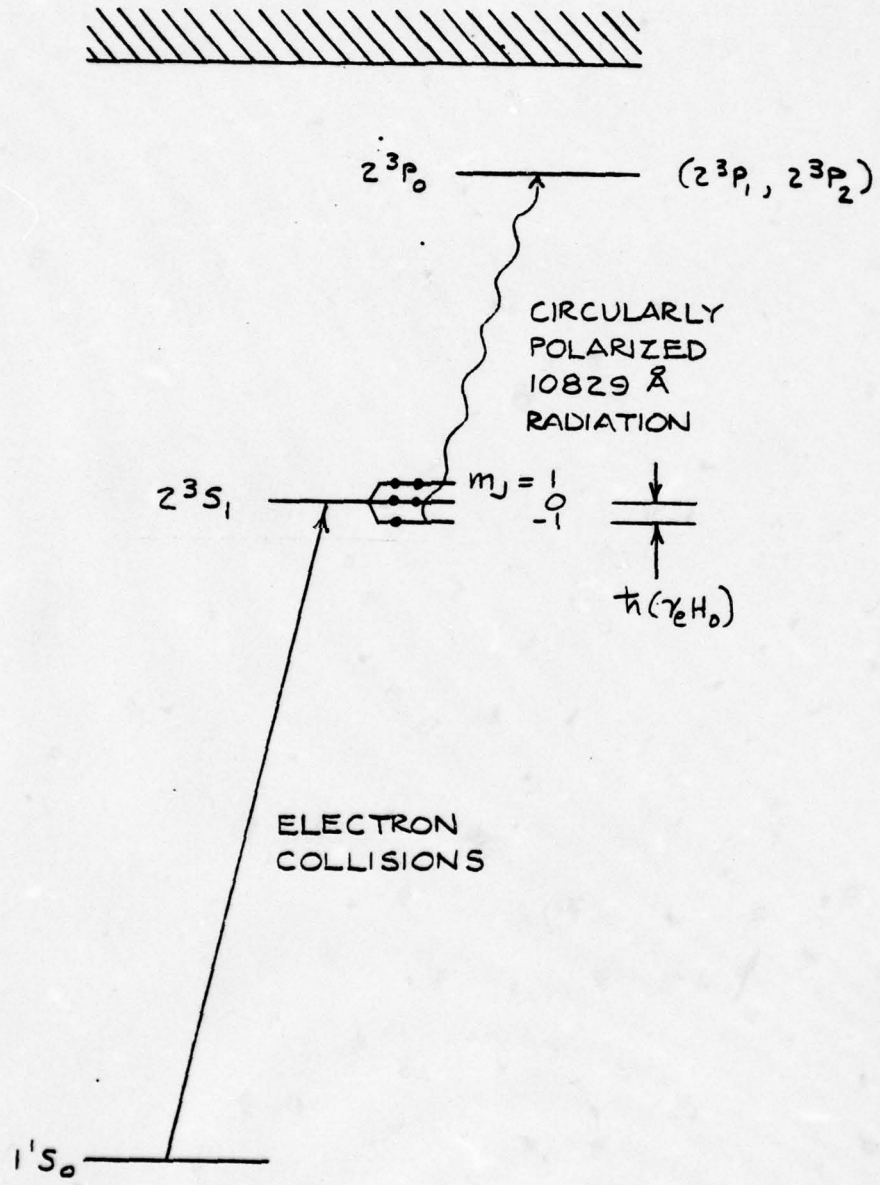

FIGURE 2.2 ^{4}He ENERGY LEVELS IMPORTANT IN ^{4}He OPTICAL PUMPING AND MAGNETIC RESONANCE.

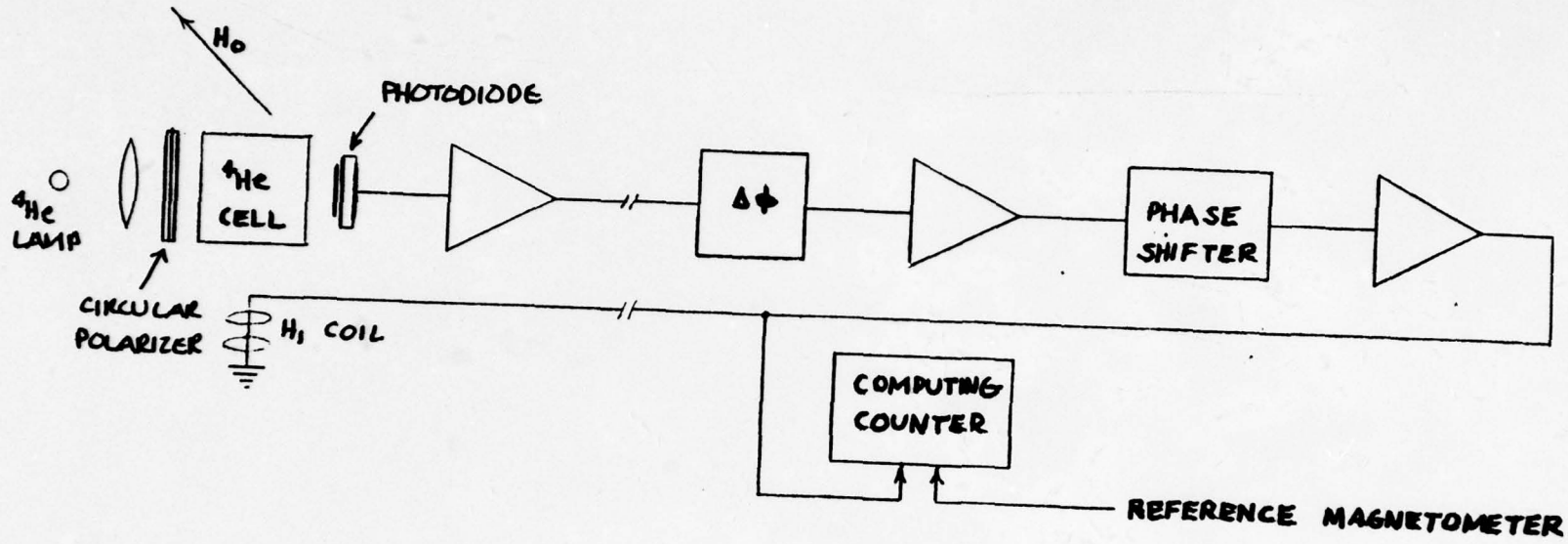

FIGURE 2.3 BLOCK DIAGRAM OF ^4He POLARIZATION AND RELAXATION EXPERIMENT.

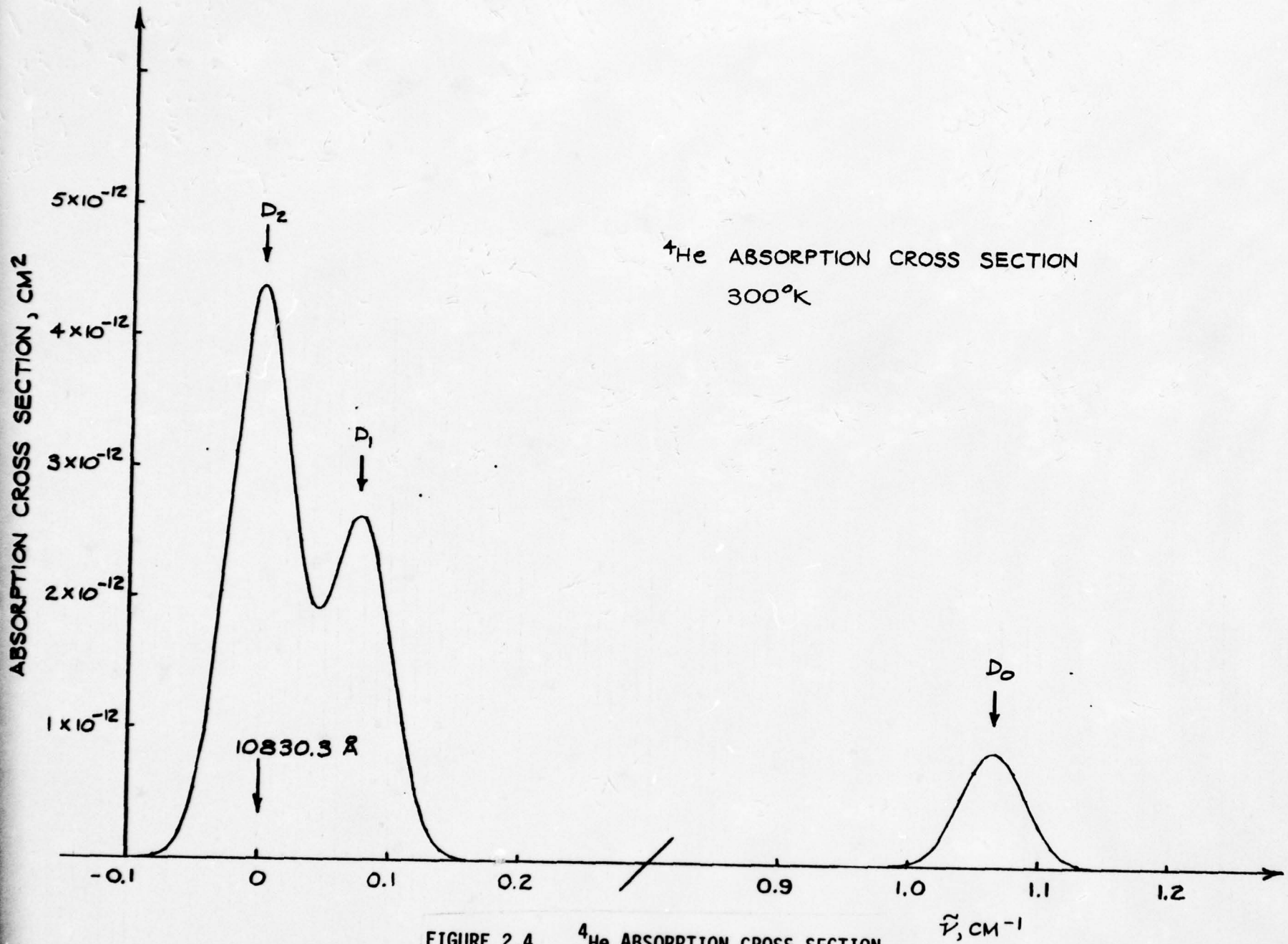

FIGURE 2.4 ^{4}He ABSORPTION CROSS SECTION VERSUS OPTICAL FREQUENCY.

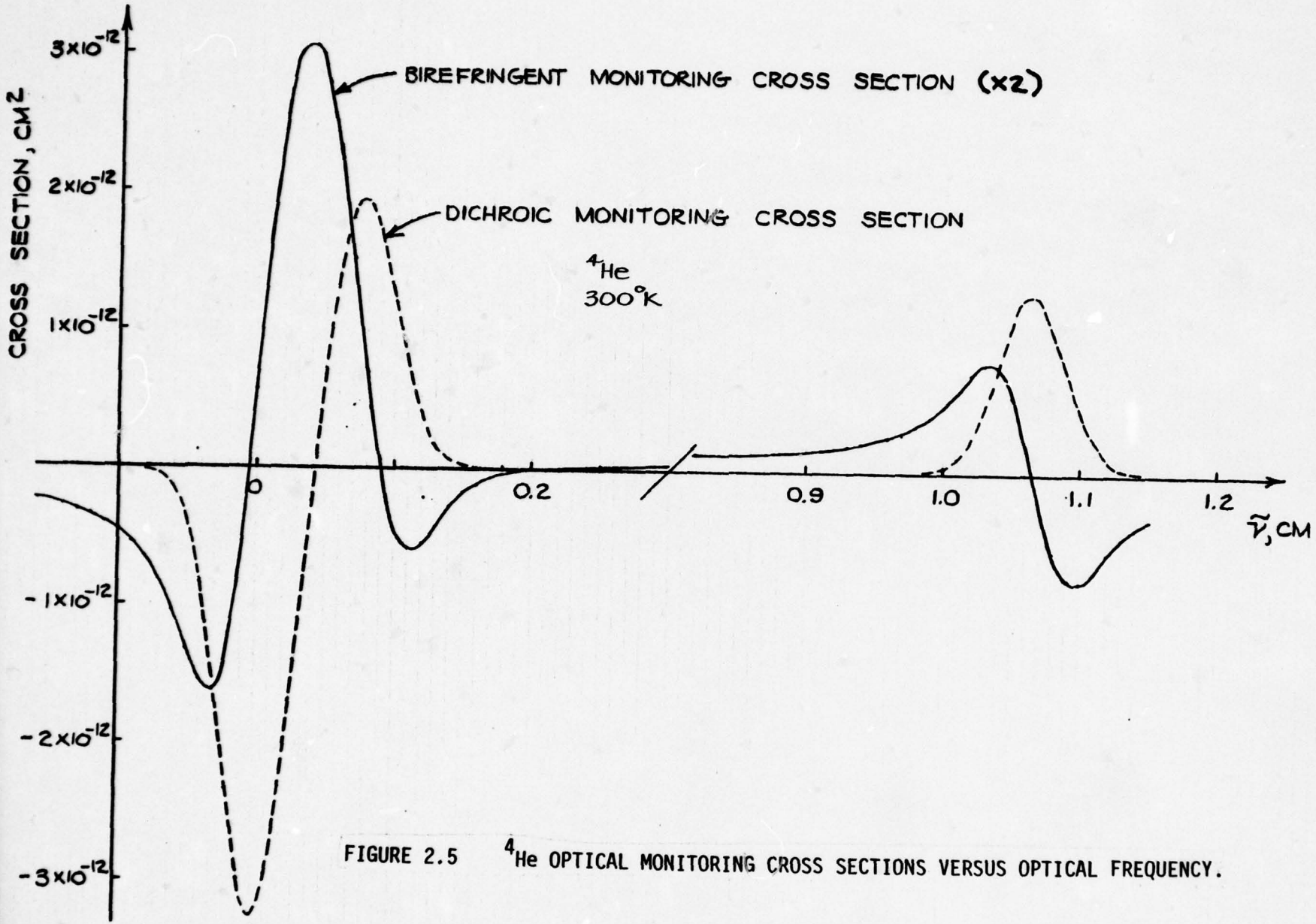

FIGURE 2.5 ^{4}He OPTICAL MONITORING CROSS SECTIONS VERSUS OPTICAL FREQUENCY.

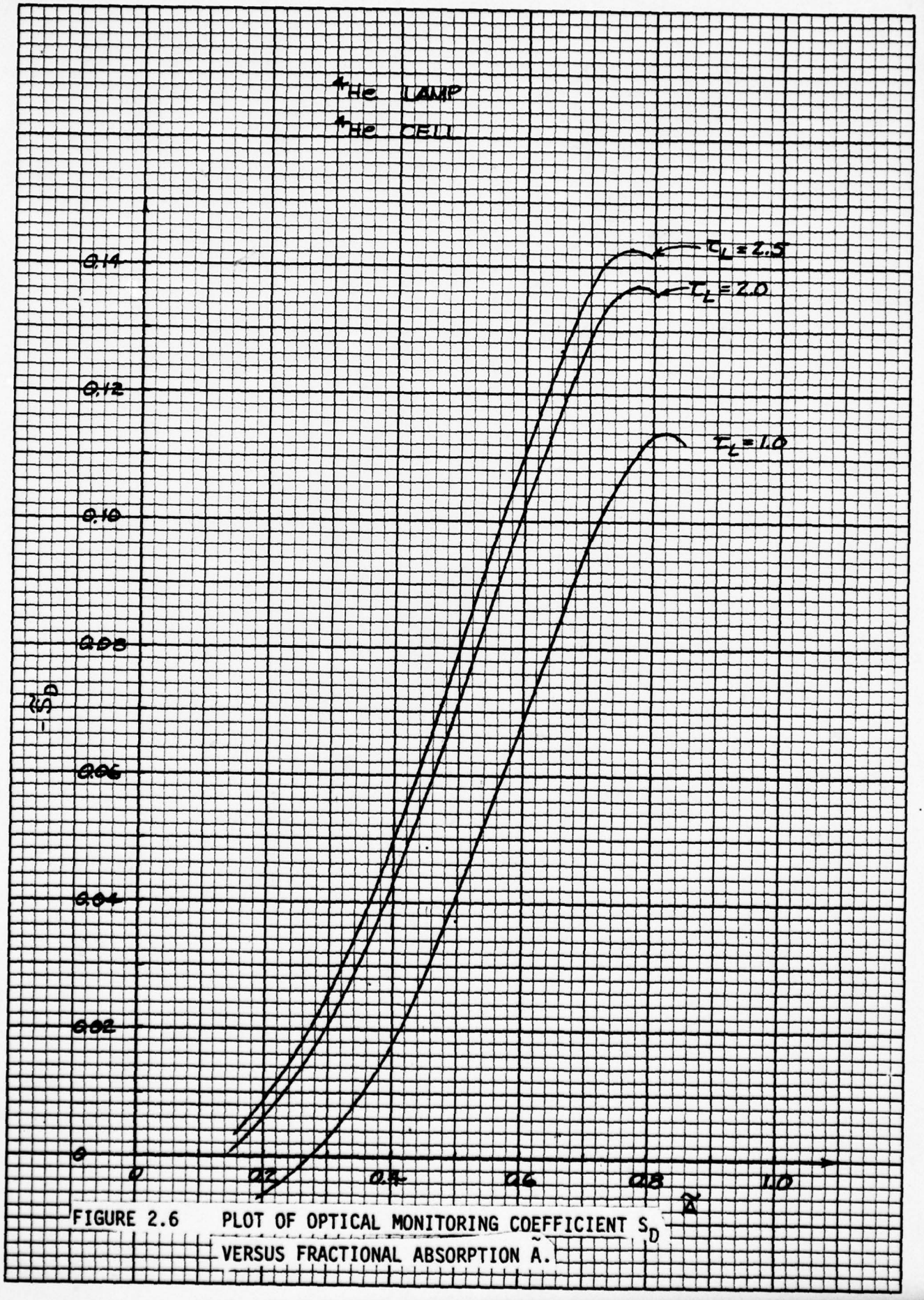

FIGURE 2.6 PLOT OF OPTICAL MONITORING COEFFICIENT S_D VERSUS FRACTIONAL ABSORPTION A.

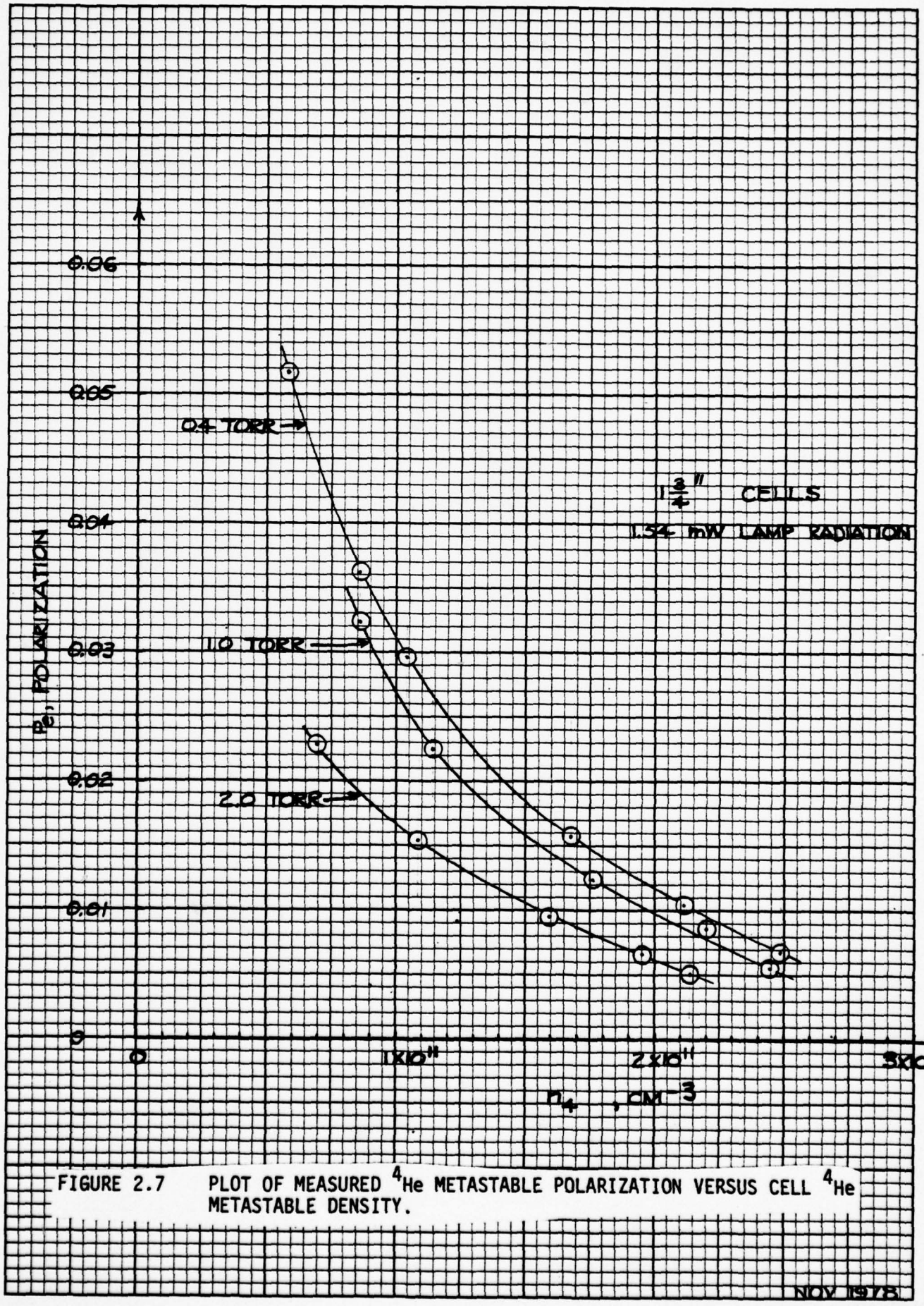

FIGURE 2.7 PLOT OF MEASURED ^{4}He METASTABLE POLARIZATION VERSUS CELL ^{4}He METASTABLE DENSITY.

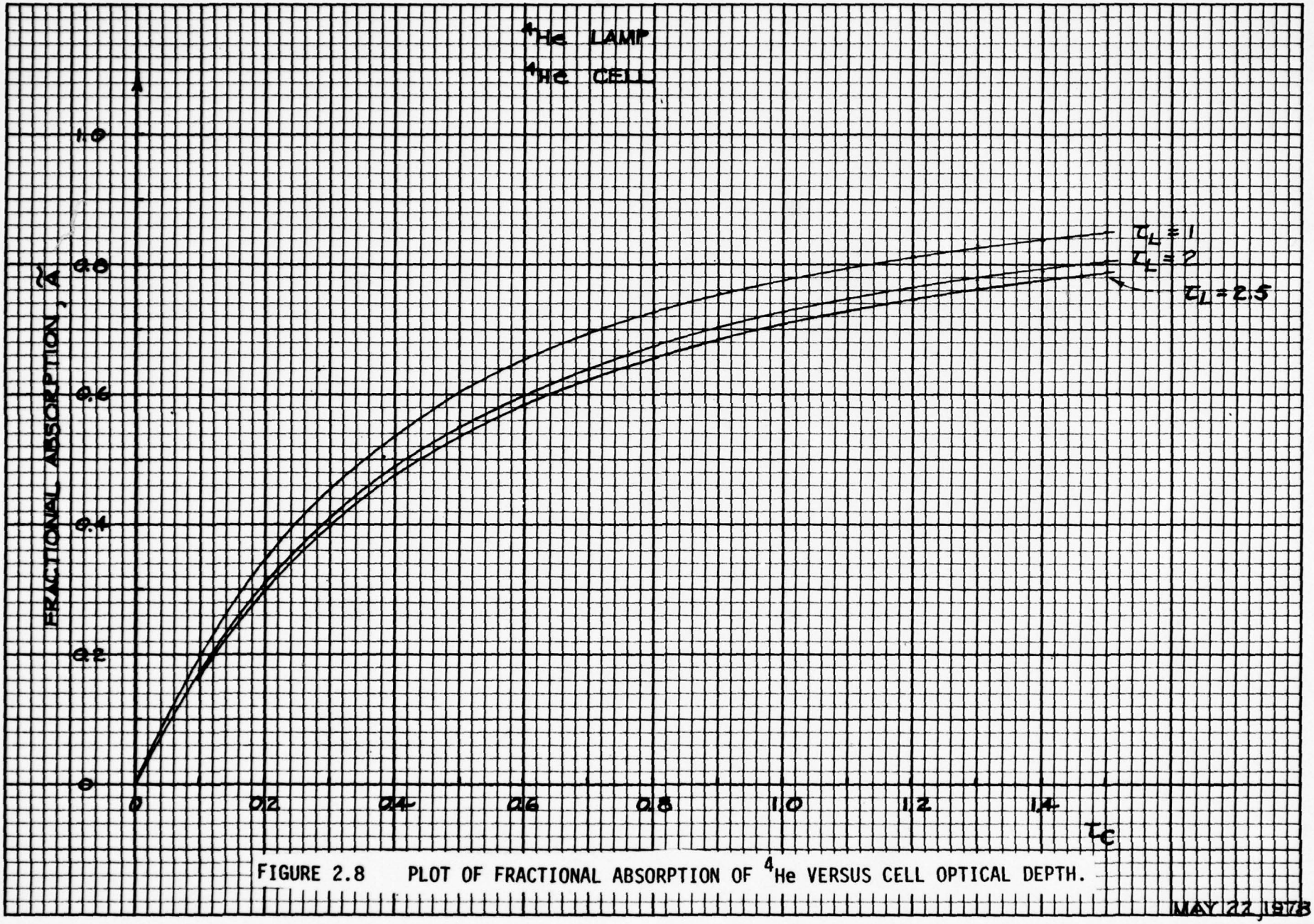

FIGURE 2.8 PLOT OF FRACTIONAL ABSORPTION OF ^{4}He VERSUS CELL OPTICAL DEPTH.

MAY 22, 1978

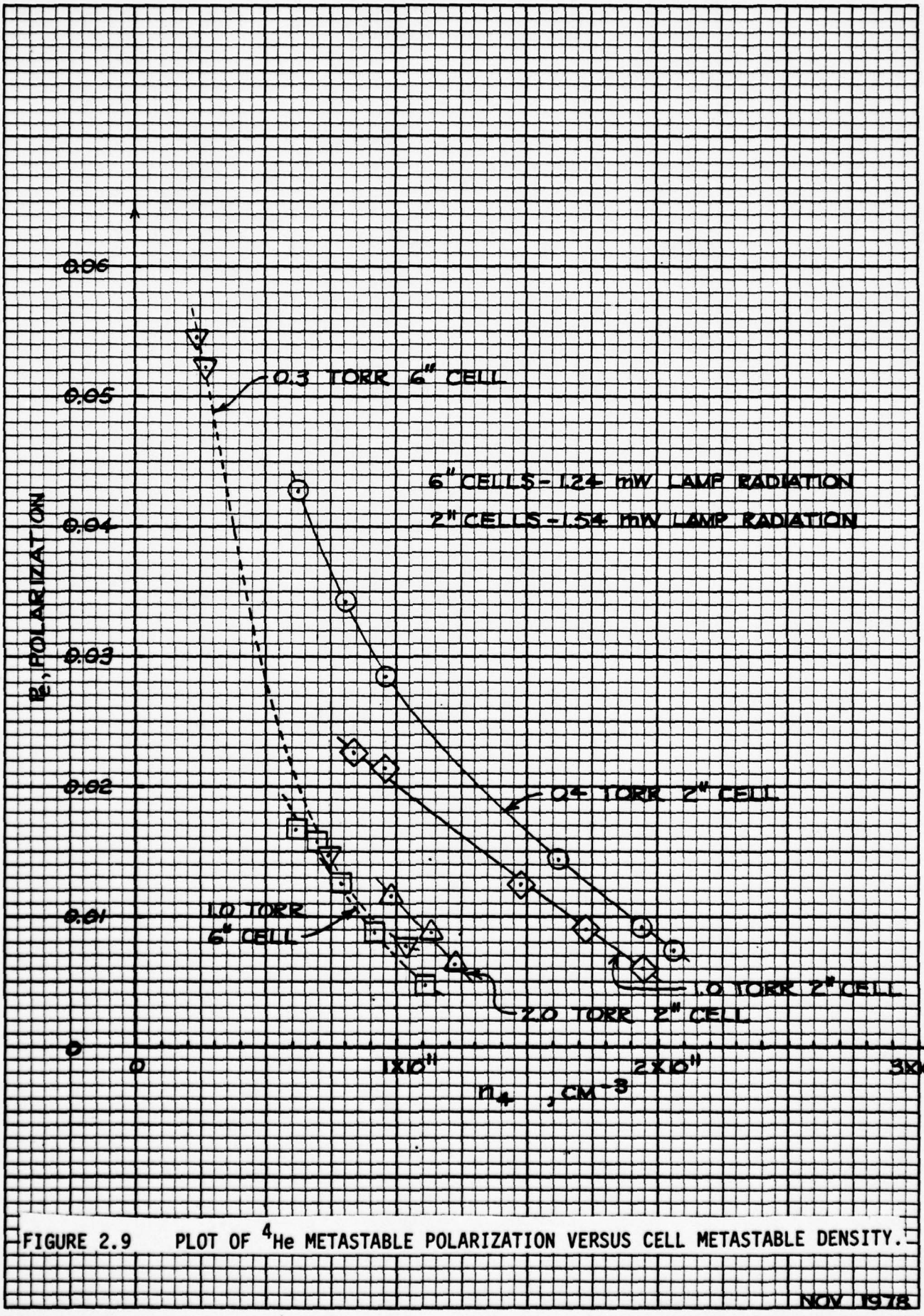

FIGURE 2.9 PLOT OF ^{4}He METASTABLE POLARIZATION VERSUS CELL METASTABLE DENSITY.

NOV 1978

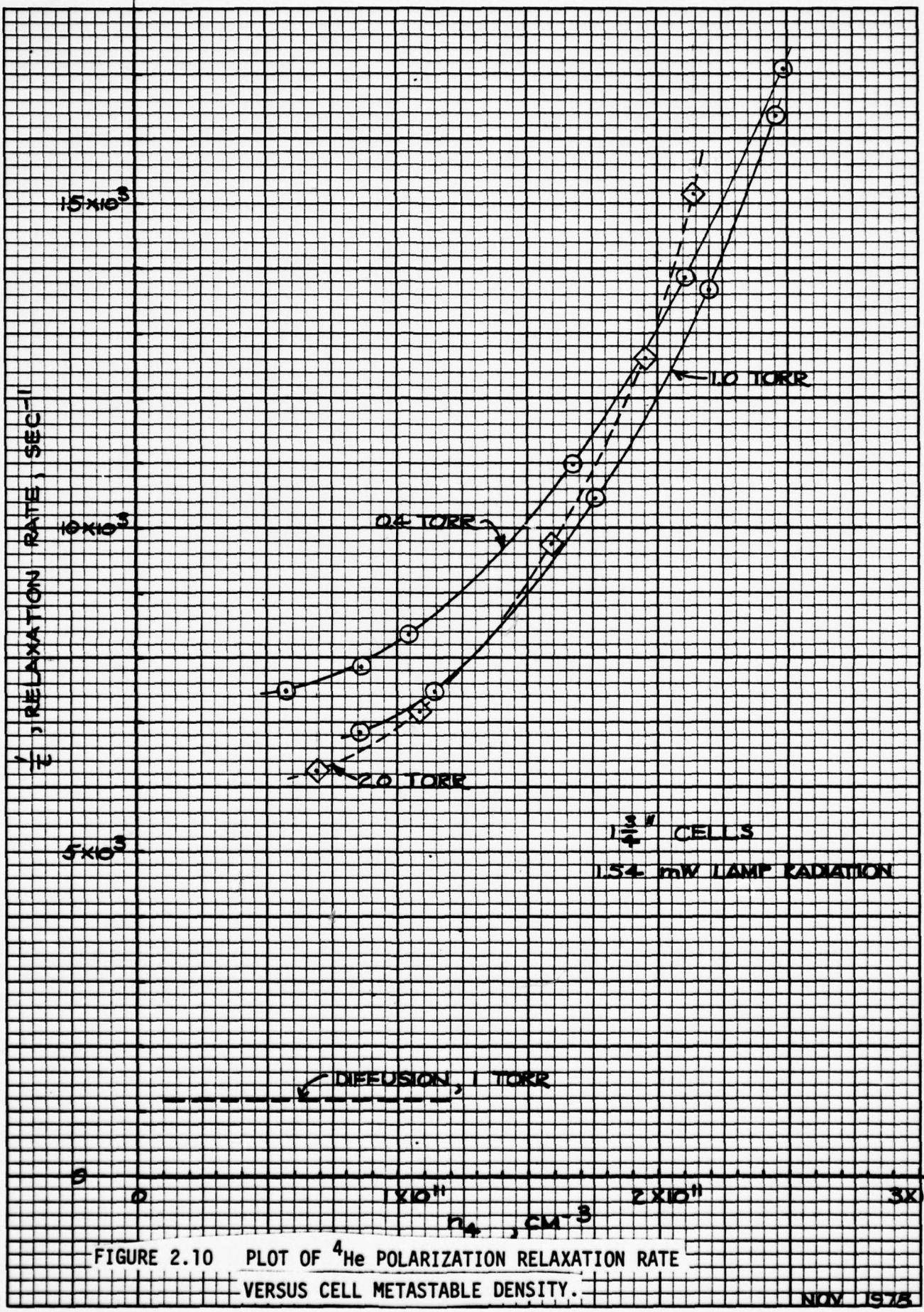

FIGURE 2.10 PLOT OF ^{4}He POLARIZATION RELAXATION RATE VERSUS CELL METASTABLE DENSITY.

NOV 1978

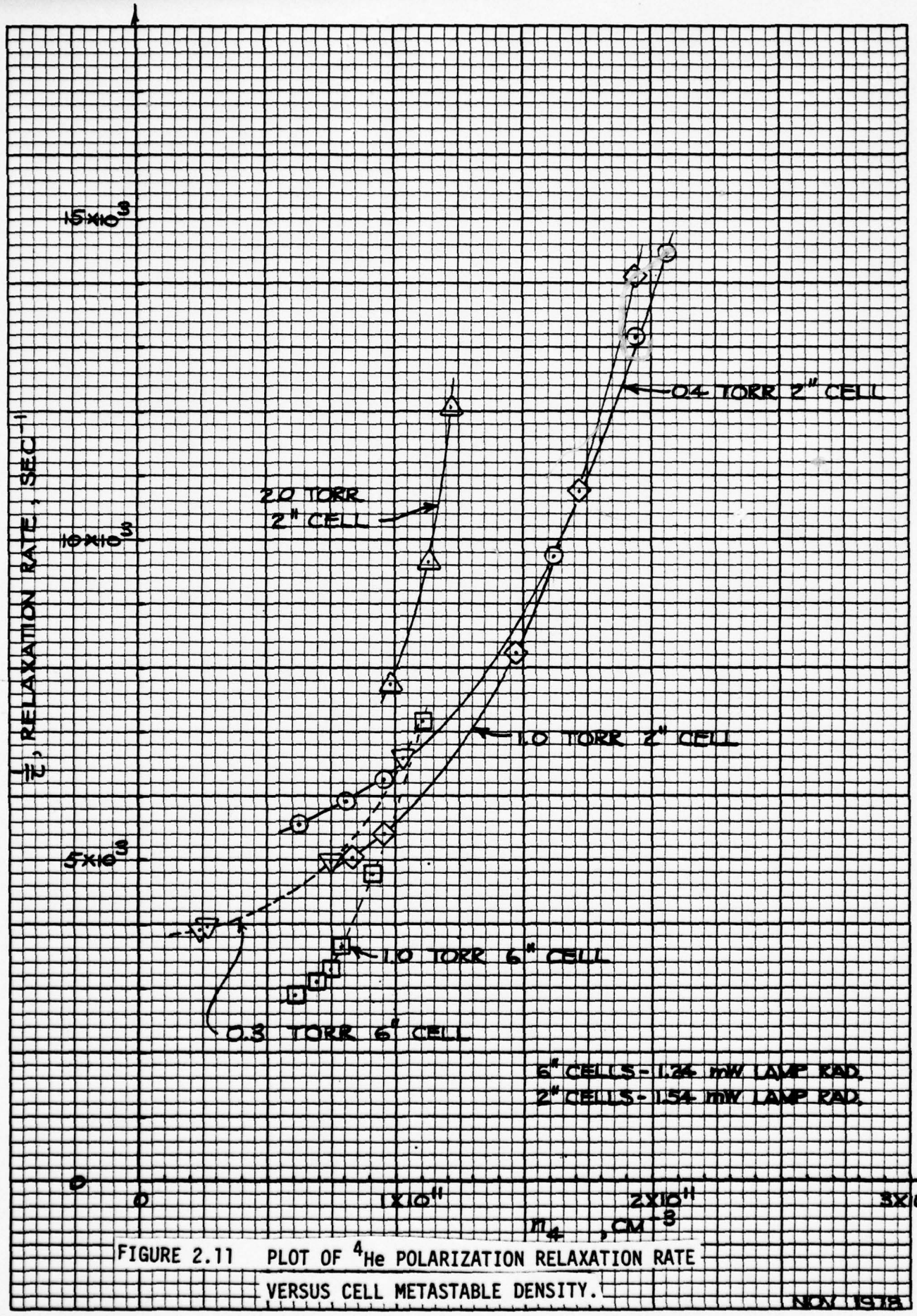

FIGURE 2.11 PLOT OF ^{4}He POLARIZATION RELAXATION RATE VERSUS CELL METASTABLE DENSITY.

NOV 1978

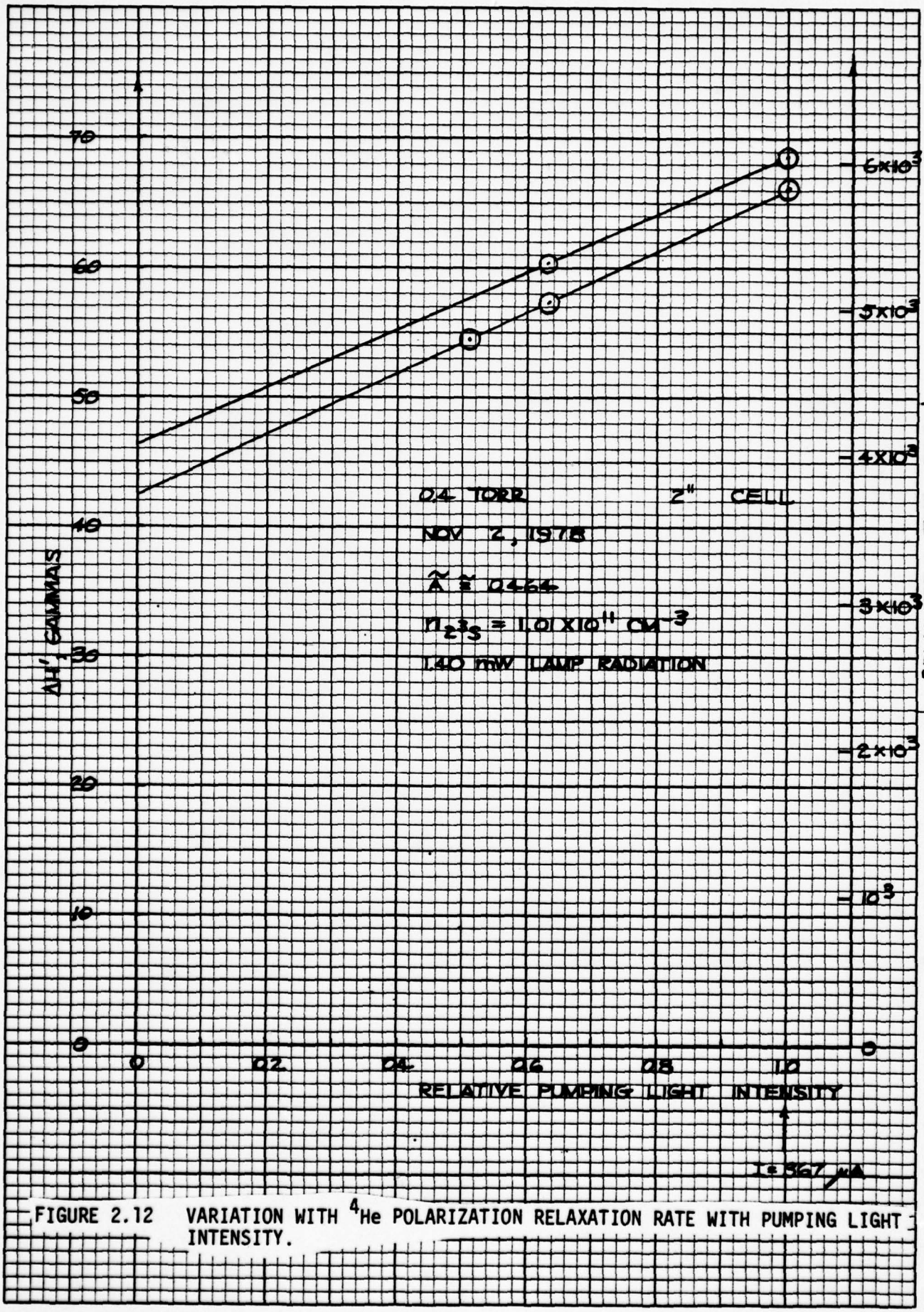

FIGURE 2.12 VARIATION WITH ^4He POLARIZATION RELAXATION RATE WITH PUMPING LIGHT INTENSITY.

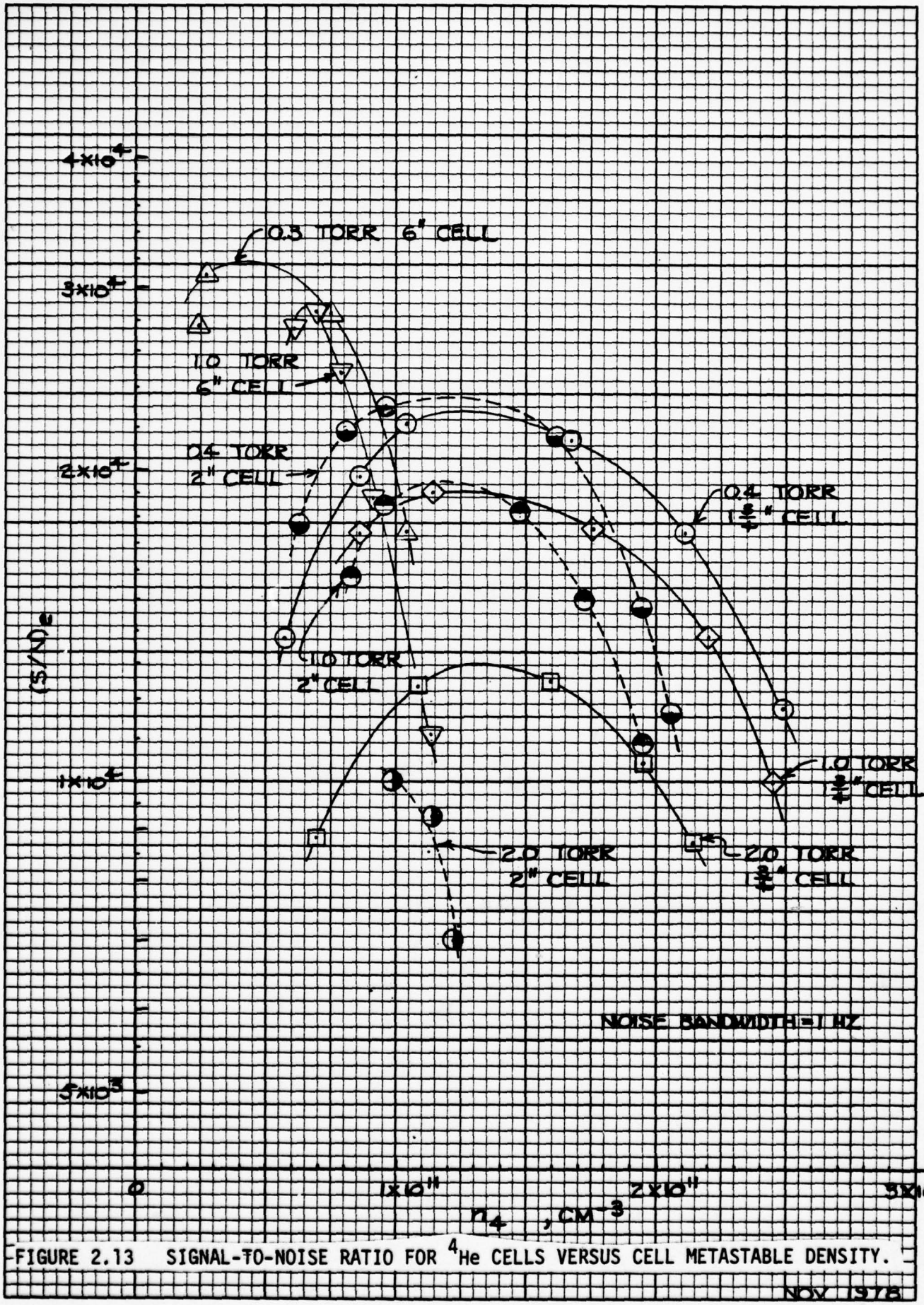

FIGURE 2.13 SIGNAL-TO-NOISE RATIO FOR ^{4}He CELLS VERSUS CELL METASTABLE DENSITY.

NOV 1978

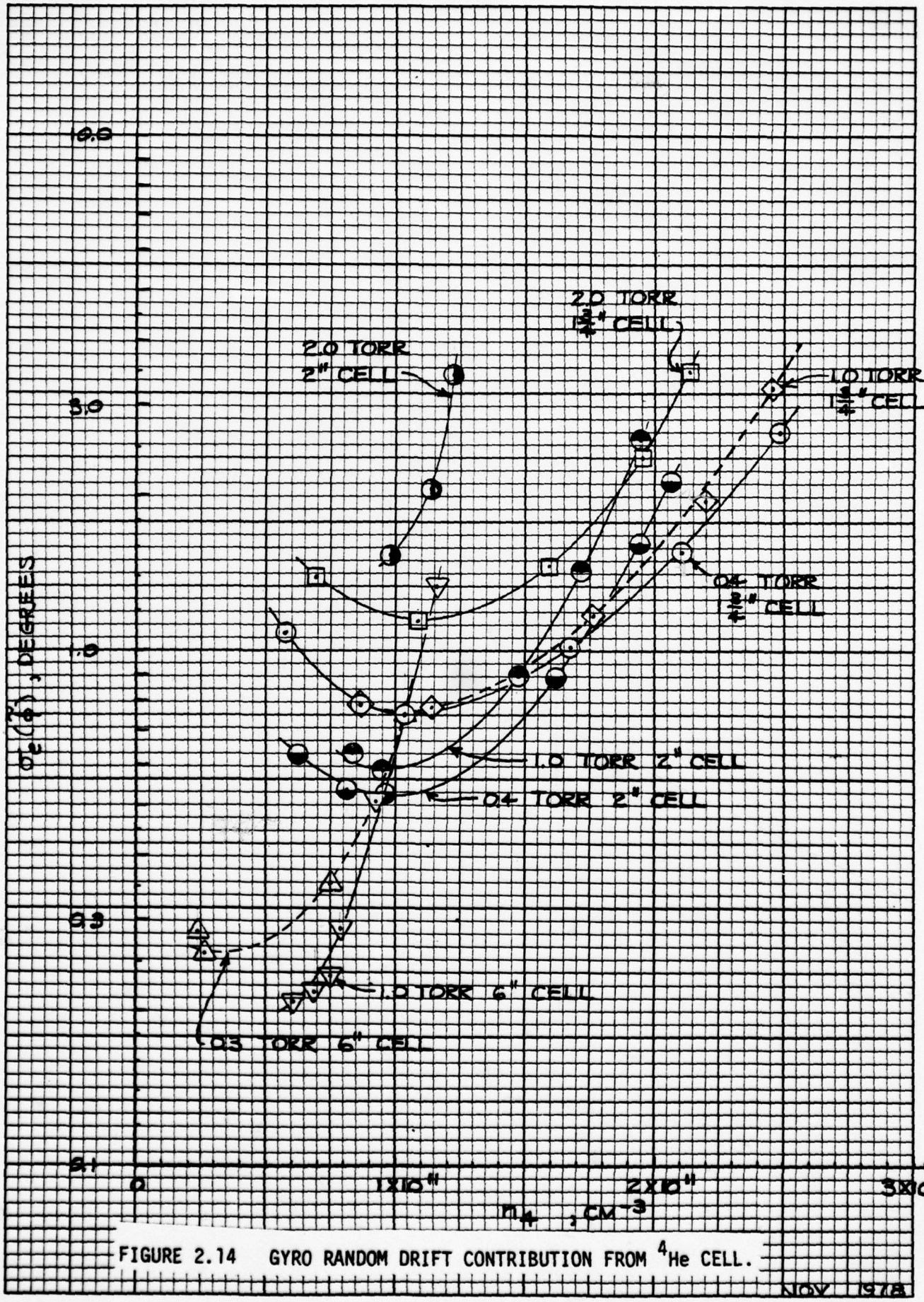

FIGURE 2.14 GYRO RANDOM DRIFT CONTRIBUTION FROM ^{4}He CELL.

NOV 1978

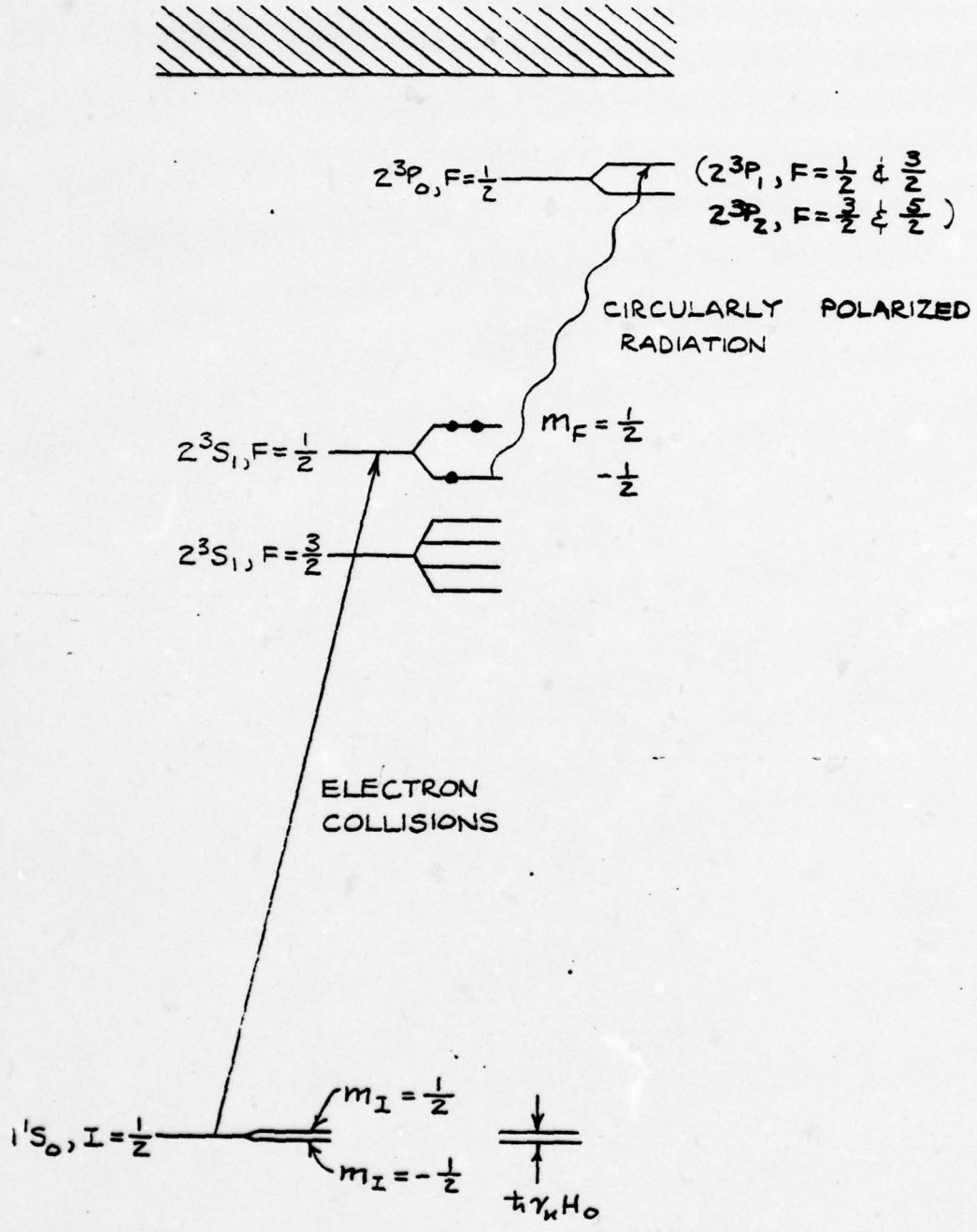

FIGURE 3.1 ^{3}He ENERGY LEVELS IMPORTANT IN ^{3}He OPTICAL PUMPING AND MAGNETIC RESONANCE.

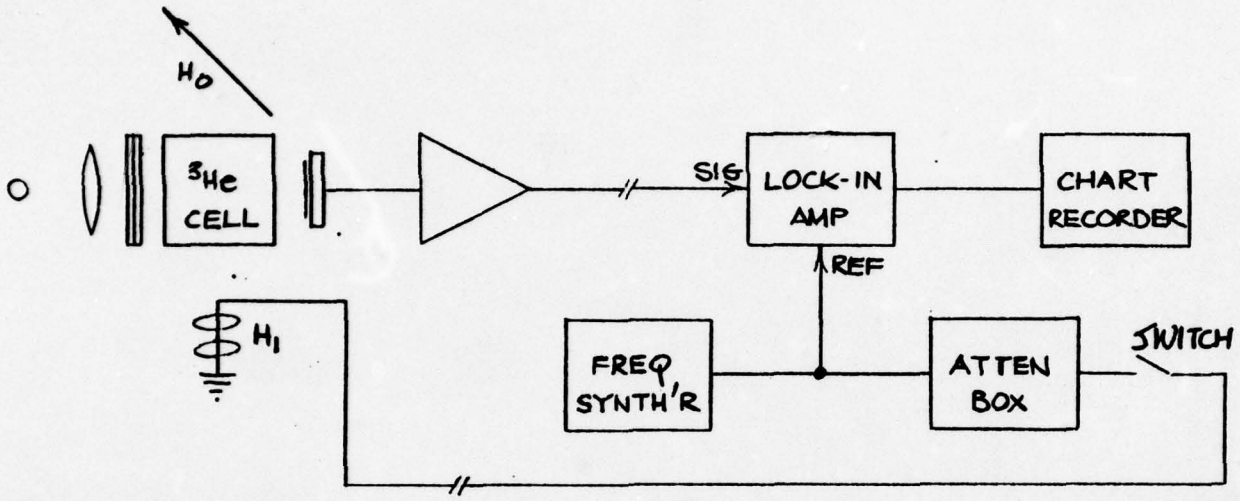

FIGURE 3.2 BLOCK DIAGRAM OF ^3He POLARIZATION AND RELAXATION EXPERIMENT.

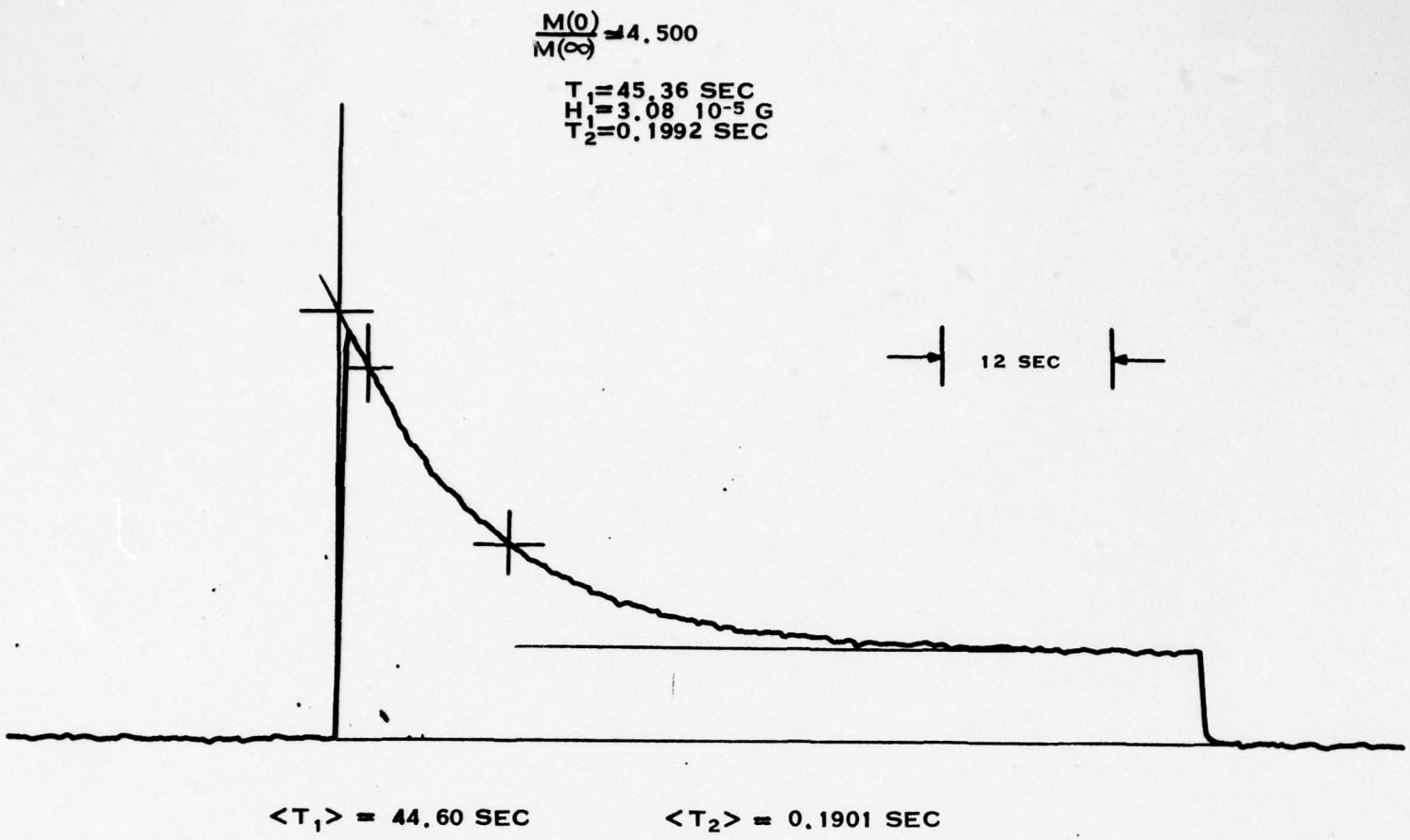

FIGURE 3.3 CHART RECORDER TRACE OF ^{3}He SIGNAL.

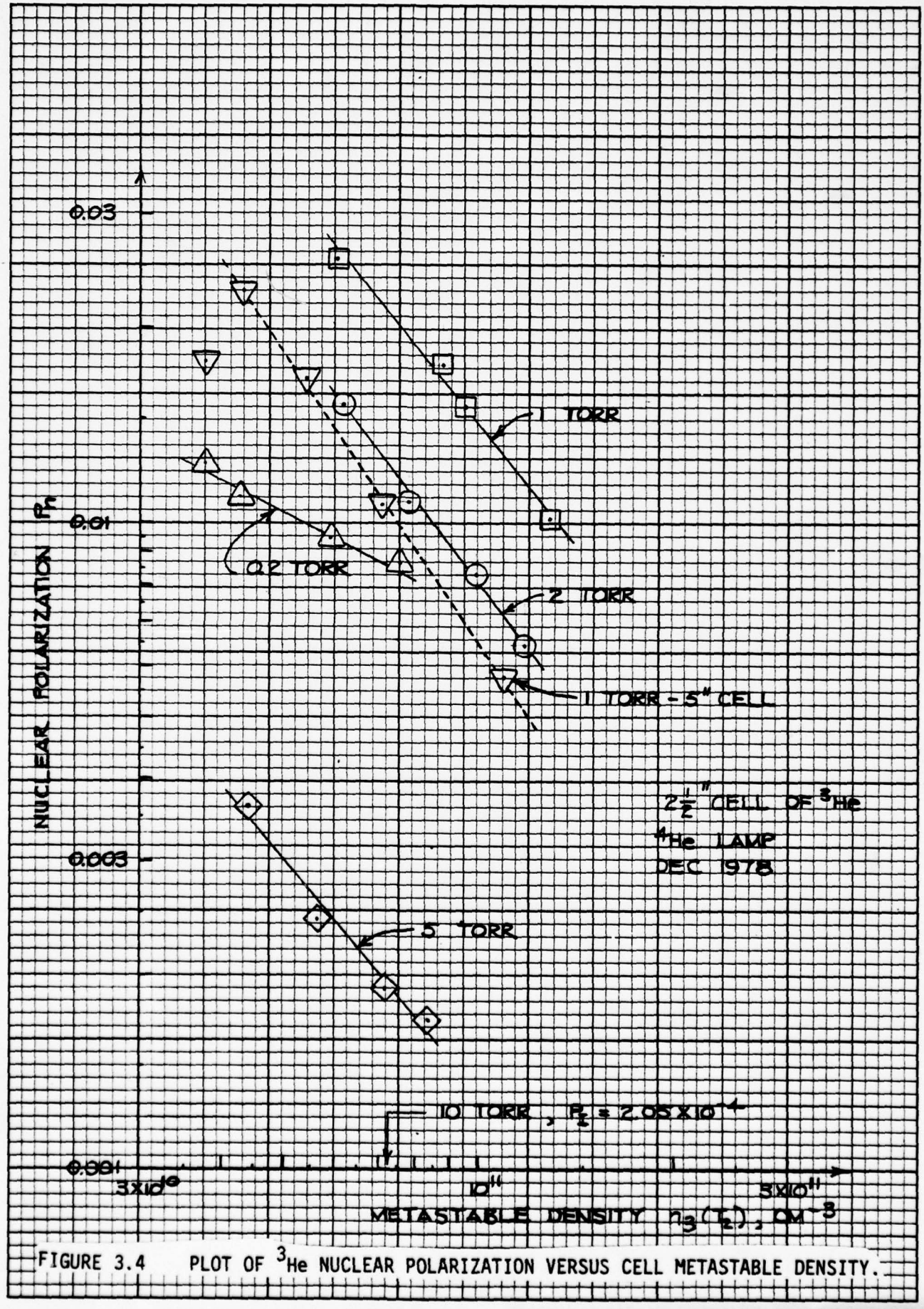

FIGURE 3.4 PLOT OF ^{3}He NUCLEAR POLARIZATION VERSUS CELL METASTABLE DENSITY.

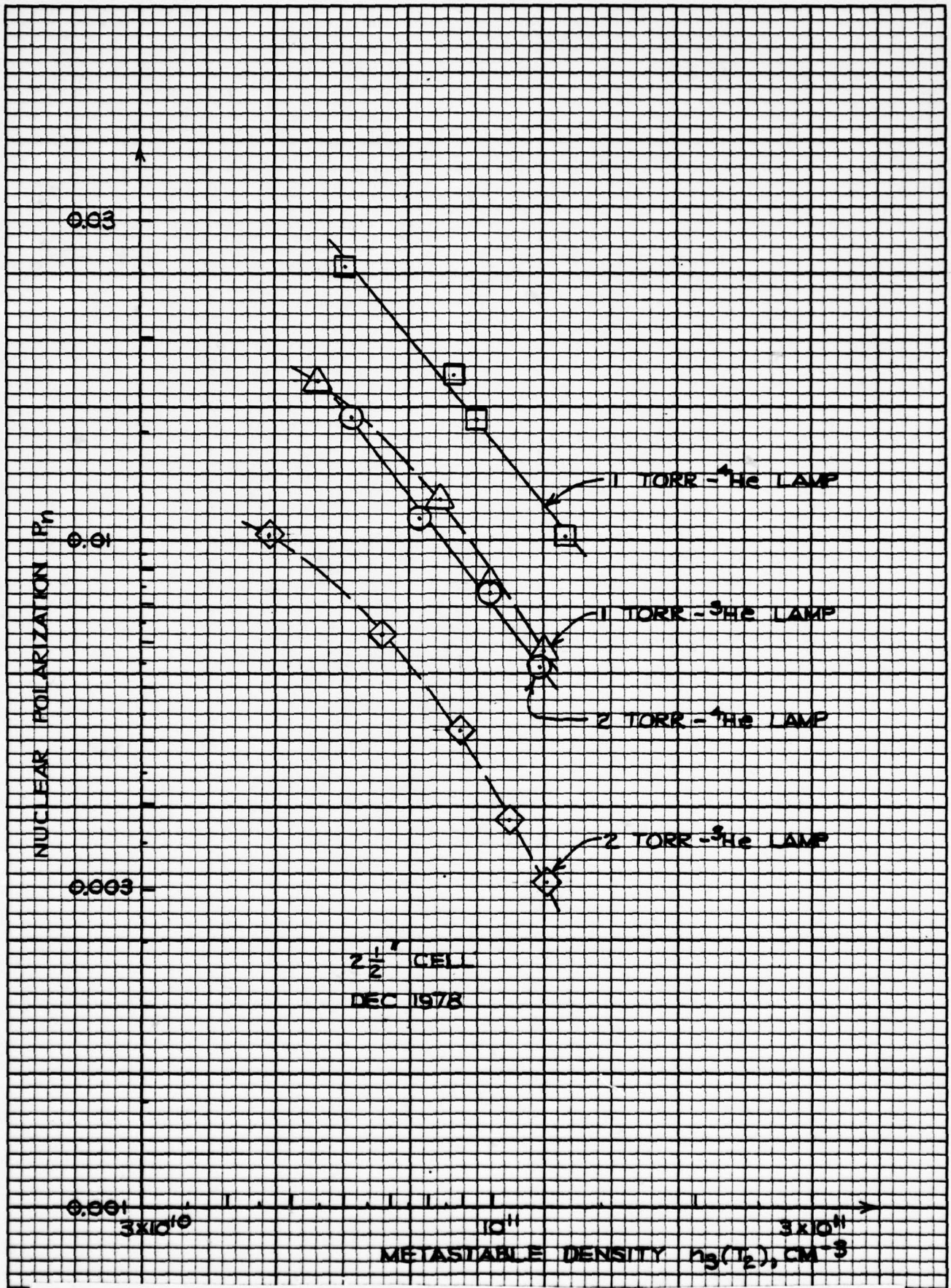

FIGURE 3.5 PLOT OF ^{3}He NUCLEAR POLARIZATION VERSUS CELL METASTABLE DENSITY.

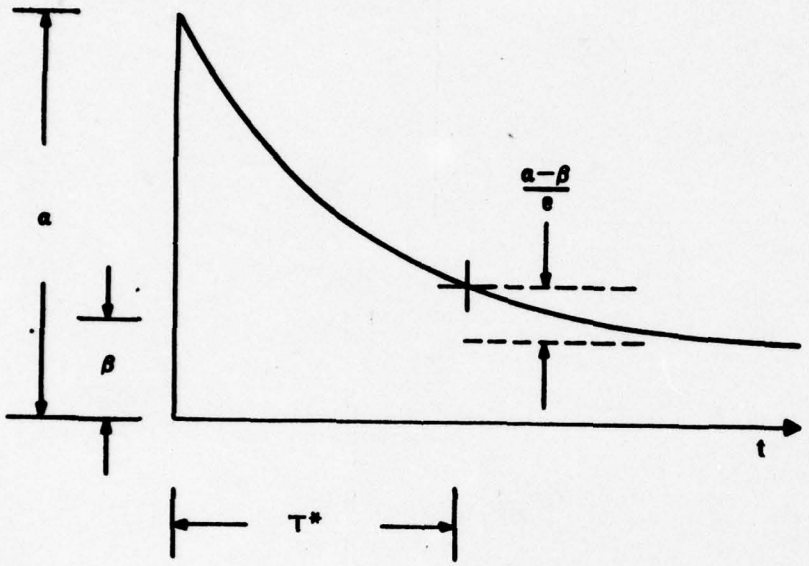

FIGURE 3.6 PARAMETERS CHARACTERIZING THE ^{3}He SIGNAL.

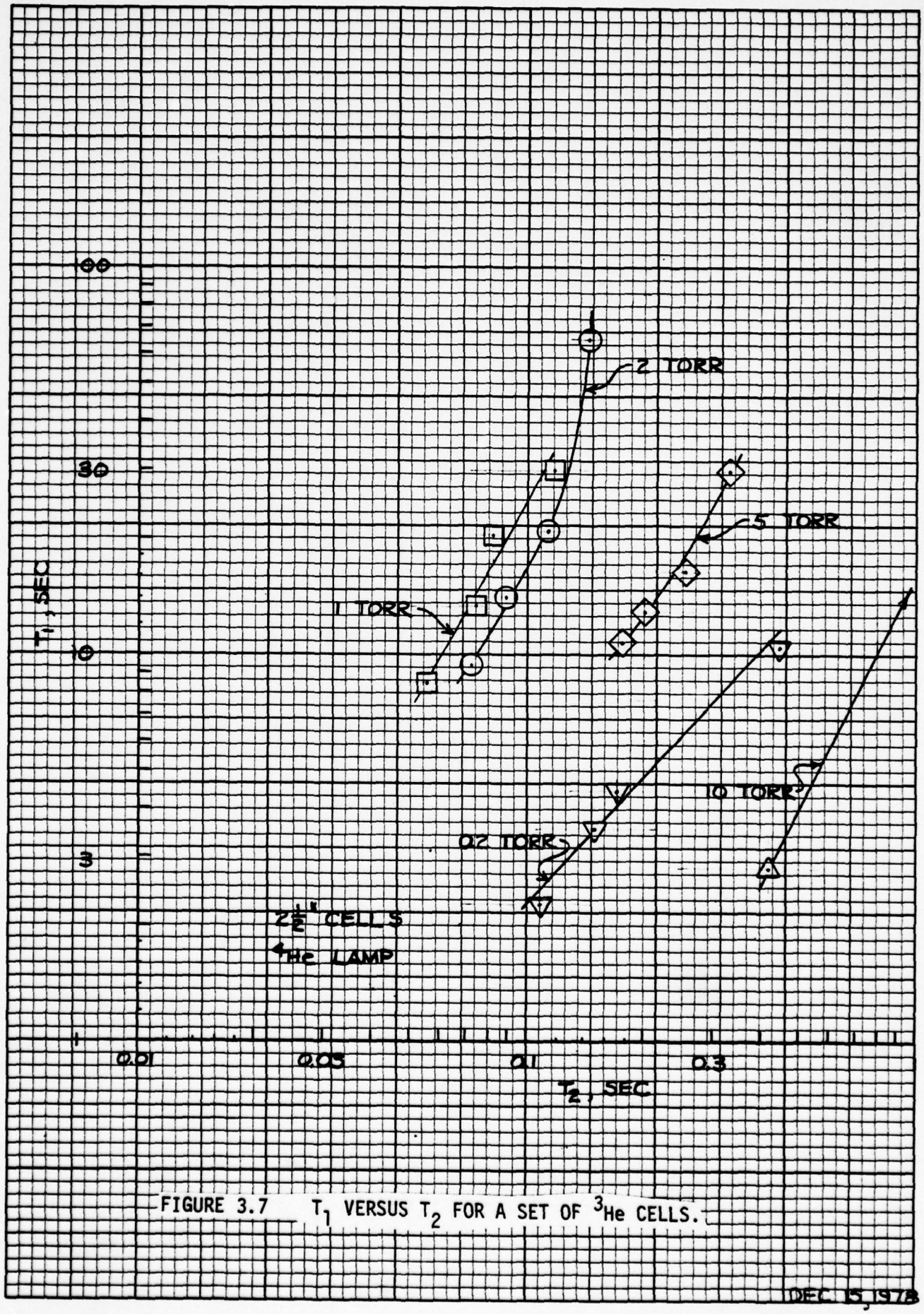

FIGURE 3.7 T_1 VERSUS T_2 FOR A SET OF ^{3}He CELLS.

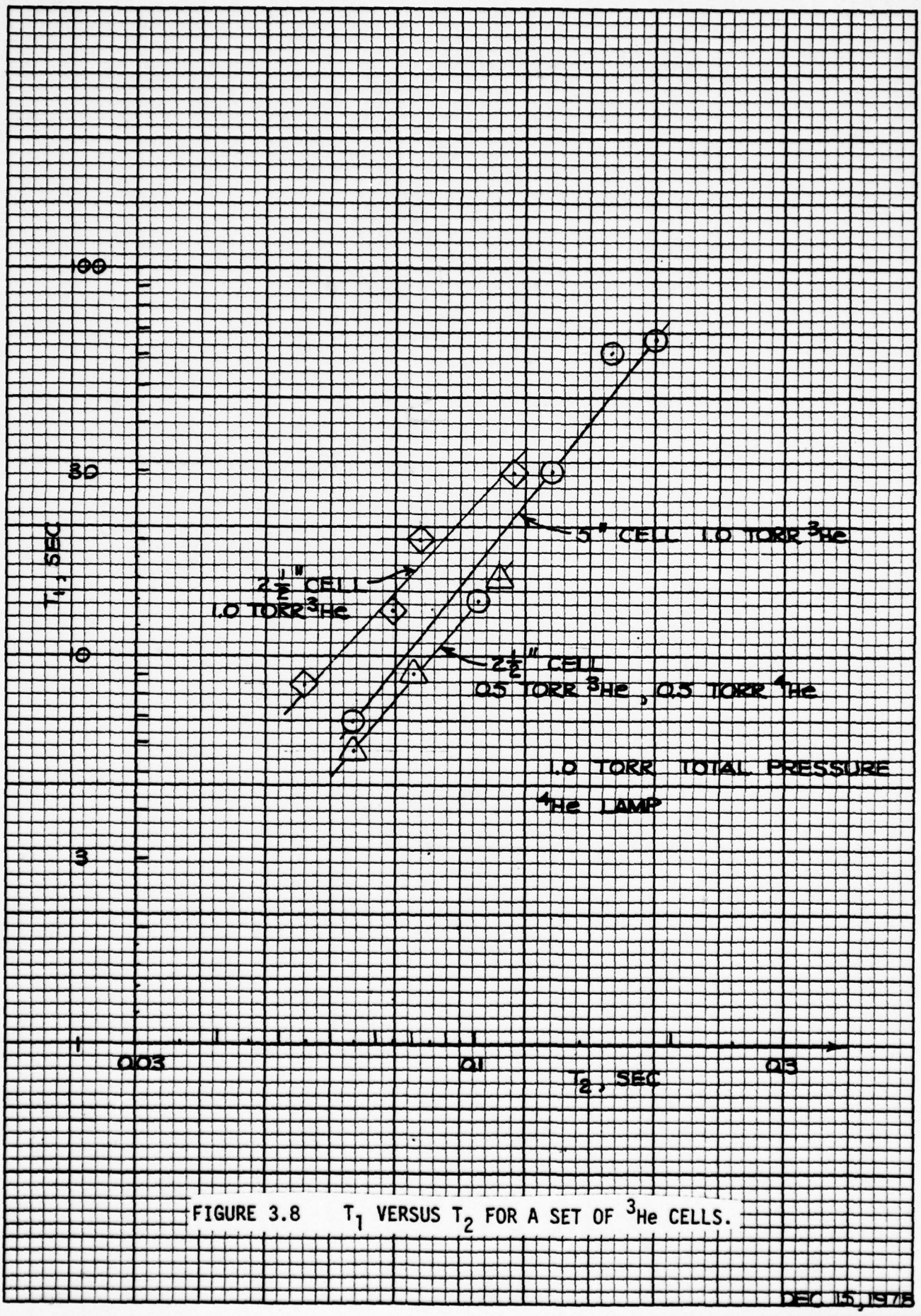

FIGURE 3.8 T_1 VERSUS T_2 FOR A SET OF ^{3}He CELLS.

DEC 15, 1978

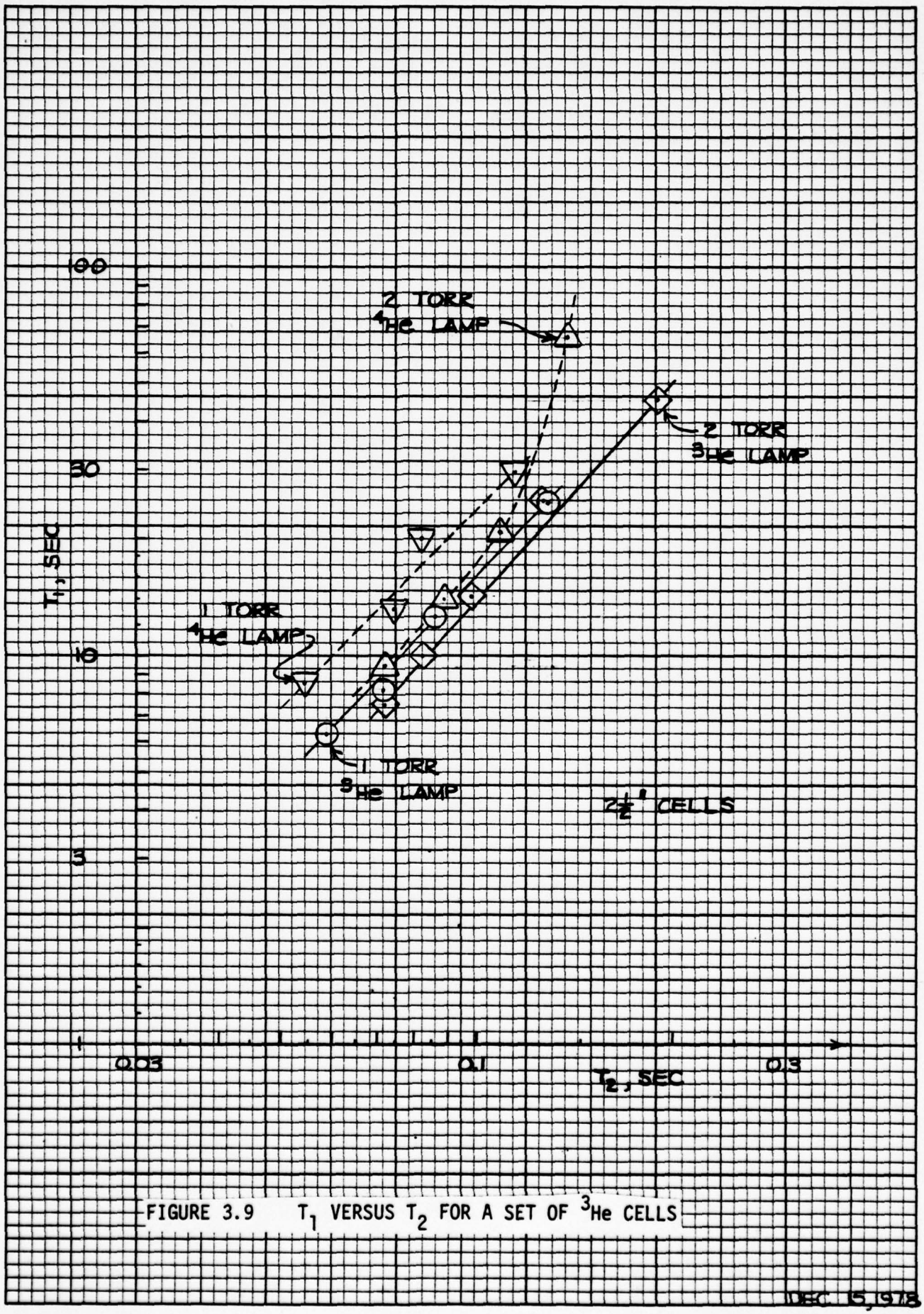

FIGURE 3.9 T_1 VERSUS T_2 FOR A SET OF ^{3}He CELLS

DEC. 15, 1978

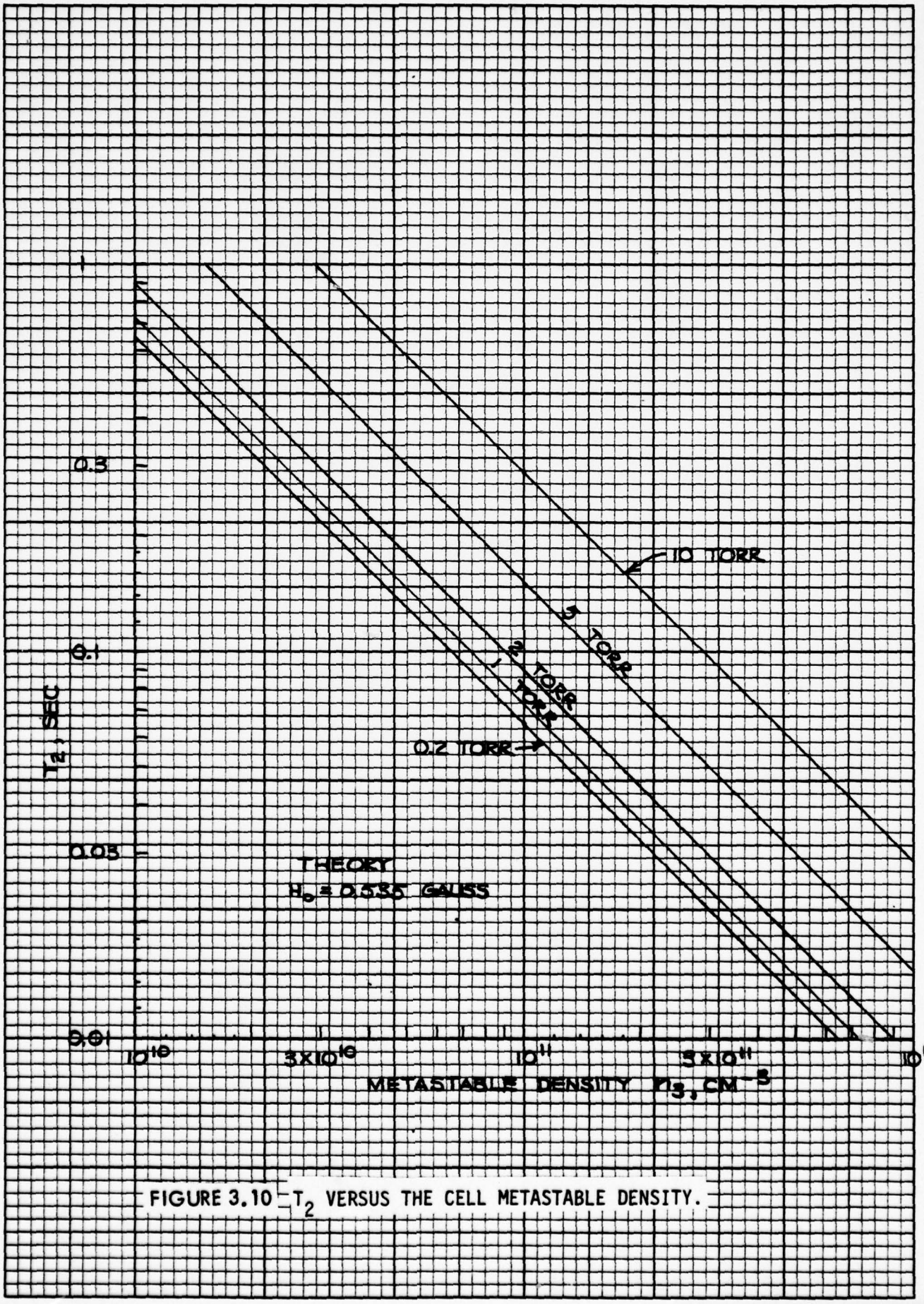

FIGURE 3.10 T_2 VERSUS THE CELL METASTABLE DENSITY.

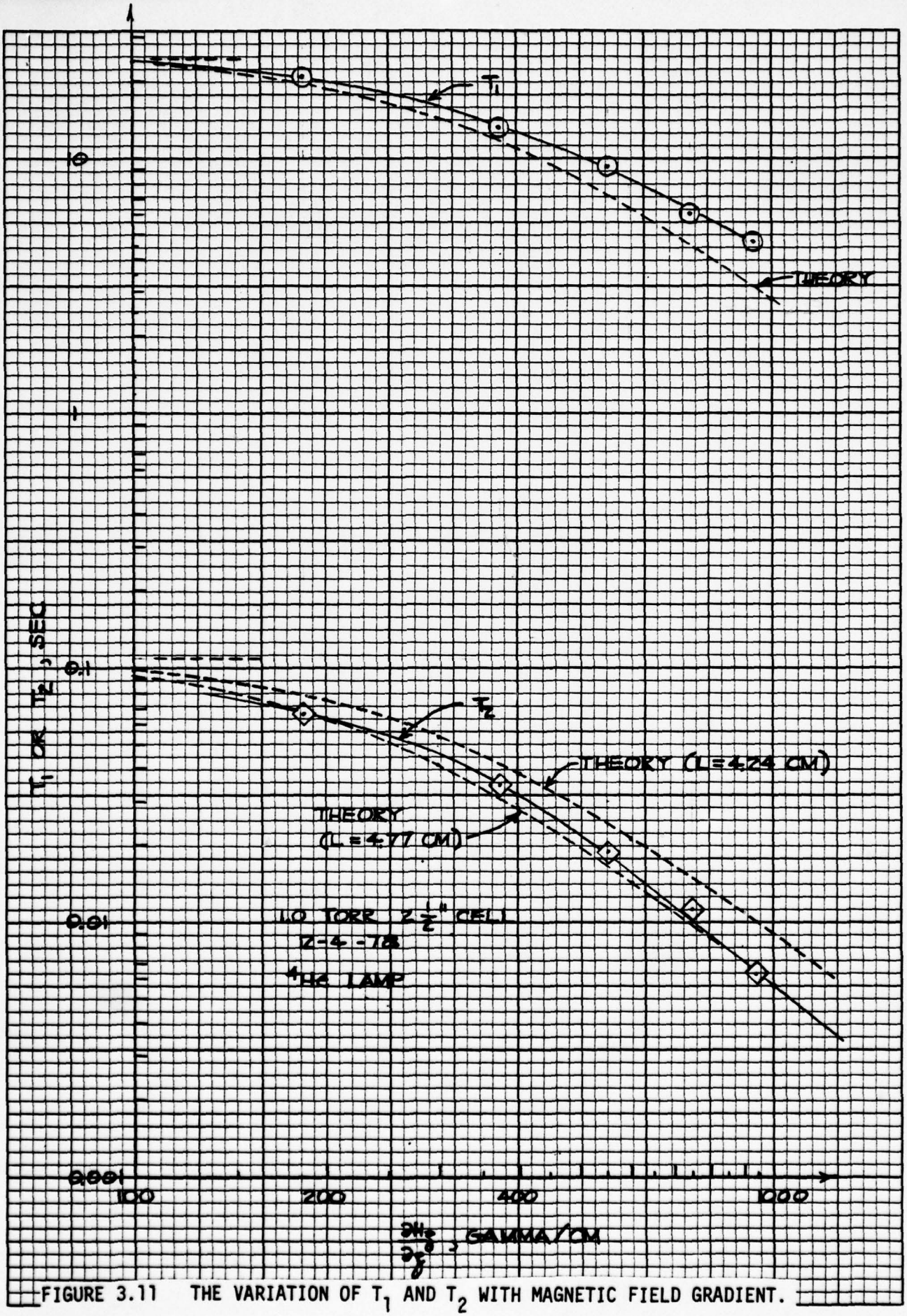

FIGURE 3.11 THE VARIATION OF T_1 AND T_2 WITH MAGNETIC FIELD GRADIENT.

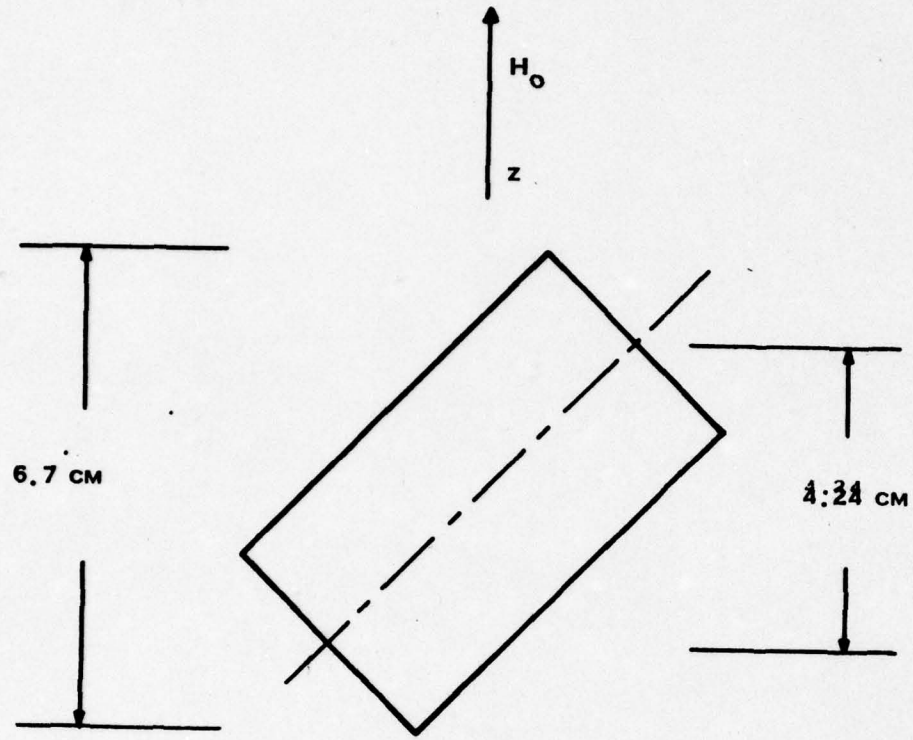

FIGURE 3.12 GEOMETRY OF ^{3}He CELL AND MAGNETIC FIELD.

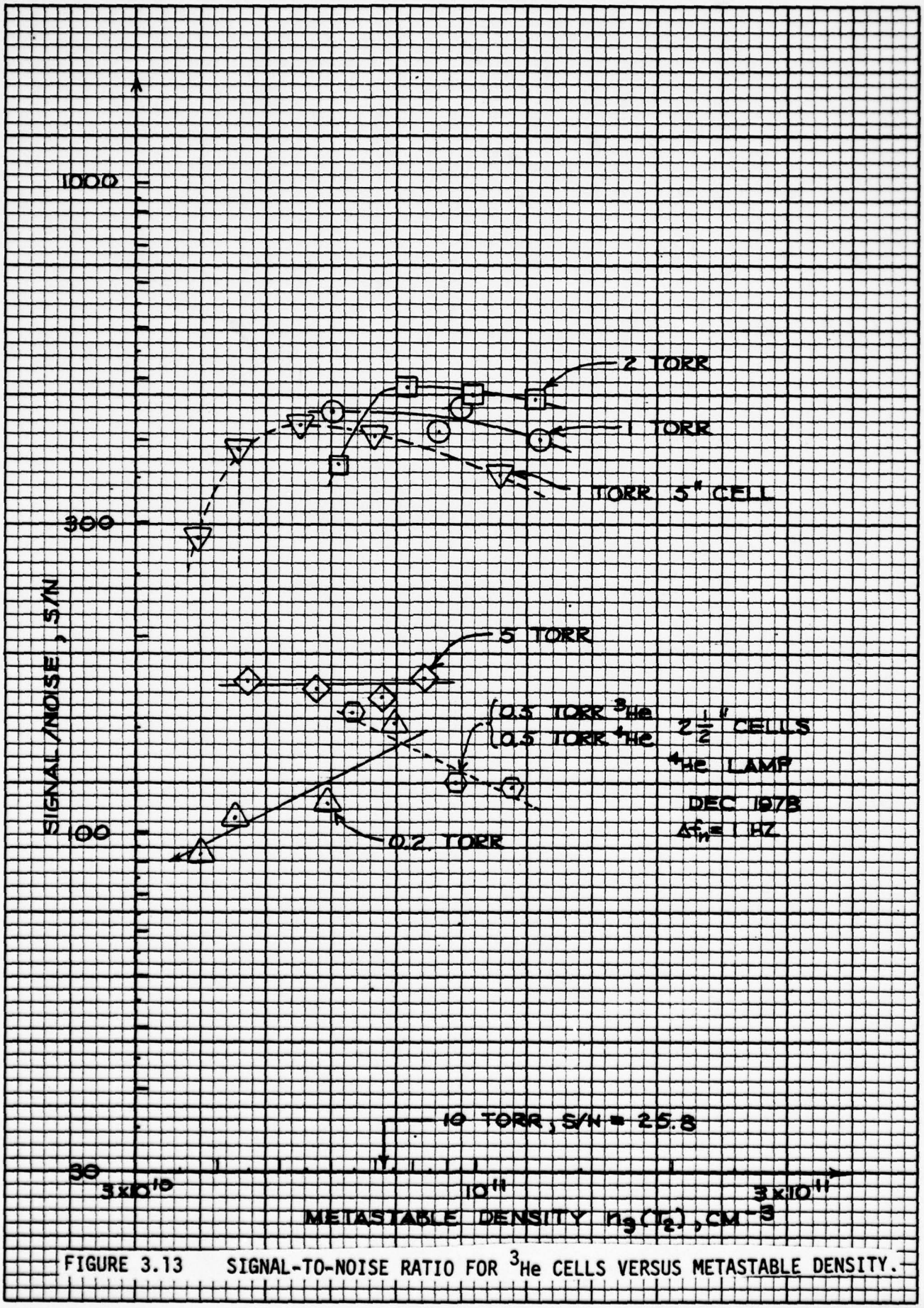

FIGURE 3.13 SIGNAL-TO-NOISE RATIO FOR ^{3}He CELLS VERSUS METASTABLE DENSITY.

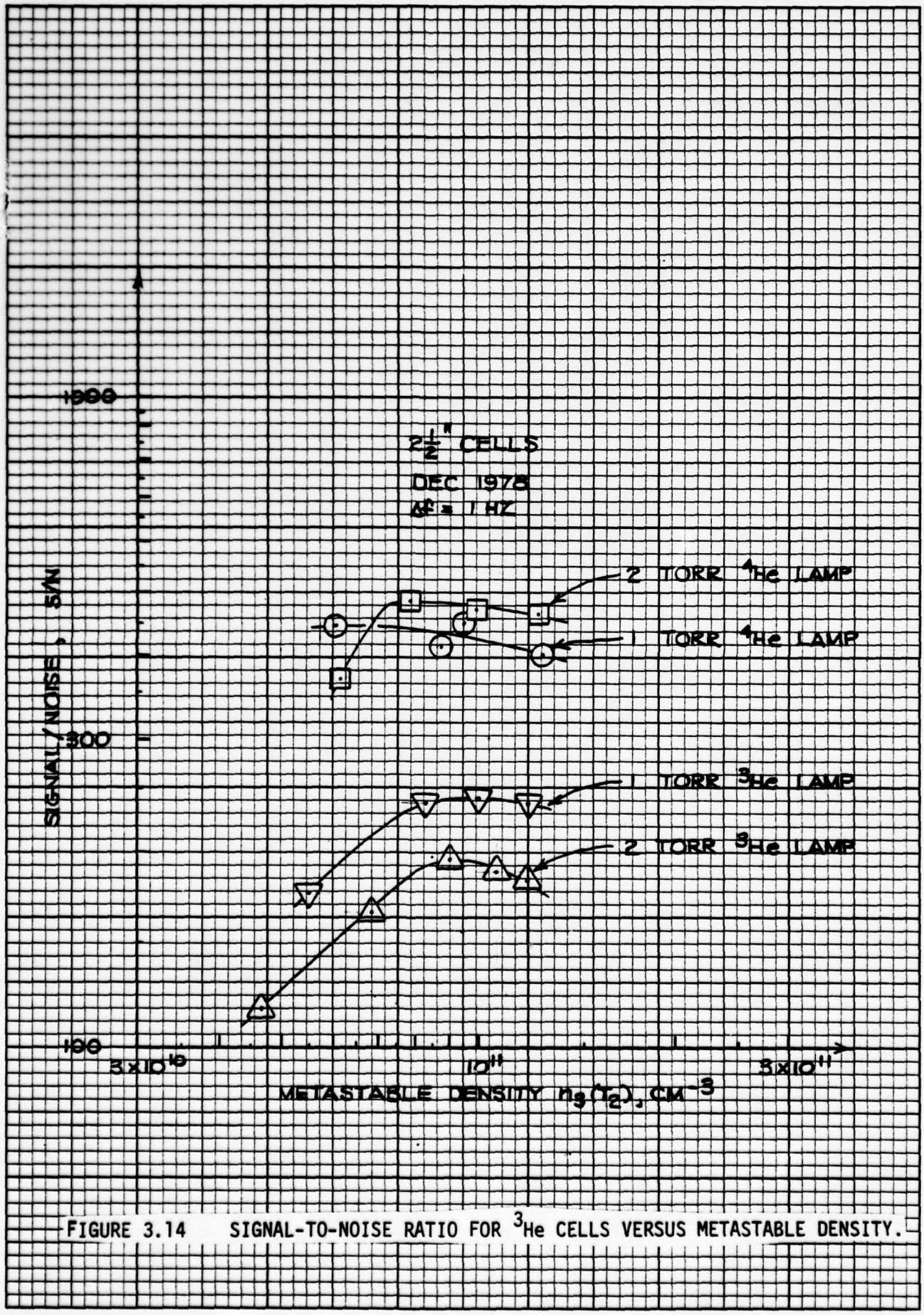

FIGURE 3.14 SIGNAL-TO-NOISE RATIO FOR ^{3}He CELLS VERSUS METASTABLE DENSITY.

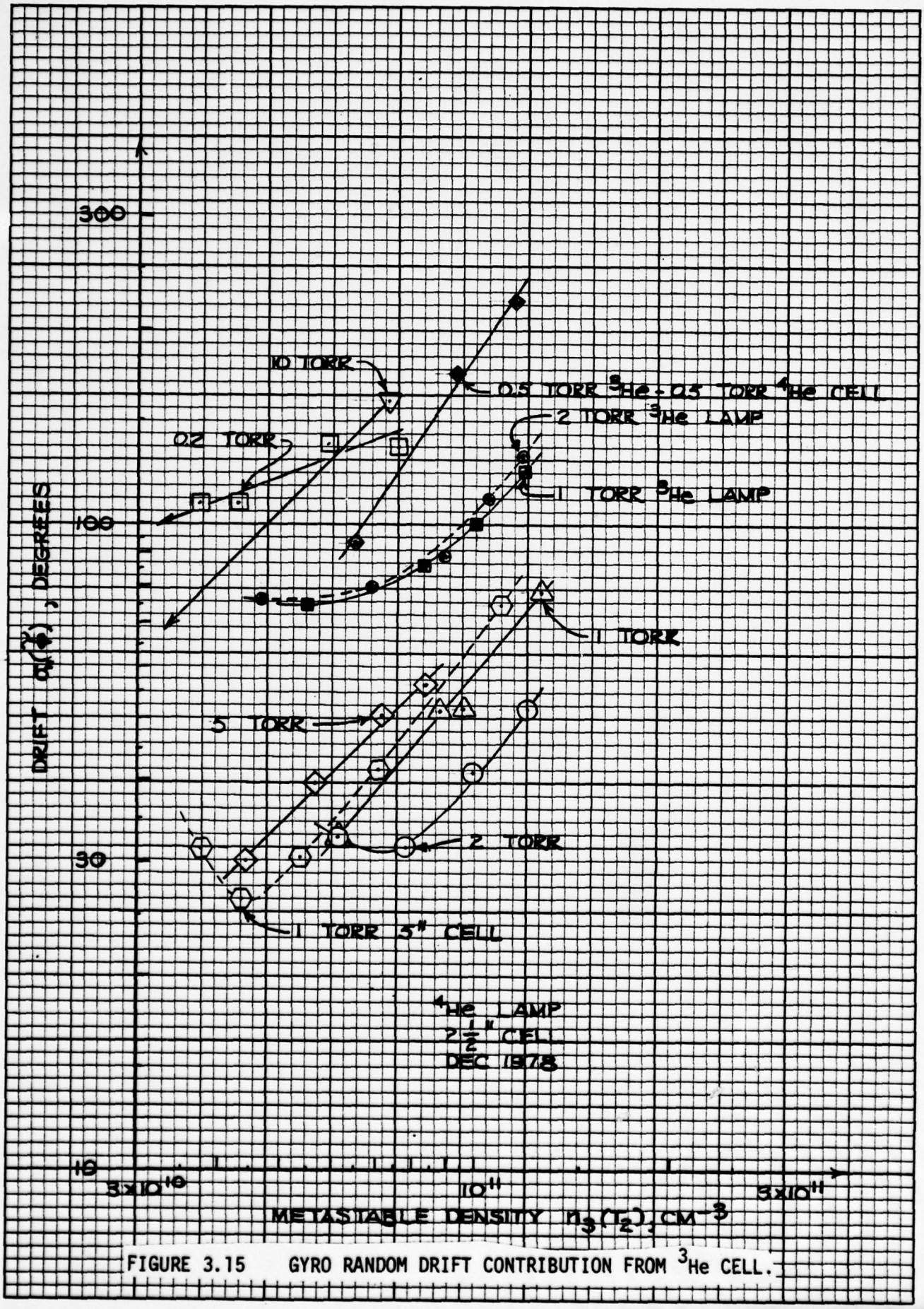

FIGURE 3.15 GYRO RANDOM DRIFT CONTRIBUTION FROM ^{3}He CELL.

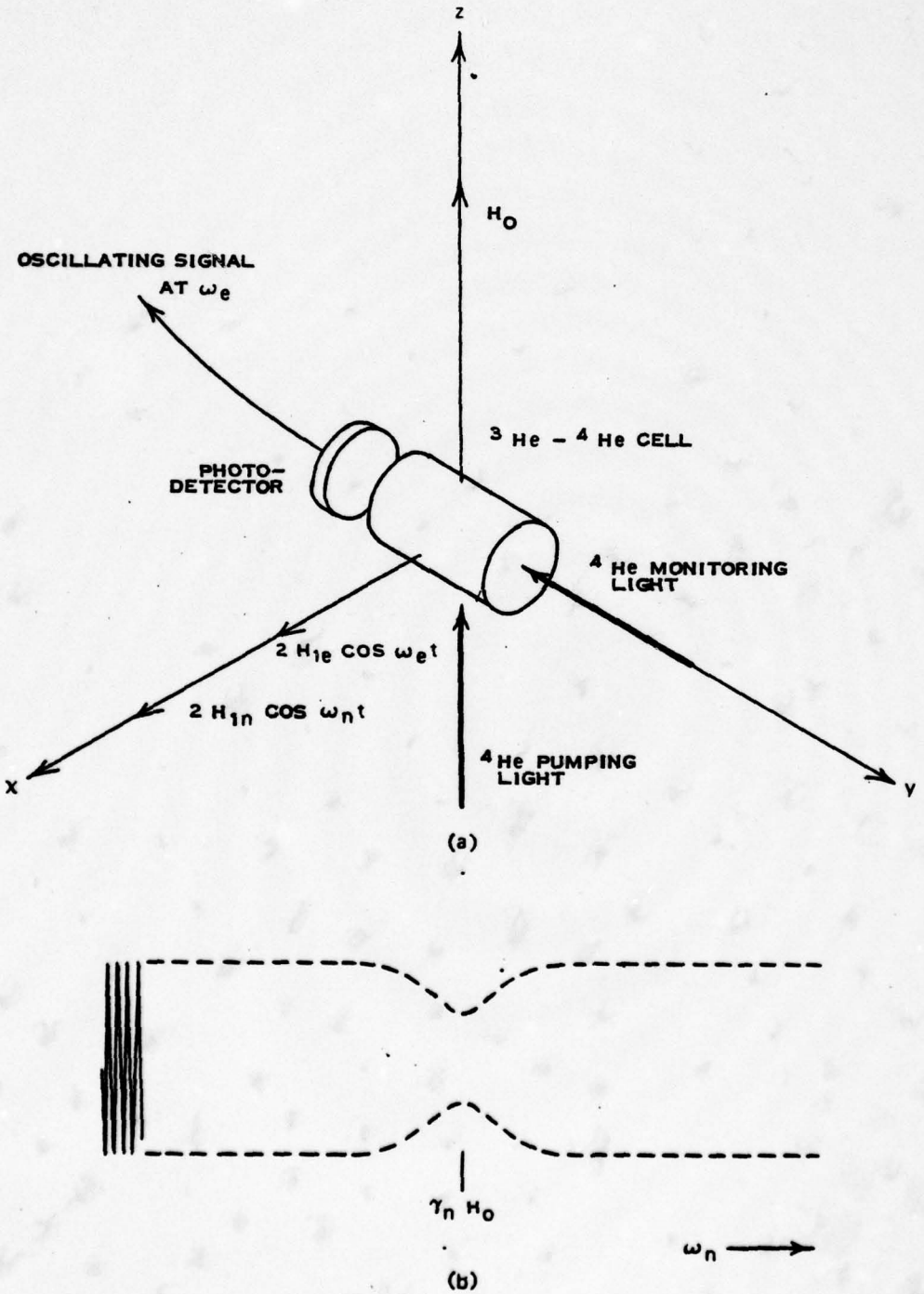

(a) SCHEMATIC OF OPTICAL PUMPING APPARATUS TO DEMONSTRATE SIMULTANEOUS MAGNETIC RESONANCE OF ^{4}He METASTABLES AND ^{3}He NUCLEI. (b) THE AMPLITUDE MODULATION OF THE OSCILLATING SIGNAL (AT ANGULAR FREQUENCY ωe) AS ω_n IS SCANNED THROUGH RESONANCE.

FIGURE 4.1

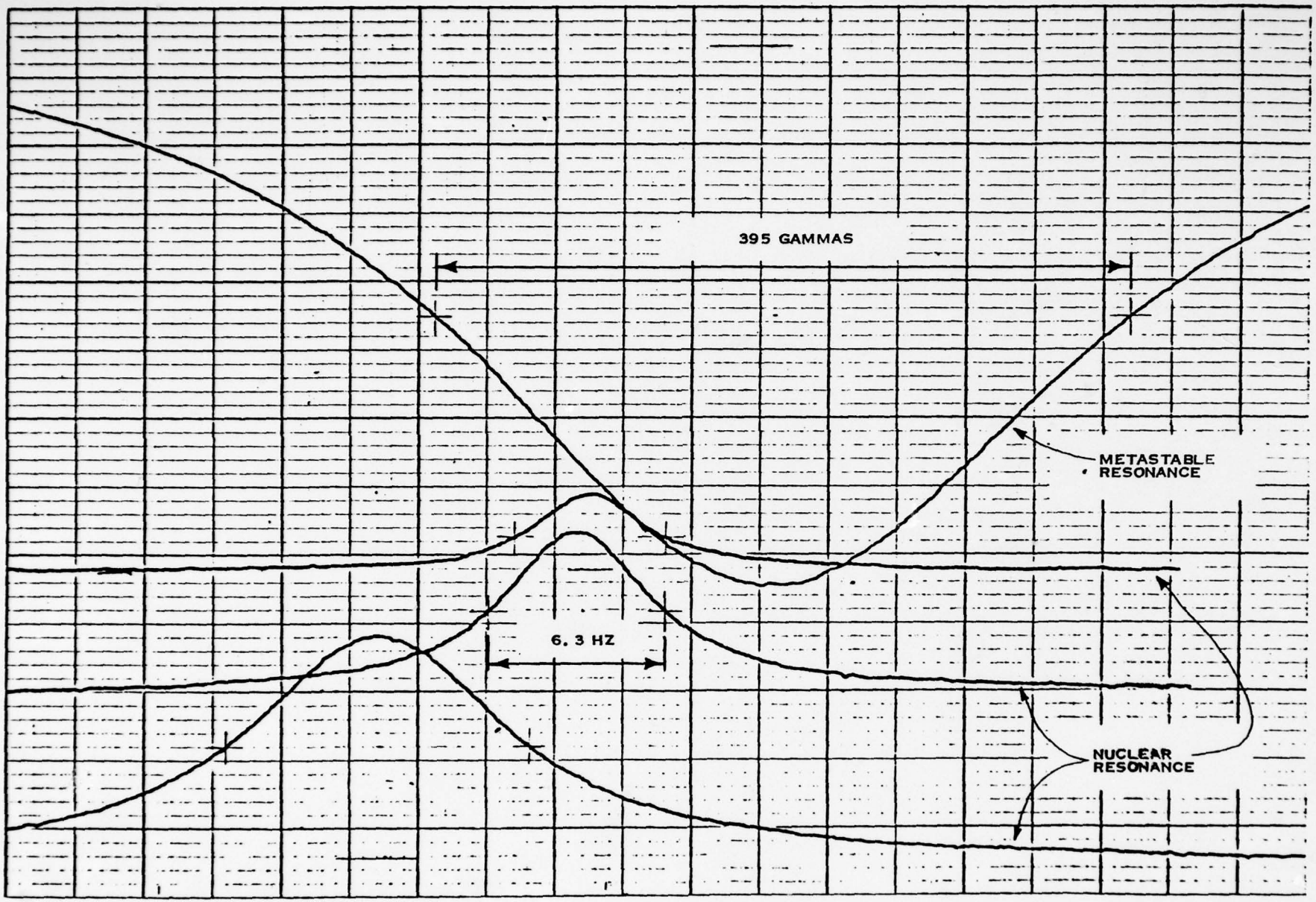

FIGURE 4.2 THE DEMODULATED AMPLITUDES OF THE PHOTODETECTOR SIGNAL. THE CURVE LABELLED "METASTABLE RESONANCE" WAS OBTAINED BY SCANNING H_0 WITH CONSTANT ω_e AND NO H_{1n}. THE CURVES LABELLED "NUCLEAR RESONANCE" WERE OBTAINED BY SCANNING ω_n WITH CONSTANT H_0 AND ω_e.

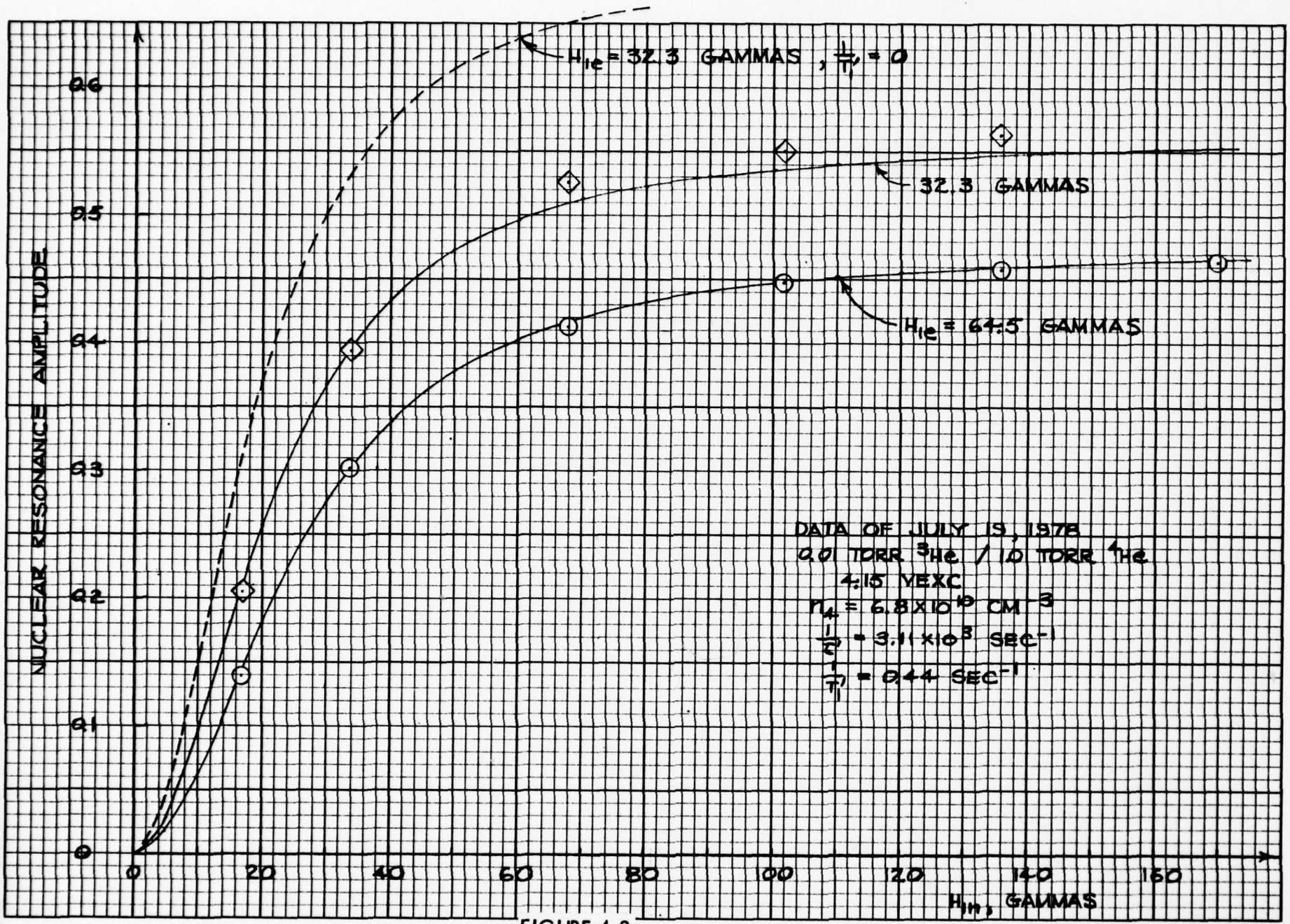

FIGURE 4.3

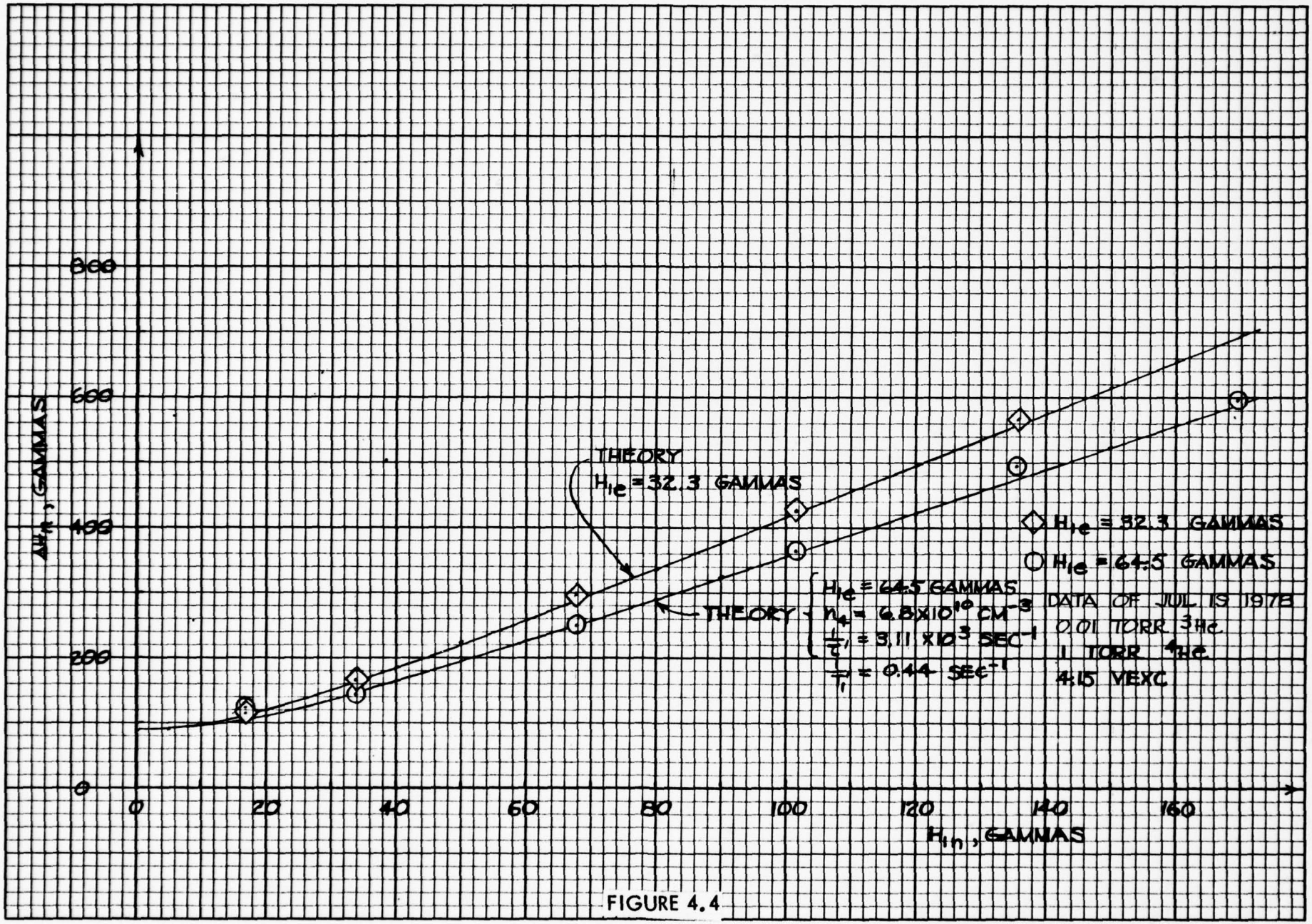

FIGURE 4.4

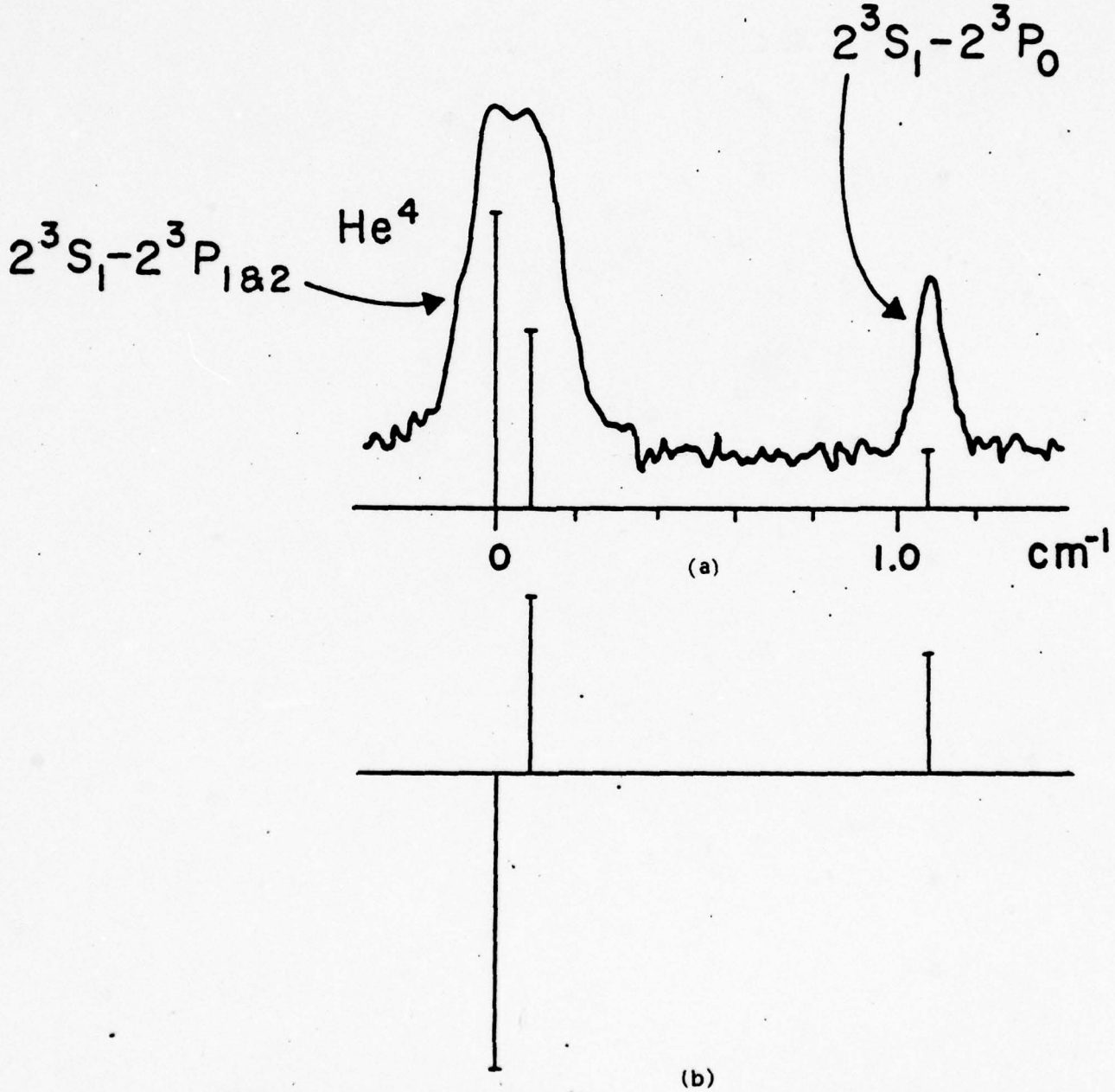

(a) THE 1.083 μm LINES OF ^{4}He IN EMISSION (FROM REFERENCE 7).
(b) THE RELATIVE PUMPING EFFICIENCIES OF THE THREE 2^3S-2^3P ABSORPTION LINES.

FIGURE 5.1

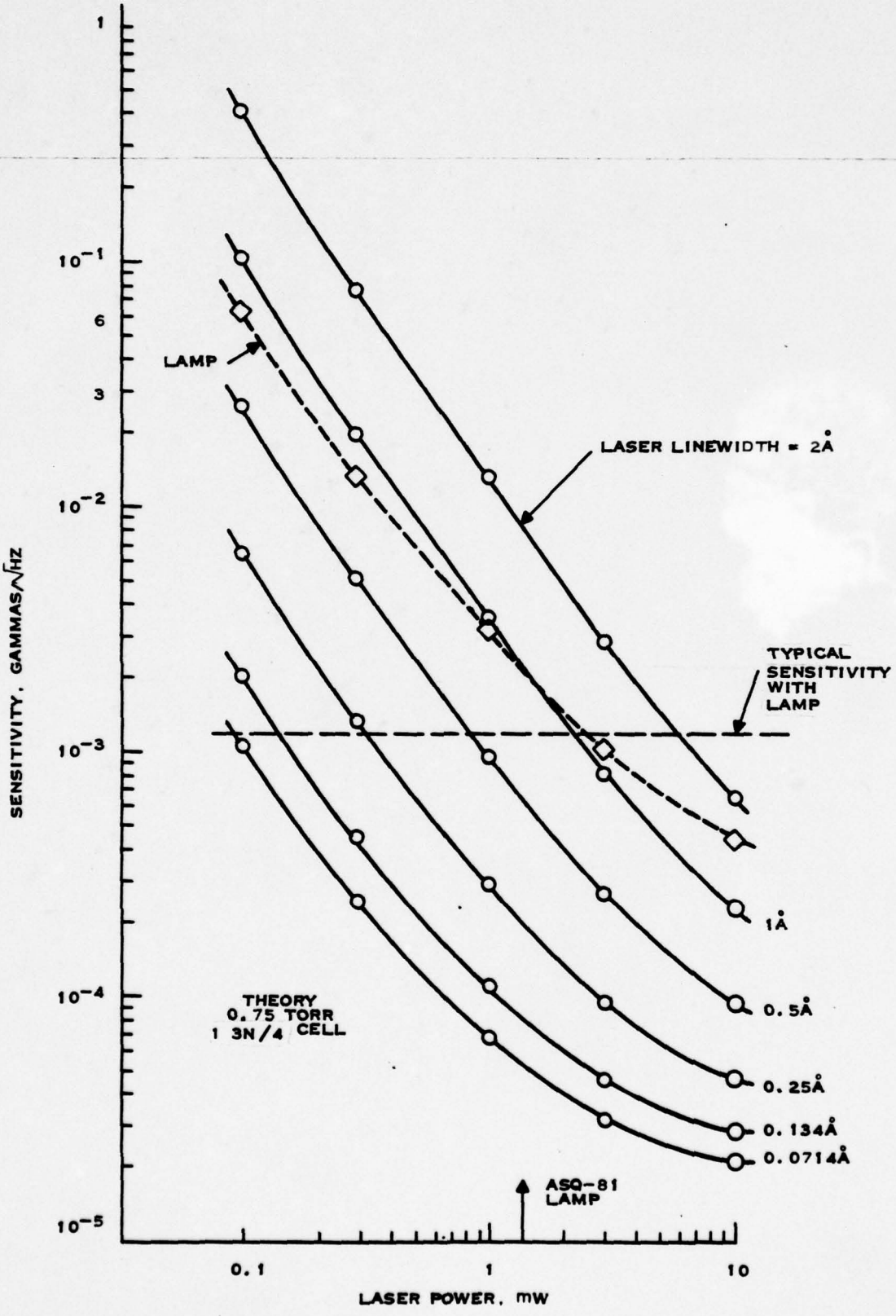

FIGURE 5.2 He^4 Magnetometer Sensitivity as a Function of Laser Radiant Power

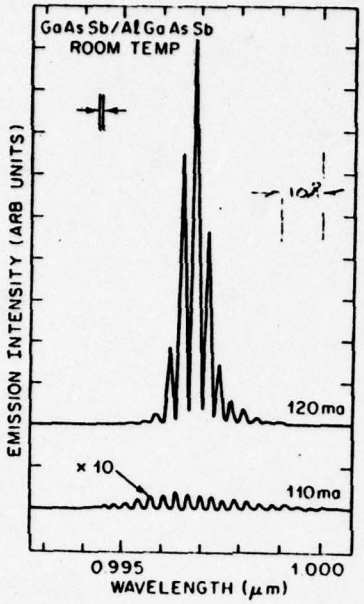

FIGURE 5.3

Spectra of a GaAsSb/AlGaAsSb DH laser operating cw at room temperature at two different currents. The spectrum for 110 mA, which is close to threshold, is shown enhanced by a factor of 10 as indicated. Mode spacing is ~ 3 Å. (Reference 8)

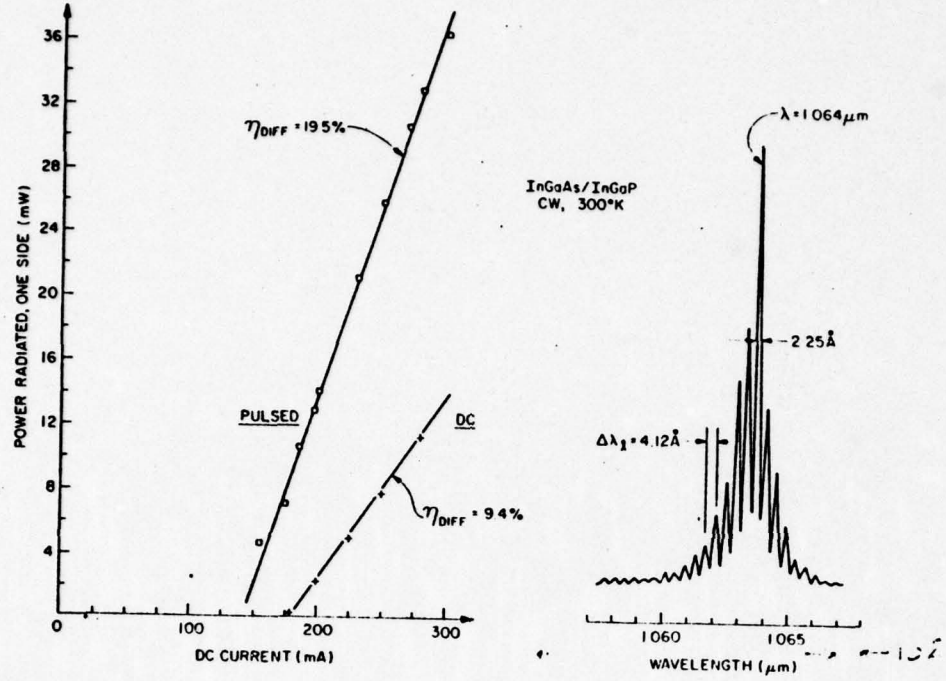

FIGURE 5.4

Room-temperature characteristics of $In_xGa_{1-x}As/In_yGa_{1-y}P$ DH sample No. 1388A. Power curve vs applied current is shown for pulsed and dc bias. Spectrum at right is for dc bias at 180 mA. (Reference 9)

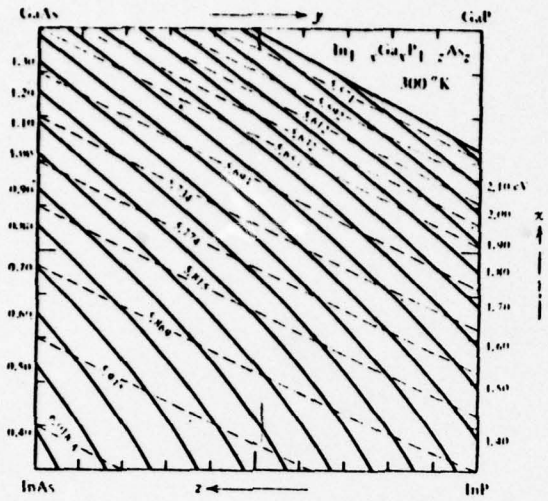

FIGURE 5.5

Figure 1. Lattice constant (dashed lines) and energy gap (solid lines) as a function of composition for the quaternary alloy $In_{1-X}Ga_XP_{1-Z}As_Z$ (300K). The figure shows that it is possible to grow a wide range of alloy compositions, and lattice-matched heterojunctions, along various isolattice constant lines. For a_o = 5.869 Å these compositions span the wavelength range (300K) from 0.92 μm at the InP corner to 1.68 μm at the $In_{1-X}Ga_XAs$ ($x \approx 0.47$) ternary boundary. (Reference 10)

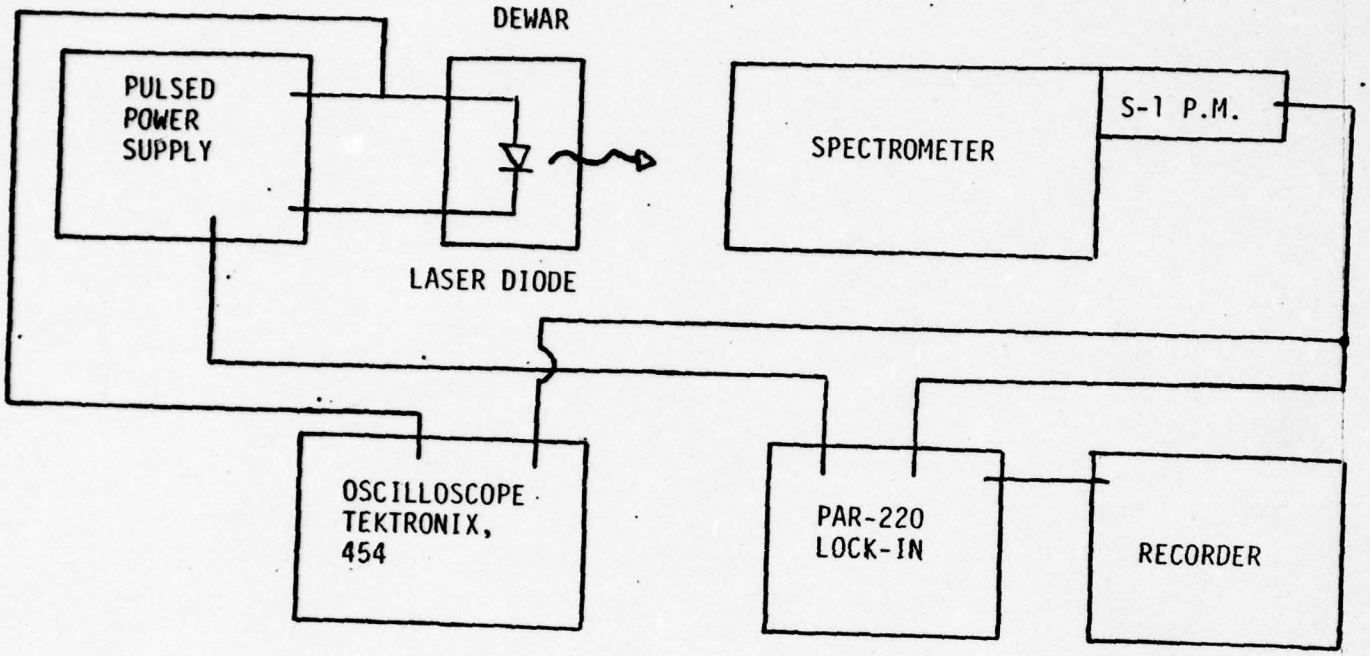

FIGURE 8: Units Employed during the Analysis of the Laser Diode Performance

FIGURE 5.6

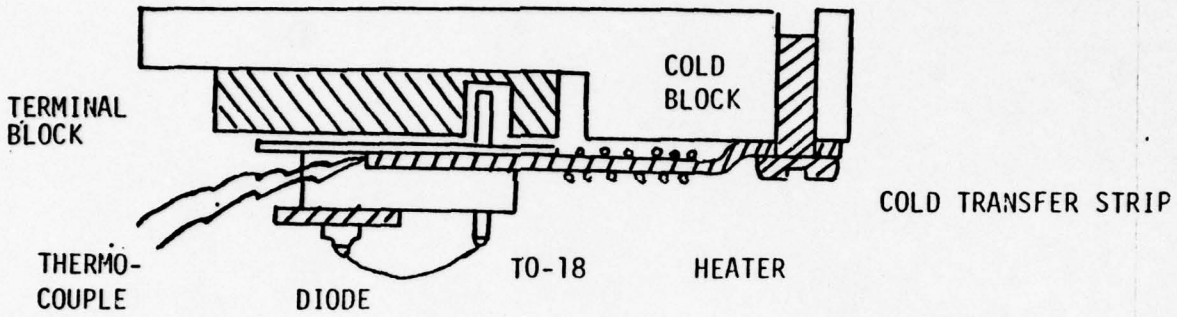

FIGURE 9: Heater, Cold Transfer Strip And Thermocouple for Controlling And Reading The Temperature of the Laser Diode

FIGURE 5.7

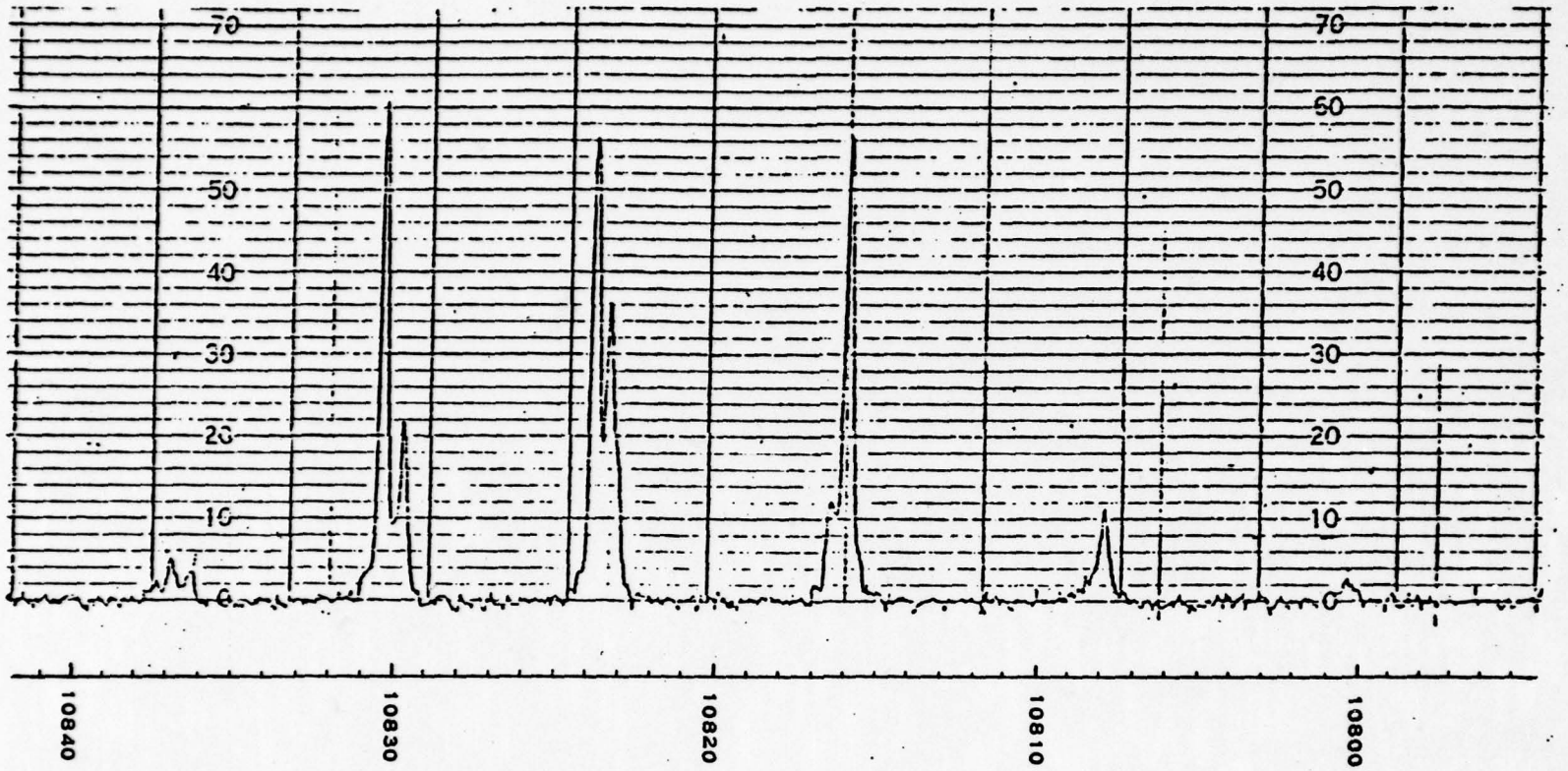

FIGURE 5.8 OUTPUT SPECTRUM OF SEMICONDUCTOR DIODE LASER. THE WAVELENGTH SCALE IS IN ANGSTROMS. PEAK CURRENT, 0.24 AMPERES; PULSE WIDTH, 3 MICRO SECONDS; PULSE RATE, 200HZ.

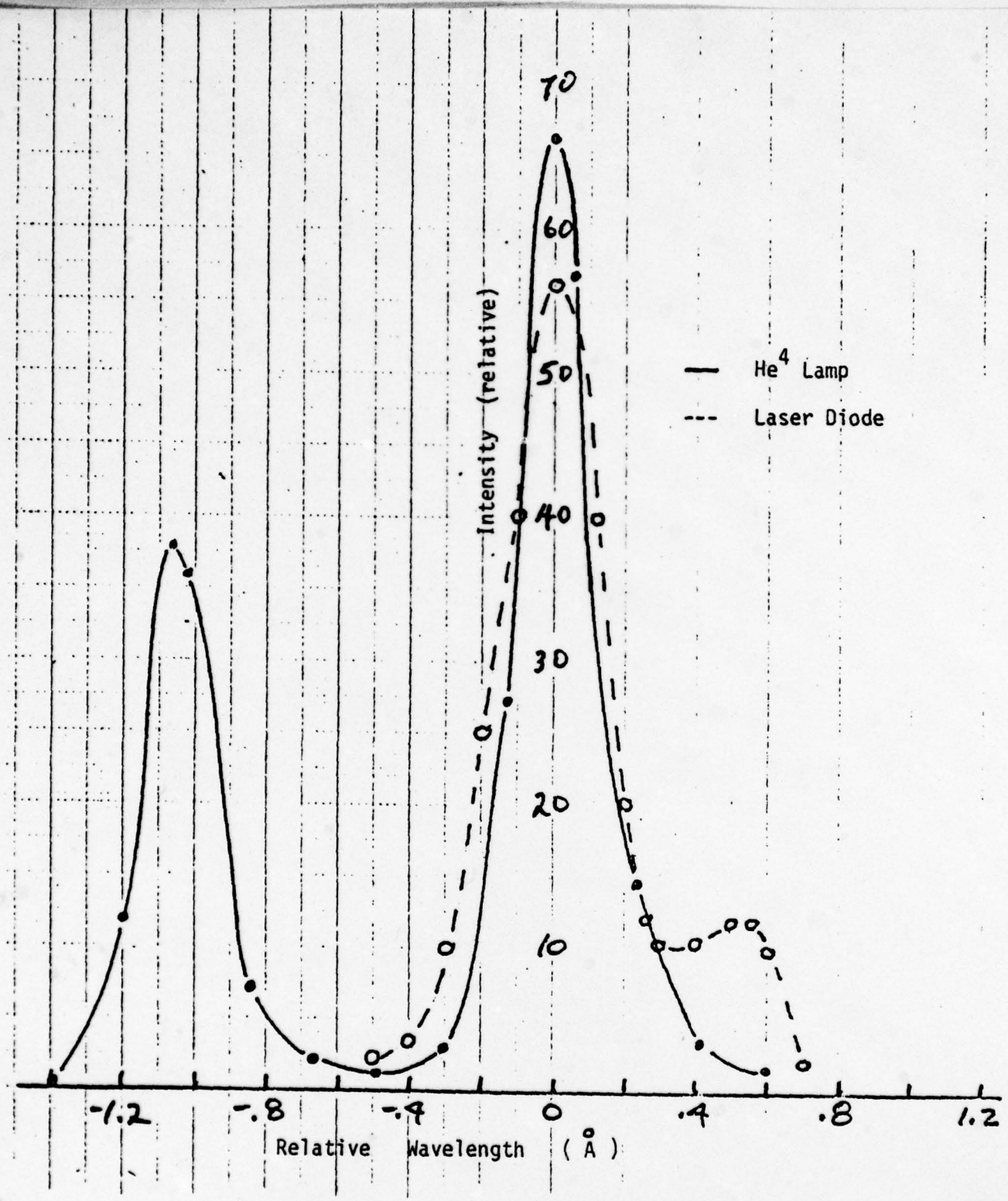

Relative intensity distribution of emission

From: He^4 lamp and laser diode

FIGURE 5.9

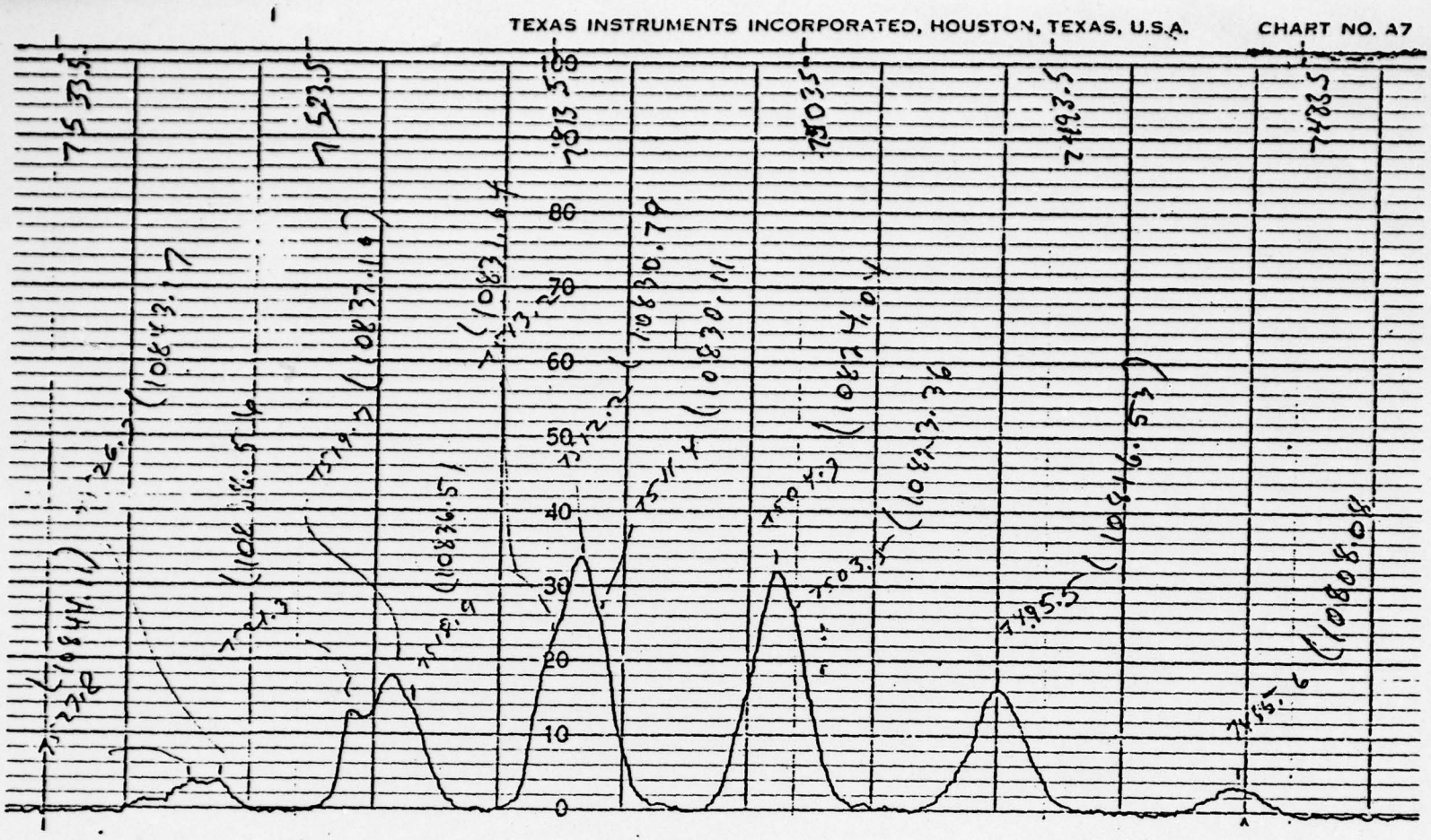

Recorder trace of Radiation from Laser Diode: Peak current 0.8 amperes; Pulse; 3 Micro Seconds; repetition rate, 200 pps.

FIGURE 5.10

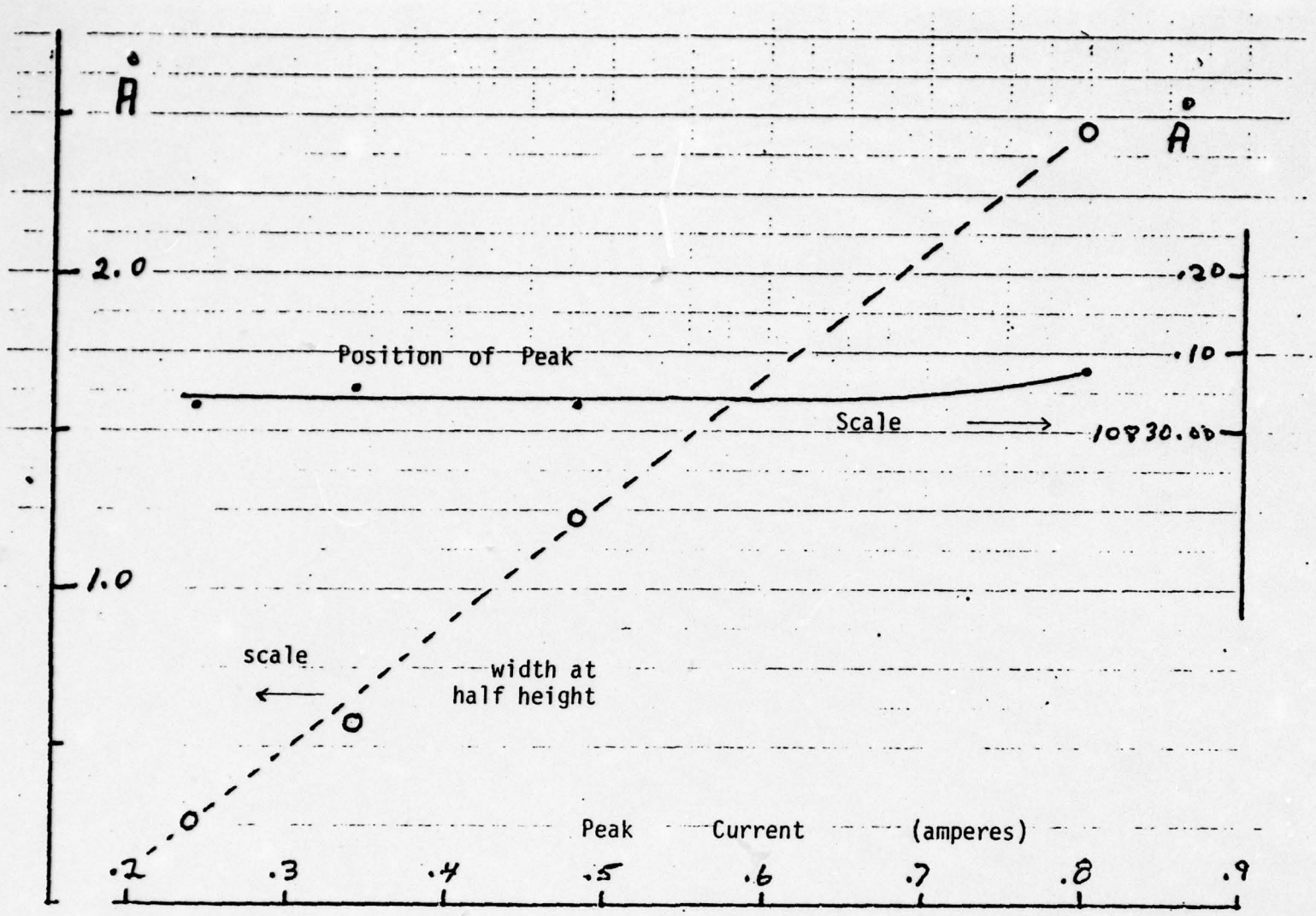

Variation of Position of Peak with driving current. Pulse, 3 micro seconds; Repetition Rate, 200 pps. Increase in current increases radiant power by increasing band width.

FIGURE 5.11

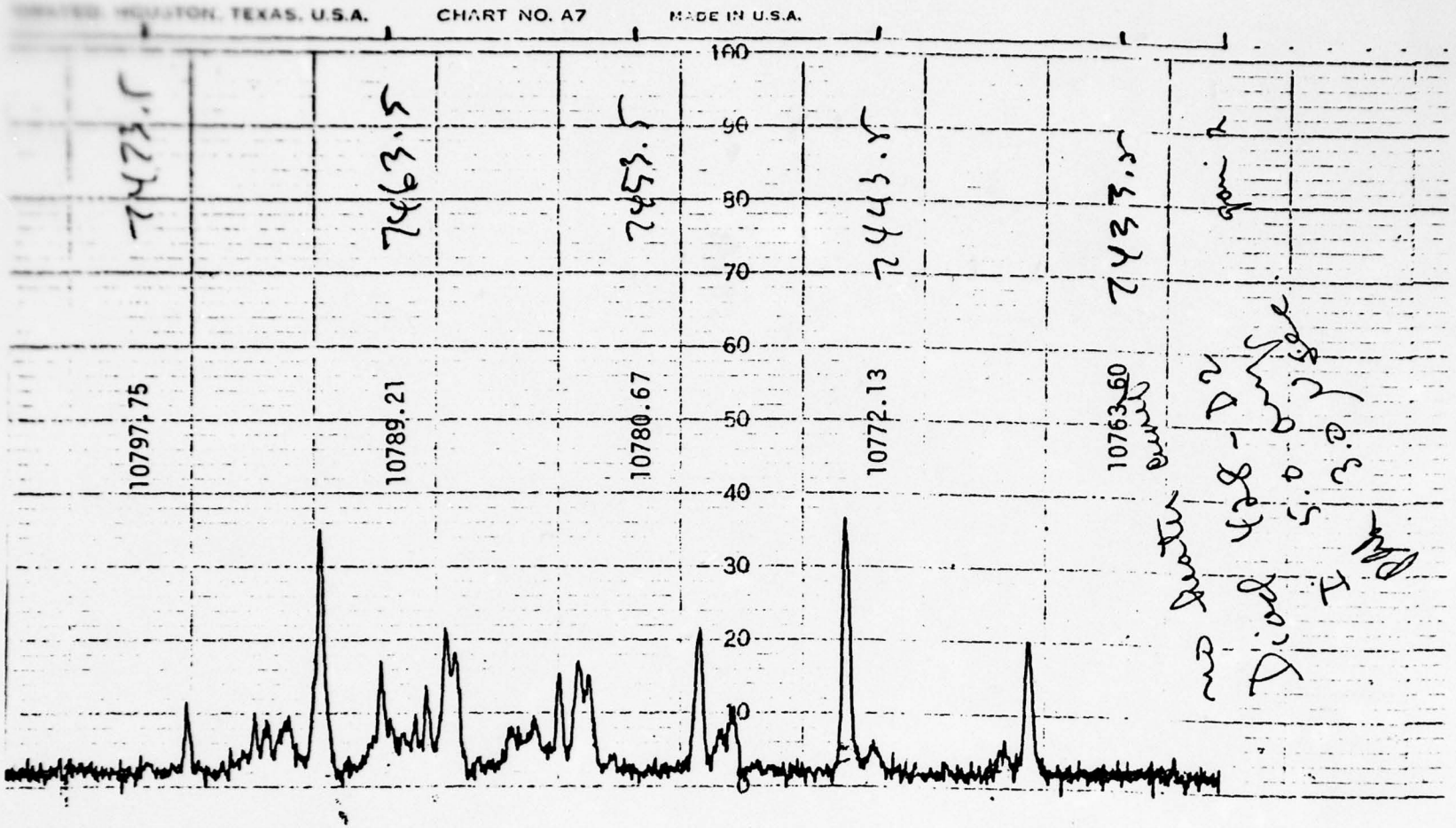

Emission from a Laser Diode at 77°K. No heater current in Temperature shifting device.

FIGURE 5.12

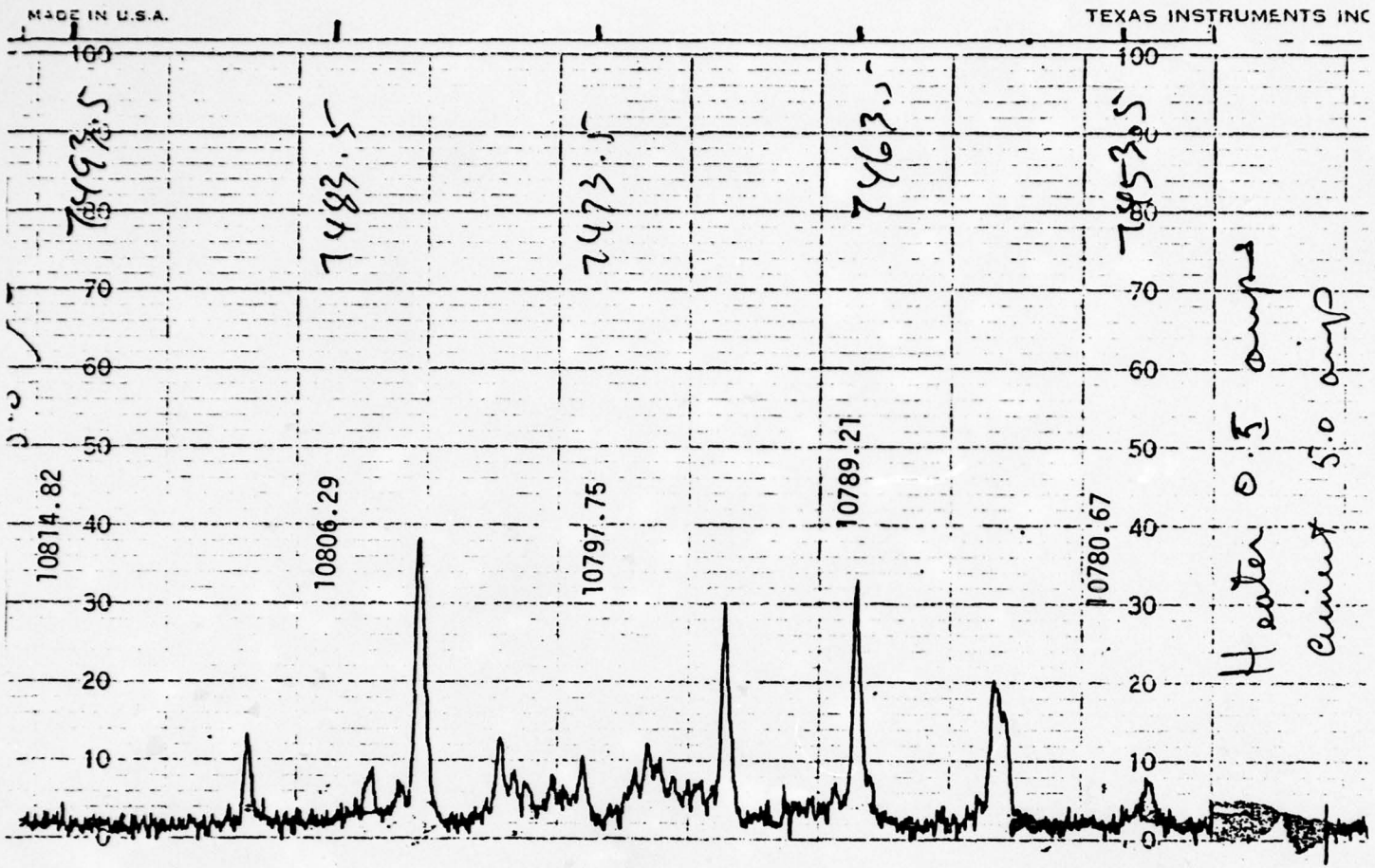

Shift in the Peaks Amplitude and Wavelength, as well as Appearance of New Peaks Produced by Passing 0.5 Amperes through the Heater.

FIGURE 5.13

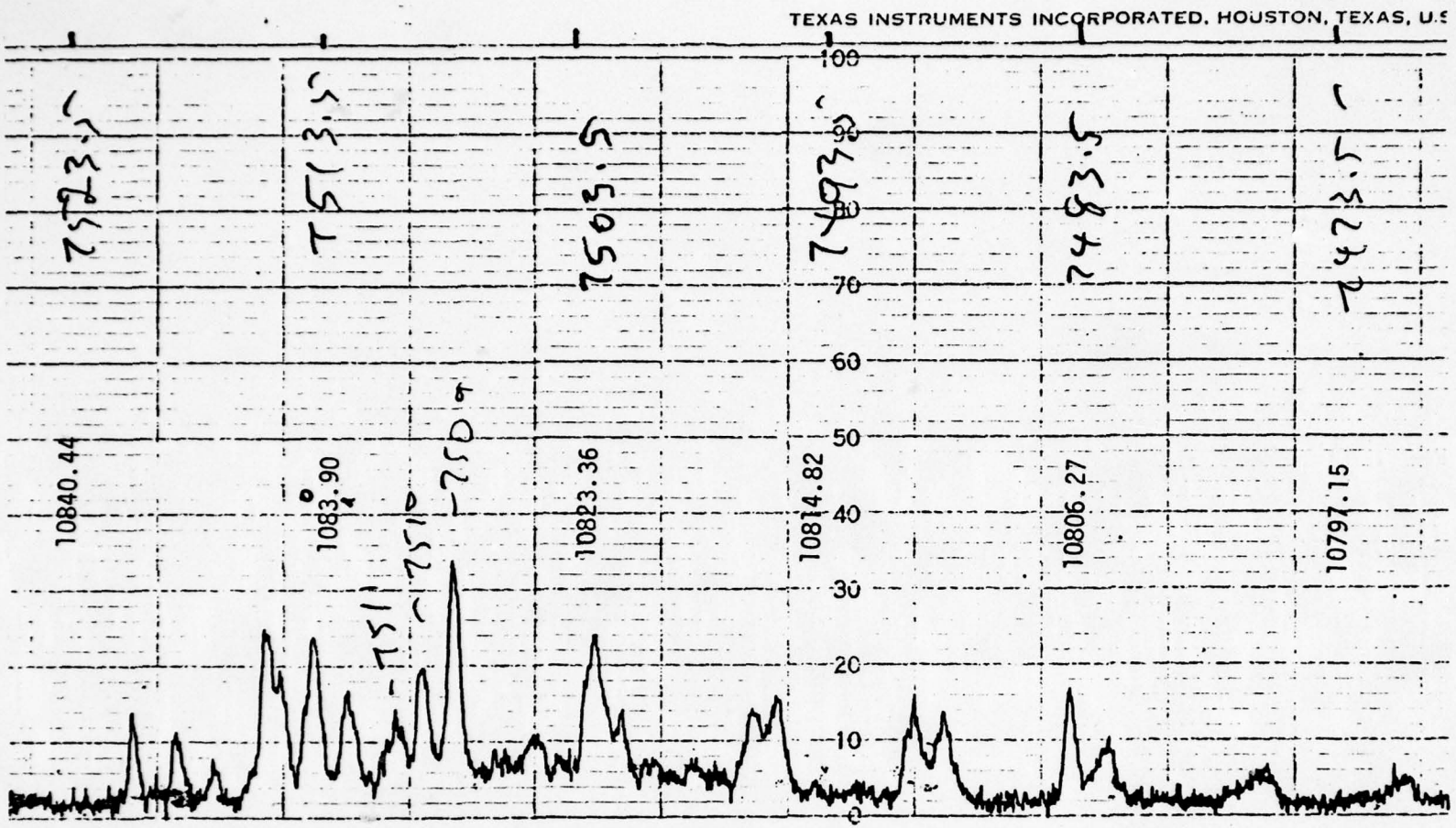

Emission from Laser has Shifted Out of the Spectral Region at which 0.0 Amperes was Passed into a Region at Longer Wavelength, and containing the 10830.0 Å, by 1.0 Amperes in the Heater.

FIGURE 5.14

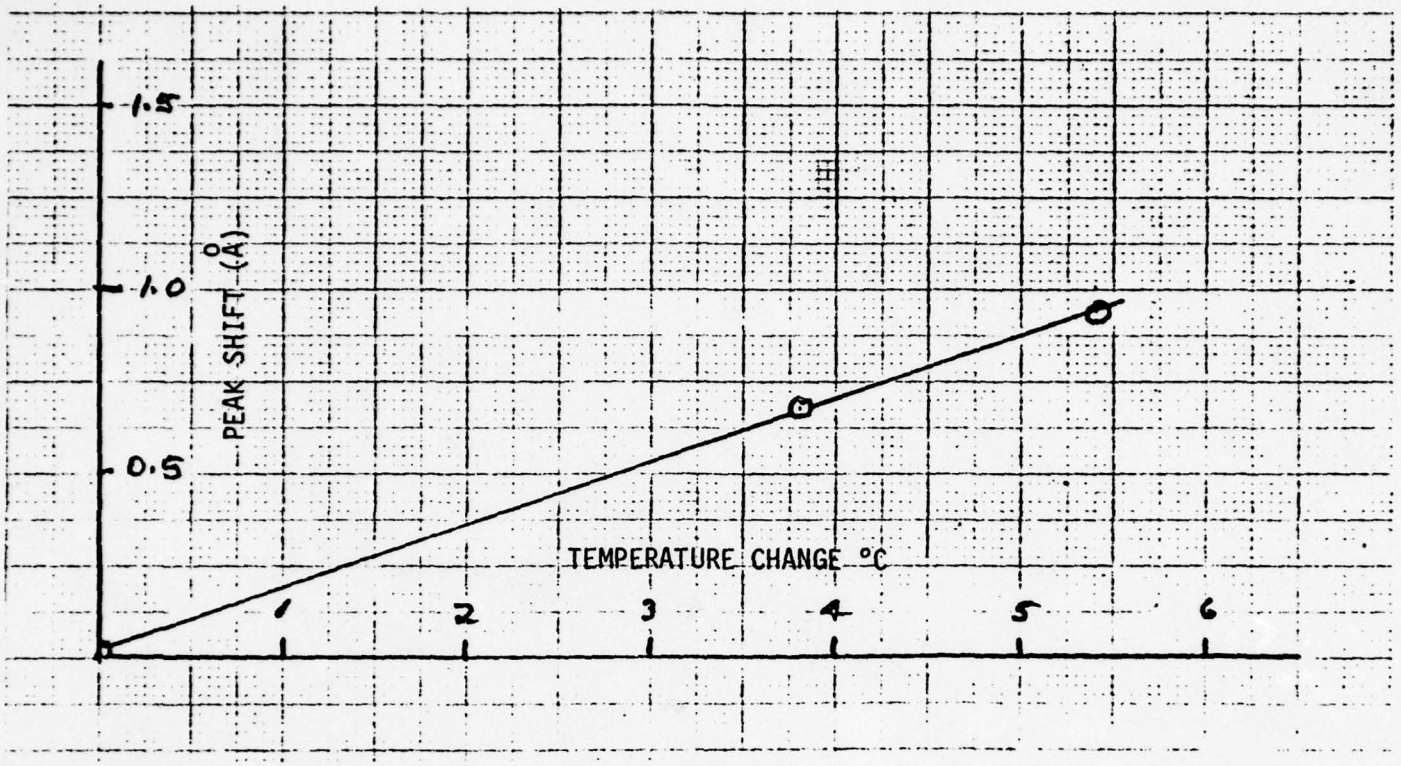

Shift in Peak Position (in Å) with change in Laser Diode Temperature (°K).

FIGURE 5.15

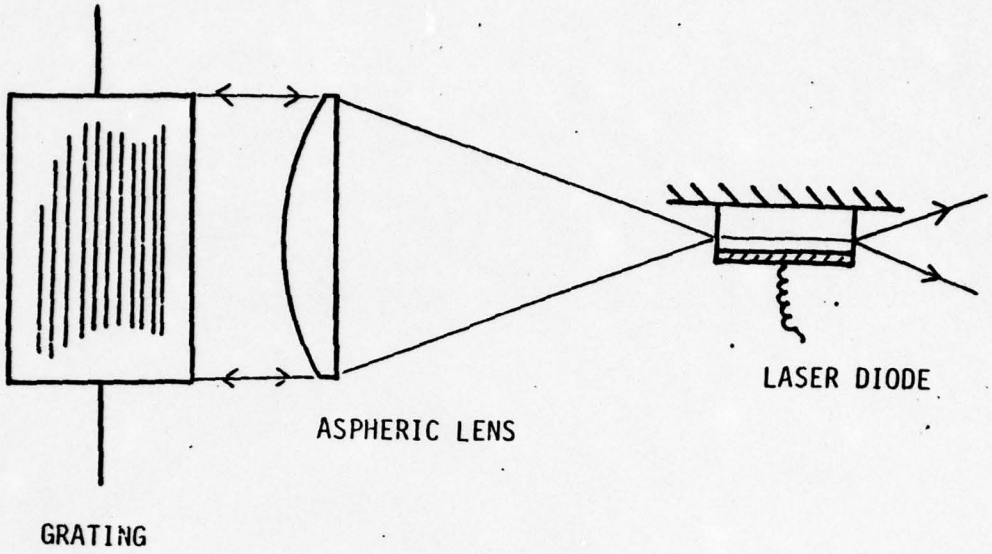

Grating, Lens And Diode Forming Tunable External Cavity

FIGURE 5.16

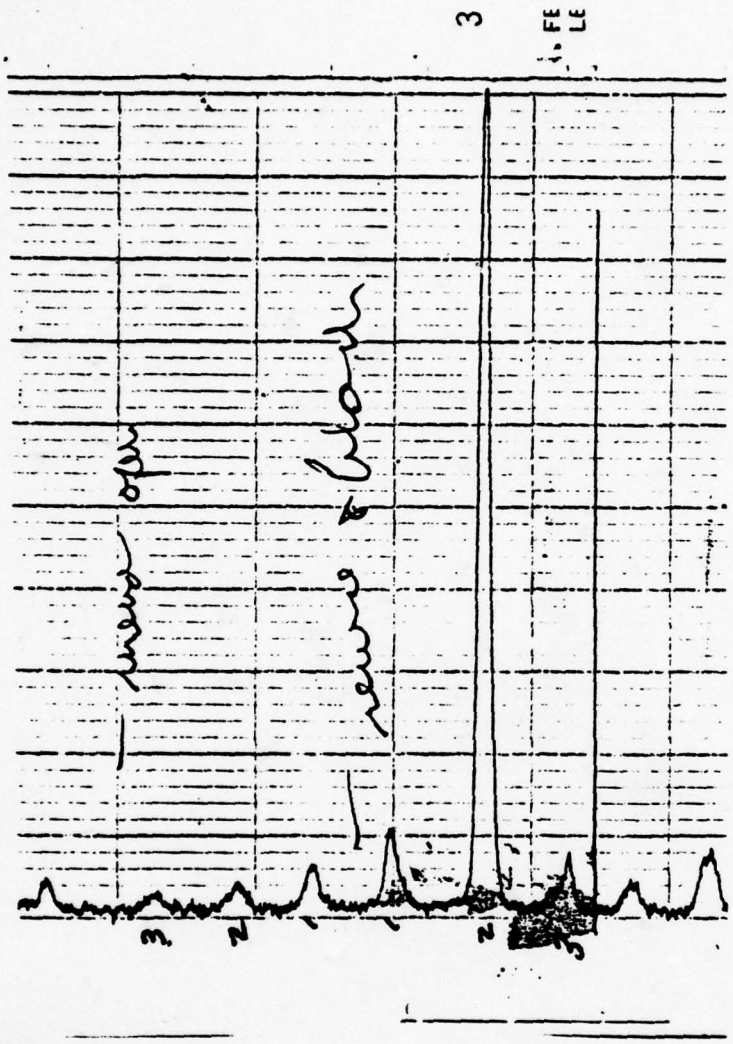

Increase in amplitude of peak #2 when the grating - lens external cavity was coupled to the laser diode. The peaks on the left labelled 1, 2, 3 were obtained without coupling.

FIGURE 5.17

Increase in amplitude of peak #2 when the grating-lens external cavity was coupled to the laser diode. The dispersed radiation was prevented from entering the spectrometer slit, except for the portion that passed through the diode

FIGURE 5.18

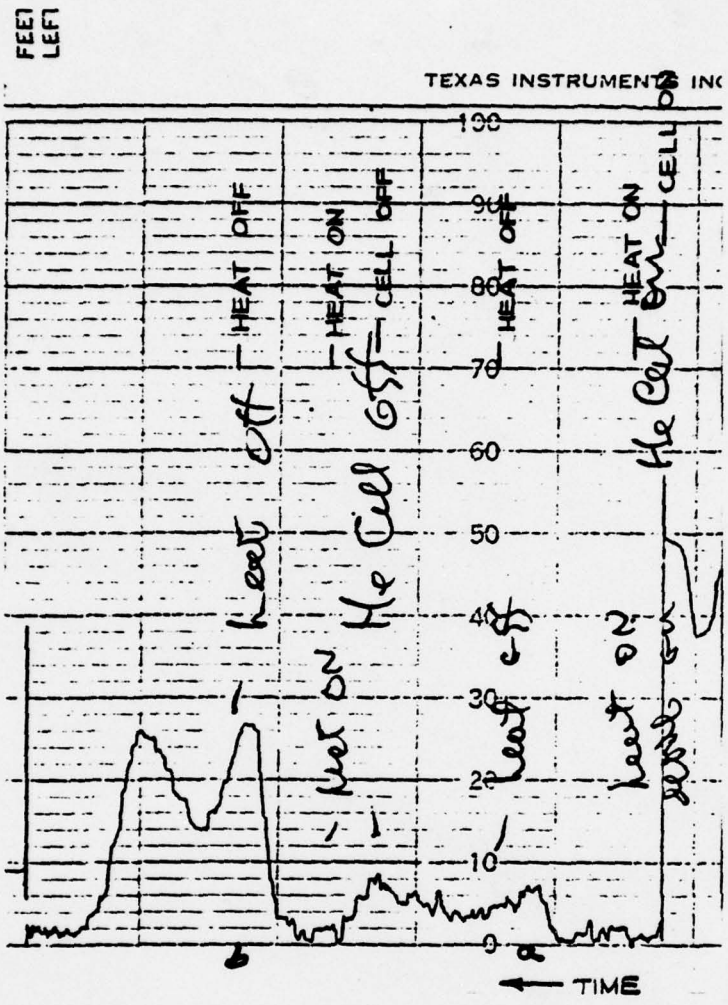

Laser diode radiation tuned through $D_{1,2}$ resonance and passed through the He absorption cell with its excitation: in a) "on" and in b). "off".

FIGURE 5.19

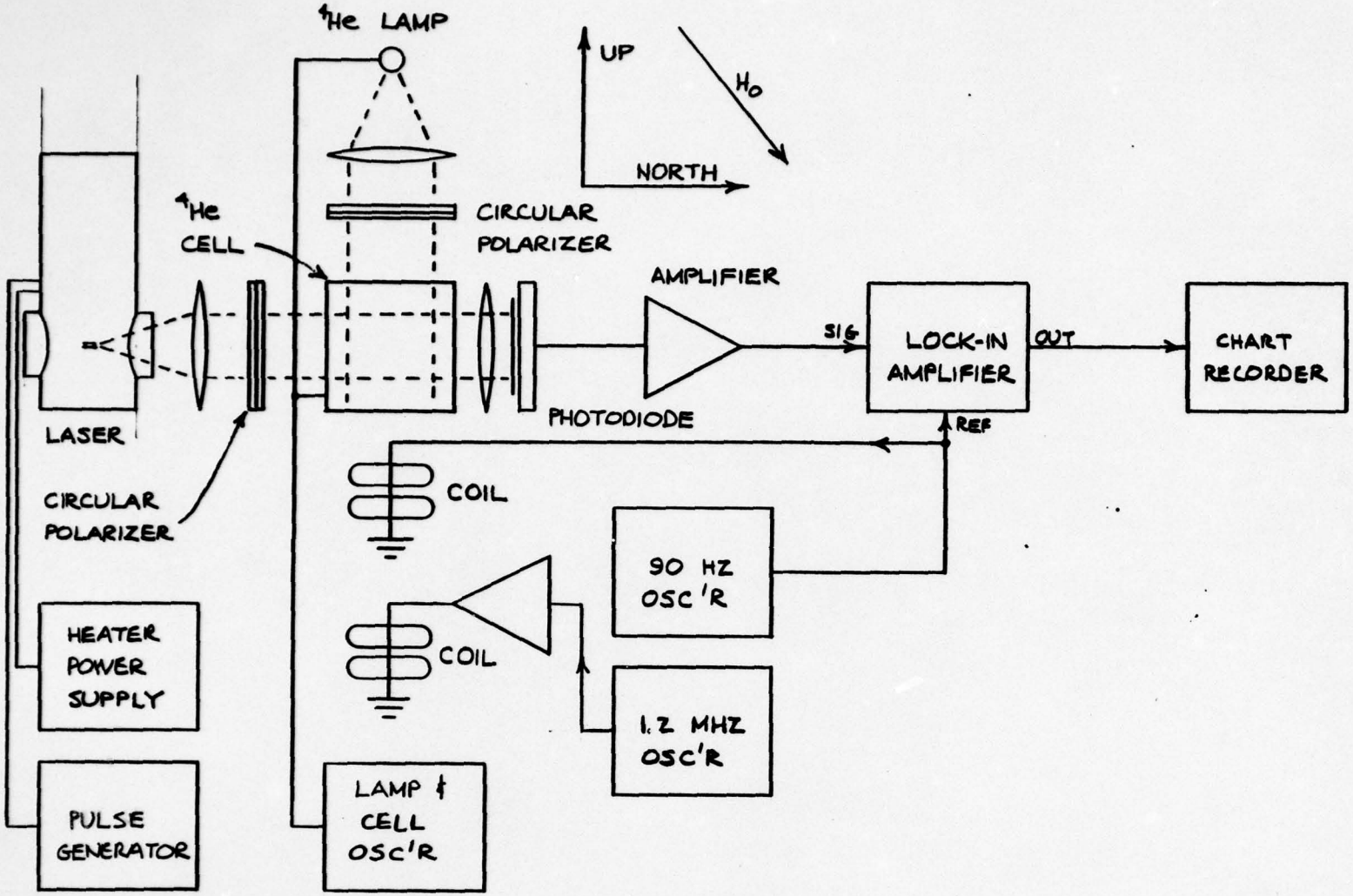

FIGURE 6.1 BLOCK DIAGRAM OF EXPERIMENT TO DEMONSTRATE MONITORING OF ^{4}He POLARIZED ATOMS BY LASER RADIATION

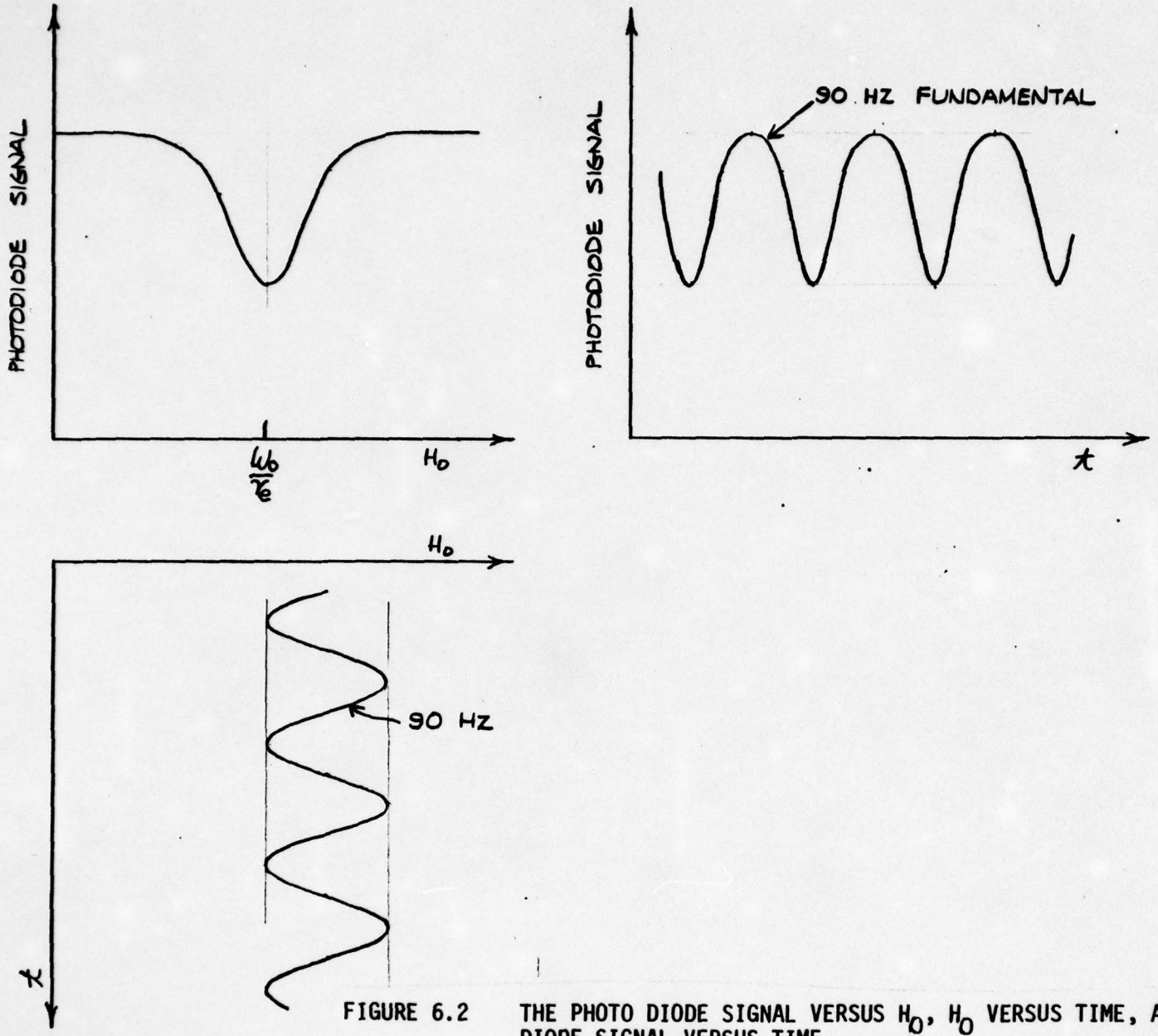

FIGURE 6.2 THE PHOTO DIODE SIGNAL VERSUS H_0, H_0 VERSUS TIME, AND THE PHOTO DIODE SIGNAL VERSUS TIME.

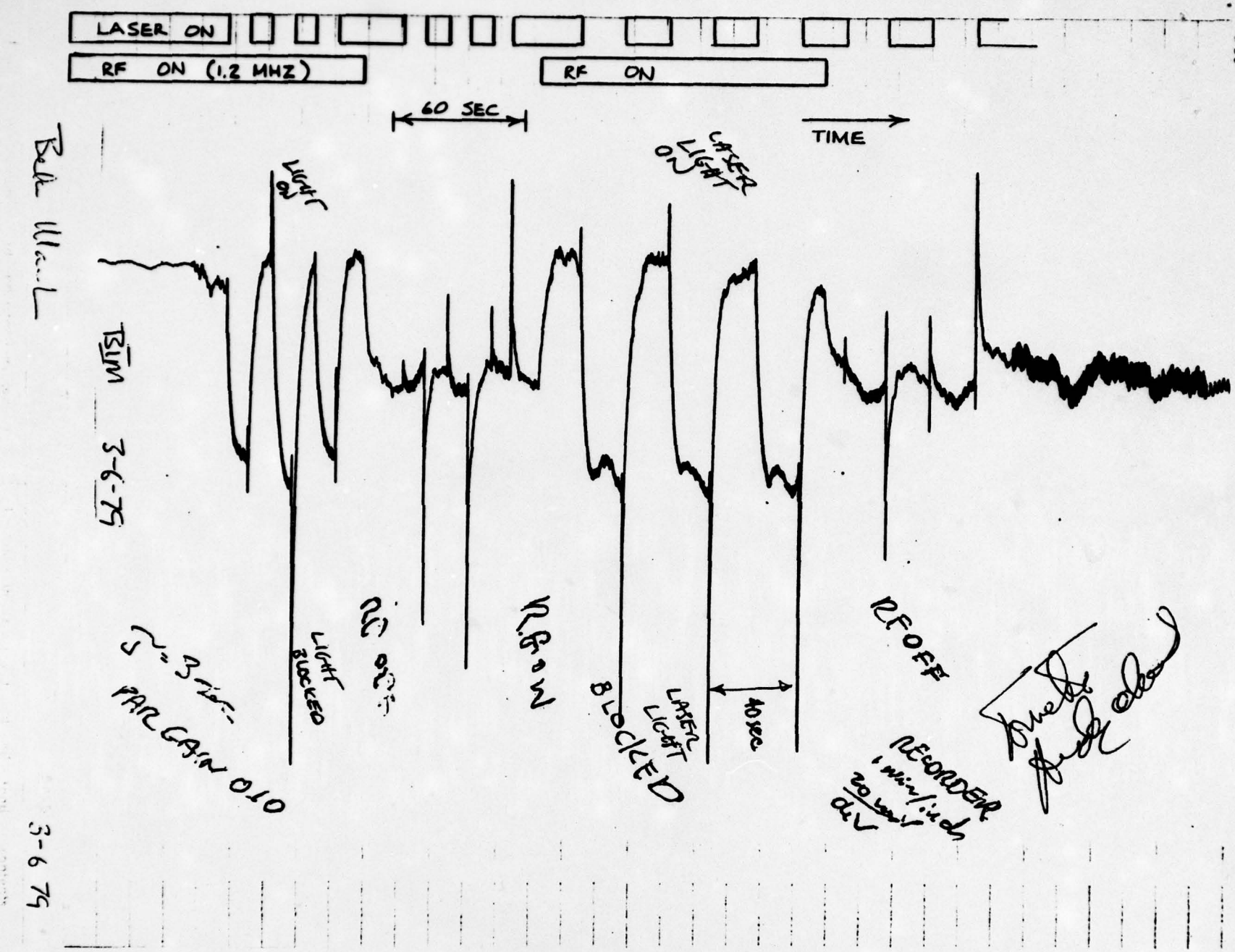

FIGURE 6.3 CHART RECORDING TRACE SHOWING DIODE LASER MONITORING SIGNAL.